UCRL-19093

c.2

RECEIVED
LAWRENCE
RADIATION LABORATORY

JAN 22 1970

LIBRARY AND
DOCUMENTS SECTION

SPECTROSCOPIC INVESTIGATION OF SOME HIGH TEMPERATURE SPECIES TRAPPED IN LOW TEMPERATURE MATRICES

John Ling-Fai Wang

(Ph. D. Thesis)

October 1969

AEC Contract No. W-7405-eng-48

TWO-WEEK LOAN COPY

This is a Library Circulating Copy which may be borrowed for two weeks. For a personal retention copy, call Tech. Info. Division, Ext. 5545

UCRL-19093 Cy. 2

LAWRENCE RADIATION LABORATORY
UNIVERSITY of CALIFORNIA BERKELEY

DISCLAIMER

This document was prepared as an account of work sponsored by the United States Government. While this document is believed to contain correct information, neither the United States Government nor any agency thereof, nor the Regents of the University of California, nor any of their employees, makes any warranty, express or implied, or assumes any legal responsibility for the accuracy, completeness, or usefulness of any information, apparatus, product, or process disclosed, or represents that its use would not infringe privately owned rights. Reference herein to any specific commercial product, process, or service by its trade name, trademark, manufacturer, or otherwise, does not necessarily constitute or imply its endorsement, recommendation, or favoring by the United States Government or any agency thereof, or the Regents of the University of California. The views and opinions of authors expressed herein do not necessarily state or reflect those of the United States Government or any agency thereof or the Regents of the University of California.

TABLE OF CONTENTS

ABSTRACT v
LIST OF FIGURES vi
LIST OF TABLES ix
I. INTRODUCTION 1
II. EXPERIMENTAL 4
A. General 4
B. Cryostat 4
1. Liquid Hydrogen Dewar 4
2. Cryo-tip 7
C. Furnaces 10
1. Carbon Resistance Furnace 10
2. Stainless Steel Knudsen Cell 10
D. Targets 10
1. Sapphire Target 10
E. Temperature Measurement 13
1. Target Temperature 13
2. Furnace Temperature 13
F. Gas Handling System 13
G. Spectrometers, Light Sources and Plates 14
H. Typical Experimental Parameters 14
III. OPTICAL ABSORPTION SPECTRA OF SOME MATRIX ISOLATED ATOMS 16
A. Introduction 16
B. General Discussions 17
1. Magnesium 17
2. Calcium 19
3. Cadmium 19
4. Lead 20
5. Barium 20
6. Silver 21
C. Results 21
1. Magnesium 21
2. Calcium 29
3. Cadmium 30

LIST OF FIGURES

Fig. 1 Photograph of liquid hydrogen dewar and the setup. 5

Fig. 2 Cutaway of liquid hydrogen dewar. 6

A. Stainless steel dewar

B. Ball bearings

C. O-ring

D. Gear arrangement

E. Copper block

F. Copper target holder

G. Germanium thermistor

H. Aluminized mylar foil

V. Pump-out port

W. Quartz windows

Fig. 3 Photograph of Cryo-tip system 8

Fig. 4 Photograph of Cryo-tip system 9

Fig. 5 Drawing of carbon resistance furnace 11

A. Vacuum chamber wall

B. Flange

C. Kovar ceramic seal for water-cooled electrode

D. Copper electrodes

E. Radiation shield

F. Carbon resistance furnace

G. Effusion hole

I. Vacuum O-ring

Fig. 6 Drawing of stainless steel Knudsen cell and optical arrangement 12

A. Stainless steel Knudsen cell

B. Tungsten foil

C. Resistance wire

D. Water cooling jacket

E. Epoxy joint

F. Flange

G. Thermal couple

H. Magnetic shutter

I. Target

J. Window

K. Lens

L. O-ring

M. Gas inlet

N. Aperture

O. Lens

P. Light source

Fig. 7 Energy levels diagram of atoms 18

Fig. 8 Spectra of magnesium in rare gas matrices 25

Fig. 9 Spectra of magnesium in xenon as a function of temperature 26

Fig. 10 Energy vs temperature for Mg spectra in xenon 27

Fig. 11 Spectra of calcium in Xe matrix as a function of temperature. 32

Fig. 12 Spectra of cadmium in Xe matrix at 20°K 36

Fig. 13 Spectra of lead in rare gas matrices at 20°K 38

Fig. 14 Splitting of ^1P state by a D_2 field 47

Fig. 15 Absorption spectra of magnesium and cadmium isolated in xenon simultaneously. 50

Fig. 16 Absorption spectra of Mg_2 in rare gas matrices 62

Fig. 17 Site stability of Mg in xenon solid as a function of temperature 65

Fig. 18 Potential energy curves of Mg_2 in krypton matrix at 20°K . 67

Fig. 19 Furnace for synthesizing MgO 76

a. Target

b. Gas mixture inlet

c. Discharge cavity

d. Knudsen cell

Fig. 20 Infrared absorption of O_3^{16} in xenon and O_3^{18} in xenon . . . 80

Fig. 21 Energy levels diagram of MgO 84

Fig. 22 Energy levels diagram of CaO 85

Fig. 23 Molecular absorption bands of Mg + O_2 (discharged) in xenon solid 89

Fig. 24 Molecular absorption bands of Mg + O_2 (discharged) in a Kr matrix 90

Fig. 25 Molecular absorption bands of Ca + O_2 in xenon matrix . 96

Fig. 26 Infrared absorption of Ca + O_2 in the xenon matrix . . . 102

Fig. 27 Infrared absorption of Ba + O_2 in the xenon matrix . . . 106

LIST OF TABLES

Table I. Absorption spectrum of matrix-isolated magnesium at 20°K. . 22

Table II. Absorption spectrum of the magnesium $^1P \leftarrow {}^1S$ transition in solid matrices. 24

Table III. Absorption features of magnesium in xenon as a function of temperature. 28

Table IV. Absorption spectrum of the calcium $^1P \leftarrow {}^1S$ transition in solid matrices. 31

Table V. Absorption features of calcium in xenon as a function of temperature. 33

Table VI. Absorption spectra of the cadmium $^1P \leftarrow {}^1S$ transition in solid matrices. 35

Table VII. Absorption spectra of the lead in solid matrices. 37

Table VIII. Absorption spectra of the barium in solid matrices. . . . 40

Table IX. Studies on gas phase homonuclear diatomic molecules of Group II. 56

Table X. Studies on matrix isolated homonuclear dimer of metal. . . 58

Table XI. Spectroscopic data of Mg_2 in gas phase. 61

Table XII. Absorption features of Mg_2 in solid matrices. 63

Table XIII. Constants of the $A^3\Sigma_u^+$ state of O_2 in the crystal and in the free molecule 72

Table XIV. Frequencies of the series of $^3\Sigma_u^+ \leftarrow {}^3\Sigma_g^-$ in the spectra of solid oxygen and gas phase 73

Table XV. Infrared absorption bands of ozone in solid matrices. . . 77

Table XVI. Infrared absorption bands of ozone in various phases and xenon matrix. 79

Table XVII. Experimental parameters for synthesizing of MgO. 87

Table XVIII. Ultraviolet absorption spectra of Mg + O (discharged) in solid matrices. 91

Table XIX. Infrared absorption of Mg + O_2 in solid matrices. 94

Table XX. Infrared absorption of Mg + O_2 (discharged) in solid matrices. 95

Table XXI. Molecular bands of Ca + O_2 in xenon matrices. 97

Table XXII. Molecular bands of Ca + O_2 in krypton matrices 98

Table XXIII. Infrared absorption of Ca + O_2 in rare gas matrices. . . 101

Table XXIV. Molecular bands of Ba + O_2 in rare gas matrices. 105

Table XXV. Infrared absorption of Ba + O_2 in rare gas matrices. . . 107

I. INTRODUCTION

Determination of the correct ground electronic state and sometimes low-lying electronic states makes a substantial difference in calculating the thermodynamic properties of a system. As an example one might consider diatomic molecule MgO where a question exists as to whether the ground state is a singlet sigma state or $^3\Pi$ state.[1-3] Because of a degeneracy factor of 6 of the $^3\Pi$ state and of greater contribution to entropy by vibration and rotation, the partition function calculated on the basis of a possible $^3\Pi$ state might be a factor of ten greater than that of a $^1\Sigma$ state. This in turn would yield an equilibrium concentration of MgO ten times higher than that calculated on the basis of a $^1\Sigma$ state with a heat of formation obtained by a second law method.

The characterization of ground and low lying electronic states of most high temperature molecules is very incomplete. Even for the diatomic molecules the ground states have been characterized only for a relatively small fraction of molecules of interest. This is mostly due to the complexity of molecular spectra. For each electronic transition there is a large number of lines corresponding to rotational and vibrational excitations. The overlapping of this multitude of lines from different electronic configurations often makes analysis extremely difficult.

When one deals with a molecule which can be produced in gaseous state at low temperature, it is relatively easy to determine the ground electronic state in an absorption experiment because at low temperature any absorption could come only from the ground electronic state. Whereas at high temperature, occurrence of an absorption band does not mean that the absorbing level is the ground electronic state since low-lying states

may be sufficiently populated to give strong absorption.

An alternative to the investigation of gaseous molecules by high-temperature spectroscopy is the use of the matrix isolation method.[4-5] In this method, gaseous molecules of interest are condensed on a cold surface along with those of rare gas. If the molecules are sufficiently isolated, interactions between molecules are negligible. Because of this it might be expected that the energy levels of the trapped molecules would be but slightly different from their gas phase values and that the spectrum observed in the matrix would be easily correlated to the gas phase spectrum. This would make the analysis of a gas phase spectrum much easier in terms of sorting out the transition due to the ground electronic state or low-lying electronic states. Molecules can also be accumulated over a long period of time from a weak source. The spectra are going to be greatly simplified because only the ground electronic state is significantly populated at temperature typically used, i.e. at liquid hydrogen temperature.

The diatomic molecules of alkaline earth oxides present an outstanding problem in determining their high temperature properties. Characterization of their ground electronic states is ambiguous. Molecular orbital correlations based on C_2 and other diatomic isoèlectrònic molecules indicate that six electronic states corresponding to the three electronic configurations $\sigma^2\sigma^2\pi^4(^1\Sigma^+)$, $\sigma^2\sigma^2\sigma\,\pi^3(^3\pi,\ ^1\pi)$ and $\sigma^2\sigma^2\sigma^2\,\pi^2(^3\Sigma^-,\ ^1\Delta,\ ^1\Sigma^+)$ could possibly lie below 20,000 cm^{-1} for all of the alkaline earth oxides.[6] To date, only some of the singlet systems of the alkaline earth oxides have been characterized and none of the predicted triplet states have been observed. The need to establish the correct ground electronic states of the alkaline earth oxides led me to working on this problem. The

approach is to synthesize the alkaline earth oxides in the rare gas matrices and study their electronic structures by means of optical spectroscopy.

The understanding of the spectra of atoms deposited in the matrices is essential because the alkaline earth oxides are synthesized through atomic reactions in the matrices. The first part of this work is devoted to understanding of the optical absorption of atomic species in rare gas matrices. The second part is a study of optical spectra of molecules synthesized in rare gas matrices.

II. EXPERIMENTAL

A. General

In recent years there has been an increasing amount of activity in studies of trapped "radicals," i.e. unstable molecular or atomic species stabilized in small concentrations in solid deposits of rare gas at low temperature. It is in part the aim of this work to develop an experimental technique for the trapping and/or synthesizing of high temperature species i.e. atomic or molecular products of vaporization of substances which have vanishingly small vapor pressure at room temperature in the rare gas matrices at low temperature. The apparatus developed allows the synthesizing of high temperature species through the diffusion processes of the atomic species trapped in the rare gas matrices controlled by the temperature of the rare gas solid. The essential parts of the apparatus include cryostat, furnace, target, gas handling system, spectrometers, light sources and photographic plates.

B. Cryostat

1. Liquid Hydrogen Dewar

Portions of this research project were performed with the metallic liquid hydrogen dewar. A photograph of the system is shown in Fig. 1. A cut-away of the liquid hydrogen insert is shown in Fig. 2. Detailed description of the cryostat has been given in B.A. King's thesis.[7]

The liquid hydrogen cryostat has few set backs. The most important one is the safety precaution needed to handle such a big quantity of liquid hydrogen. Secondly the control of the target temperature is not very flexible and it is almost impossible to do a temperature-dependent study with this system.

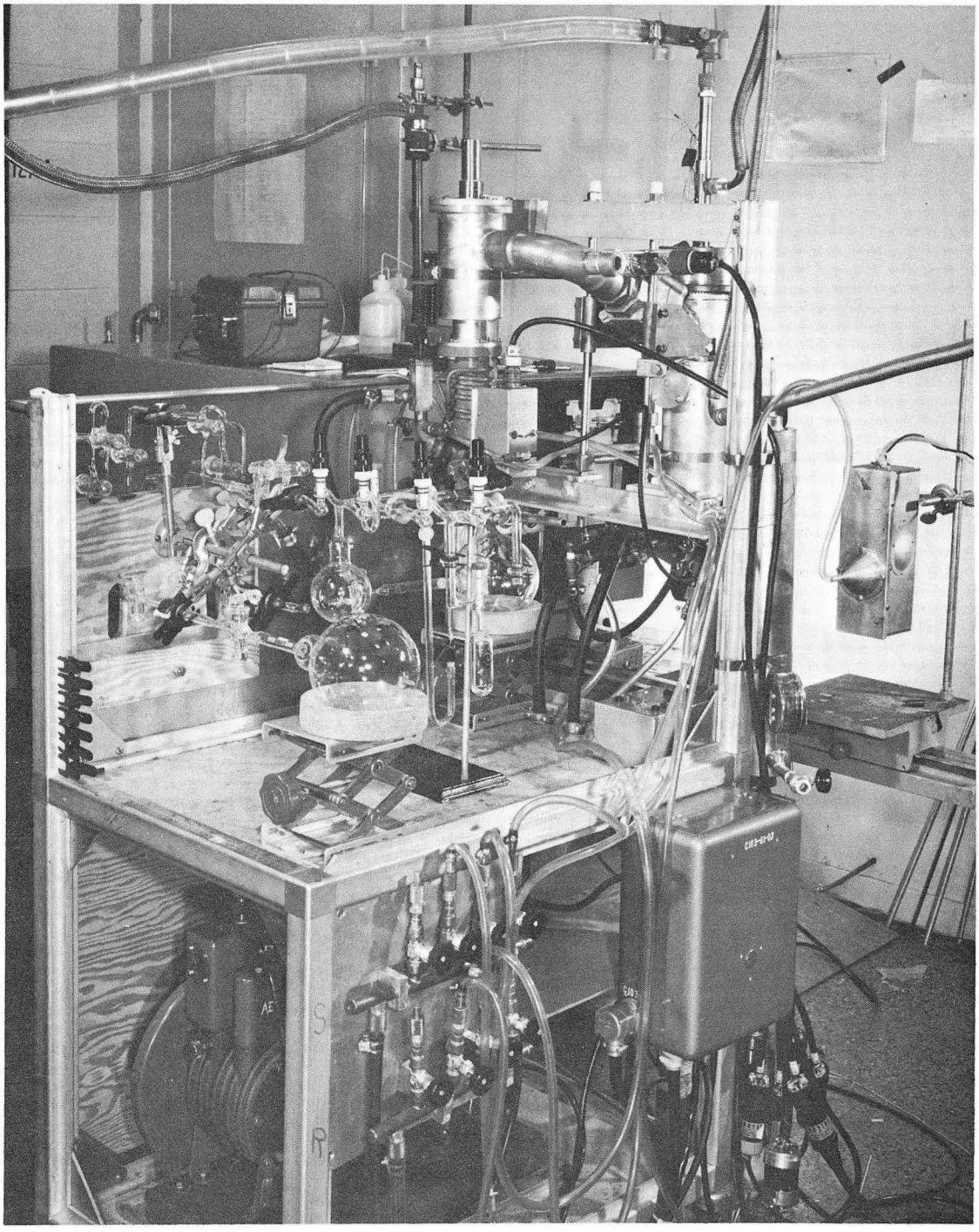

CBB 682-883

Figure 1

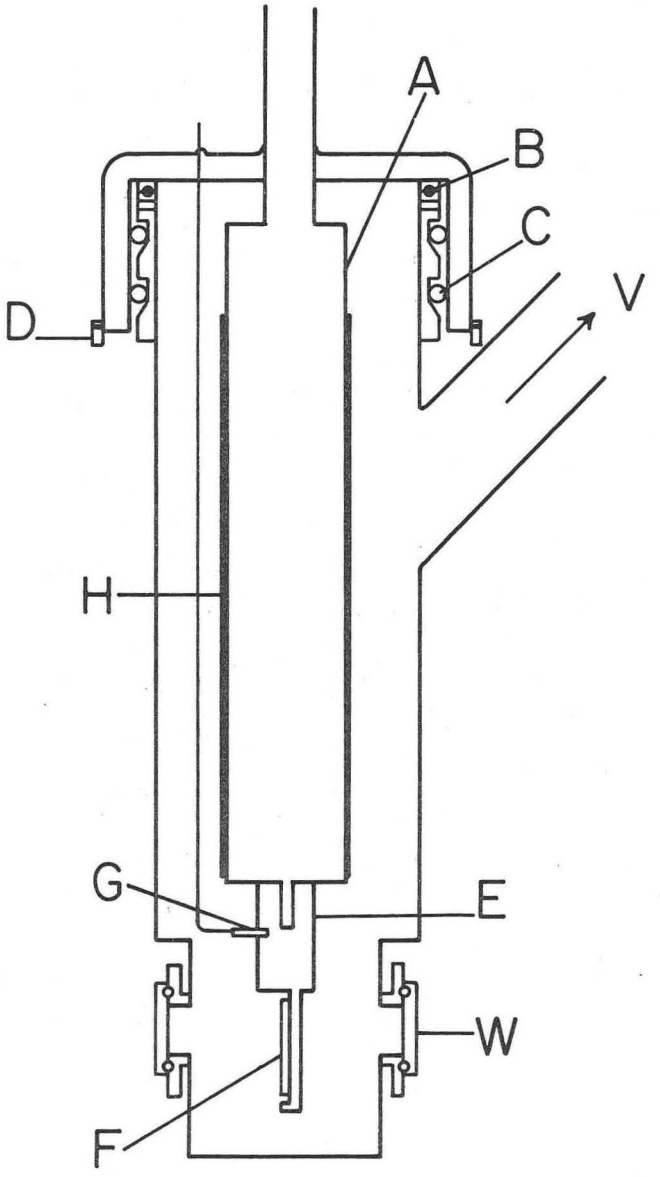

XBL 6810-6066

Figure 2

2. Cryo-tip

A commercially built cryo-tip system is used for most of the temperature dependent study. Photographs of the cryo-tip system are shown in Fig. 3 and 4. The cryo-tip model number AC-21-110, built by Air Products and Chemical Inc., is a miniature open-cycle, Joule-Thomson refrigerator. This model uses liquid nitrogen for pre-cooling and provides temperatures down to the liquid hydrogen range, using liquid nitrogen and high purity gaseous hydrogen as refrigerants. The basic components of the system are:

a. Heat exchanger (AC-2L-110)

b. Vacuum shroud WMX-1C (tailor made to fit the other equipment in the Liquid Hydrogen Room, IMRD, LRL).

c. Control panel

d. Flexible gas lines

e. Hydrogen high pressure regulators.

Detailed description of all the components are provided by Air Products and Chemicals, Incorporated.

Before Joule-Thomson cooling occurs, a gas must be cooled below its inversion temperature. A liquid nitrogen reservoir is used to cool the hydrogen below its inversion point, 160°K.

Since the exact temperature achieved at the pool of liquid gas built up in the bottom of the heat exchanger is a function of the gas pressure above the pool, the temperature at the cold tip can be controlled by adjusting the back pressure, the pressure above the pool.

The cryo-tip has a 10-W nozzling, with 1000 psi inlet and 177 gm cold tip mass and it takes about 20 minutes for the tip to cool down to liquid hydrogen temperature. After liquid gas is formed in the circuit the flow rate is reduced to conserve the gas supply as the steady state

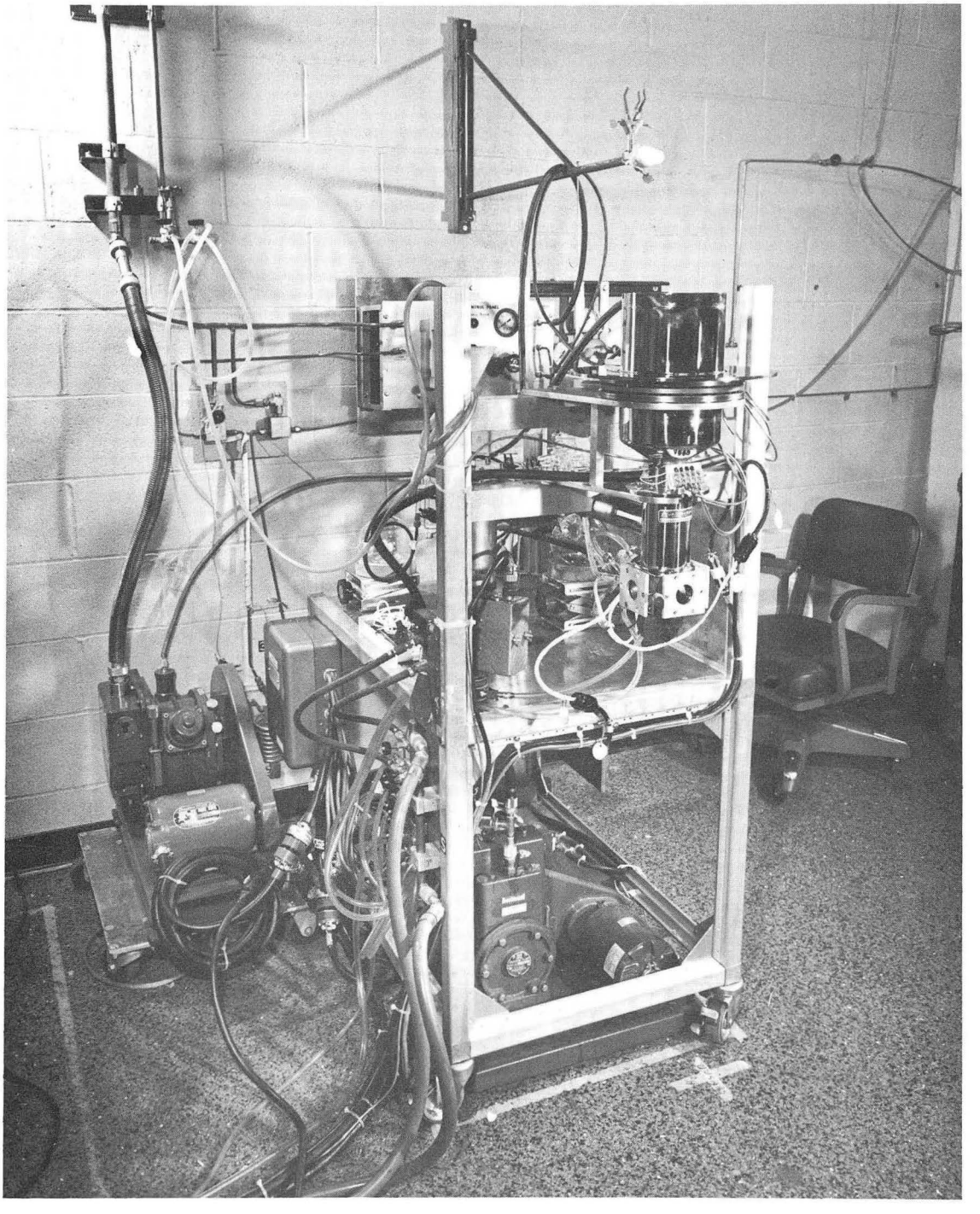

XBB 693-1632

Figure 3

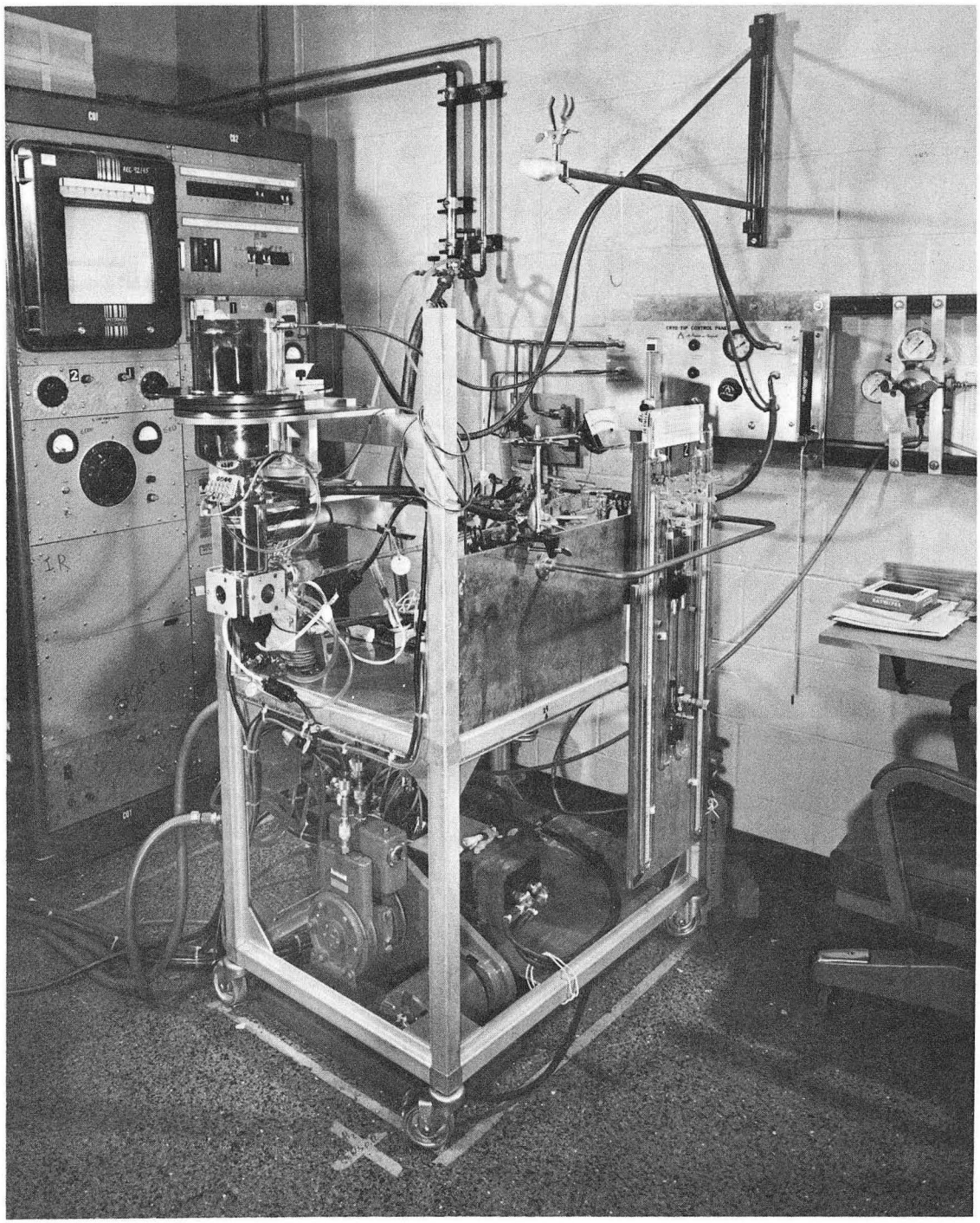

XBB 693-1633

Figure 4

refrigeration load is less than that required to cool down.

The temperature range used for experiments is from 18 K up to 70 K. Temperatures could be reproduced within ±2°.

C. Furnaces

1. Carbon Resistance Furnace

The carbon resistance furnace used for generating atomic beams was of the same design as that used by Brewer, et al.[8] and is shown in Fig. 5. This type of furnace is used to generate silver, magnesium, calcium, and lead atomic beams for atomic absorption study.

2. Stainless Steel Knudsen Cell

Due to the low temperature needed for generating the alkaline earth atomic beams, the disappearing filament optical pyrometer cannot be used to measure the furnace temperature of the carbon resistance furnace. A thermocouple is not practical either. A stainless steel Knudsen cell, illustrated in Fig. 6, was constructed for these experiments. It has an orifice with a diameter of 1 mm. The cell is placed in a quartz heater tube which is wrapped with resistance heating wire, and is lined inside with tungsten foil to prevent stray atoms from reaching the quartz.

A magnetically operated shutter is used to interrupt the atomic beam from reaching the target while outgasing the furnace.

D. Targets

1. Sapphire Target

Sapphire targets are used for all atomic absorption experiments and ultraviolet molecular absorption. A sapphire plate 3 mm thick is clamped in a copper target holder between indium gaskets to ensure proper thermal contact. The sapphire plate used in the Cryo-tip system is about half the length of the one used in the liquid hydrogen dewar system. Quartz

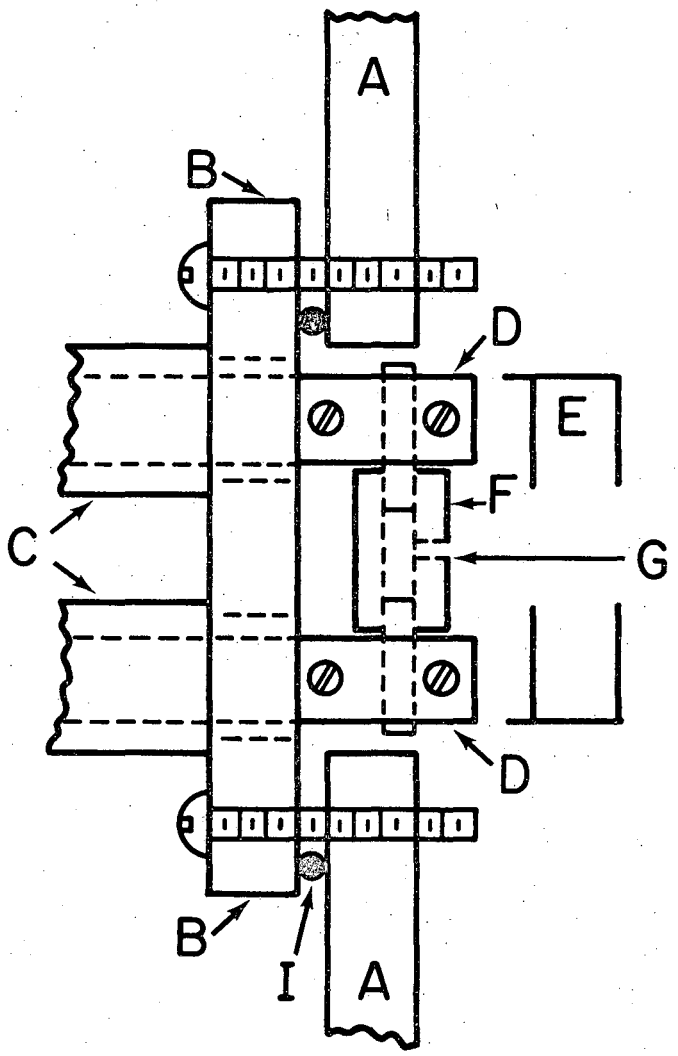

XBL 6810-6063

Figure 5

valves are used to control the rate of flow and Fisher-Porter flow meters to assure reproducible flow rates. A gas mixing system, similar to the one used by B. A. King,[7] is used to prepare different proportions of oxygen and rare gas mixtures.

High purity (>.99.99%) rare gases and oxygen (Air Product and Chemical are used without further purification. Blank tests are carried out by just depositing the rare gas along and/or oxygen mixtures. Results show that they are spectroscopically pure in infrared, visible and ultraviolet regions.

G. Spectrometers, Light Sources and Plates

The visible and ultraviolet spectra are photographed with a 0.75 meter Jarrell-Ash plane grating spectrograph, model 75-000. It has a nominal exit aperture of f/6.3. For visible region a grating blazed for 7500 A, giving a dispersion of 20 A/mm, is used. A high intensity tungsten lamp is used as a light source for this region. The spectra are recorded on Kodak 103-a-F spectroscopic plates. For an ultraviolet region a gratingblazed for 3000A giving a dispension of 5 A/mm is used. The ultraviolet continuum source is provided by a 150 watt xenon-mercury arc lamp operating at 8 amp. Spectral images are photographed on Kodak 103 -a-O spectroscopic plates.

Infrared spectra are made with a Perkin-Elmer Model 421 Spectrophotometer using Dual Grating Interchange with a spectral region covered from 4000 to 550 cm^{-1}.

H. Typical Experimental Parameters

Pressure in the vacuum system is intially $\lesssim 2\times10^{-6}$ torr and rises during deposition. Target temperature for deposition is around 20 K

or lower; for observation it is ranged from 18 K to 65 K. Rate of metal deposited is approximately 6×10^{-10} mole/sec. or less. This is obtained by measuring the weight increase of the target for a blank experiment with metal deposition only. Rate of rare gas deposited is approximately 2.0×10^{-6} mole/sec. This rate is calculated with the assumption that the condensation coefficient of rare gas is 1.0. This should be the upper limit. In reality it should be less than this rate, because the actual condensation coefficient of rare gas may be around 0.5. These rates of deposition are being used through out this work except as otherwise specified.

III. OPTICAL ABSORPTION SPECTRA OF SOME MATRIX-ISOLATED ATOMS

A. Introduction

As necessary background information for the reactions of metallic atoms with oxygen in rare gas matrices, a careful study of the behavior of atoms in rare gases is undertaken. The object of the study is to characterize the electronic spectra of atoms in solid rare gases and to determine the effects of metallic atom concentration, type of matrix, rate of deposition, and the temperature of impurity-rare gas solids upon the isolation of atoms in the matrix. A number of authors have observed complicated spectra for trapped metallic atoms which they discussed in terms of matrix perturbations. (Li,[28] Na,[10,11] K,[10,11] Rn,[10,12] Cs,[10] Mg,[13,14] Mn,[13,15] Hg,[16-20] Cu,[7] Ag,[7,8,21] Au,[7] Cd,[22,23] Zn,[22,23] In,[24]), Jahn-Teller distortions (Na,[25] Hg[25]), and interacting atomic pairs (Li,[26,27] Na,[27] Cd,[27] Hg[27]). There are some other experimental results (Pb,[29], Bi[29], Tl[29] Sc,[30] Y,[30] Fe[21]) without an interpretation. Up to now it is hard to find an adequate theory to interpret all the existing experimental data. There are also contradicting data. Apparently the conditions for laying down a doped matrix on a cold target determine to a large extent the form of the spectra obtained. Different investigators have obtained different results for the same element in the same matrix, e.g. Duley's[19] Hg in Xe had a doublet for $^1P \leftarrow {}^1S$ resonance transition while Brabson's[9] Hg in Xe had a triplet for the same transition. As far as can be determined from the published data, the obvious reason for different results is that Duley used a very fast rate of deposition and high concentrations of Hg. The fast rate of deposition does not give atoms much time to order themselves and this effect alone is almost good enough to broaden the spectral lines and cause them to overlap each other. Also, as will be shown later the

splittings of spectral lines are very much dependent on the target temperature.

In King's work, he showed that the concentration of metal atoms does not affect the apparent position of the absorption features.

The present work tries to study the sample temperature dependence and mixed impurities effects on multiplet splittings and apparent positions of spectral lines. An interpretation will be provided for the existing experimental data.

Because of the needed information for synthesizing alkaline earth oxides in the latter part of this research project, some of the alkaline earth atoms, i.e. Mg, Ba, Ca are chosen for this study. Cd and Pb are studied separately for particular reasons which will be stated in appropriate sections.

Figure 7 shows some of the atomic transitions in gas phase which were studied in matrices.

B. General Discussion

1. Magnesium

The magnesium atom has a ground state electron configuration $3s^2$ which yields a $^1S_0$ state. The lowest allowed atomic transition lies at 35051 cm^{-1} [31] to a ^1P state with an electron configuration 3s 3p. It will be seen that the separations between the observed triplet components in the free atom spectra are of a magnitude smaller than the observed line widths in the matrix spectra. It is therefore not to be expected that three components will be resolved in the matrix.

The sublimed magnesium metal was provided by Dow Chemical with a purity of 99.9948%. A spectroscopic analysis of the sample was done by Dr. John Conway. Both types of furnace have been used. The spectral region investigated covers from 2200A to 6000A. Most of the preliminary experi-

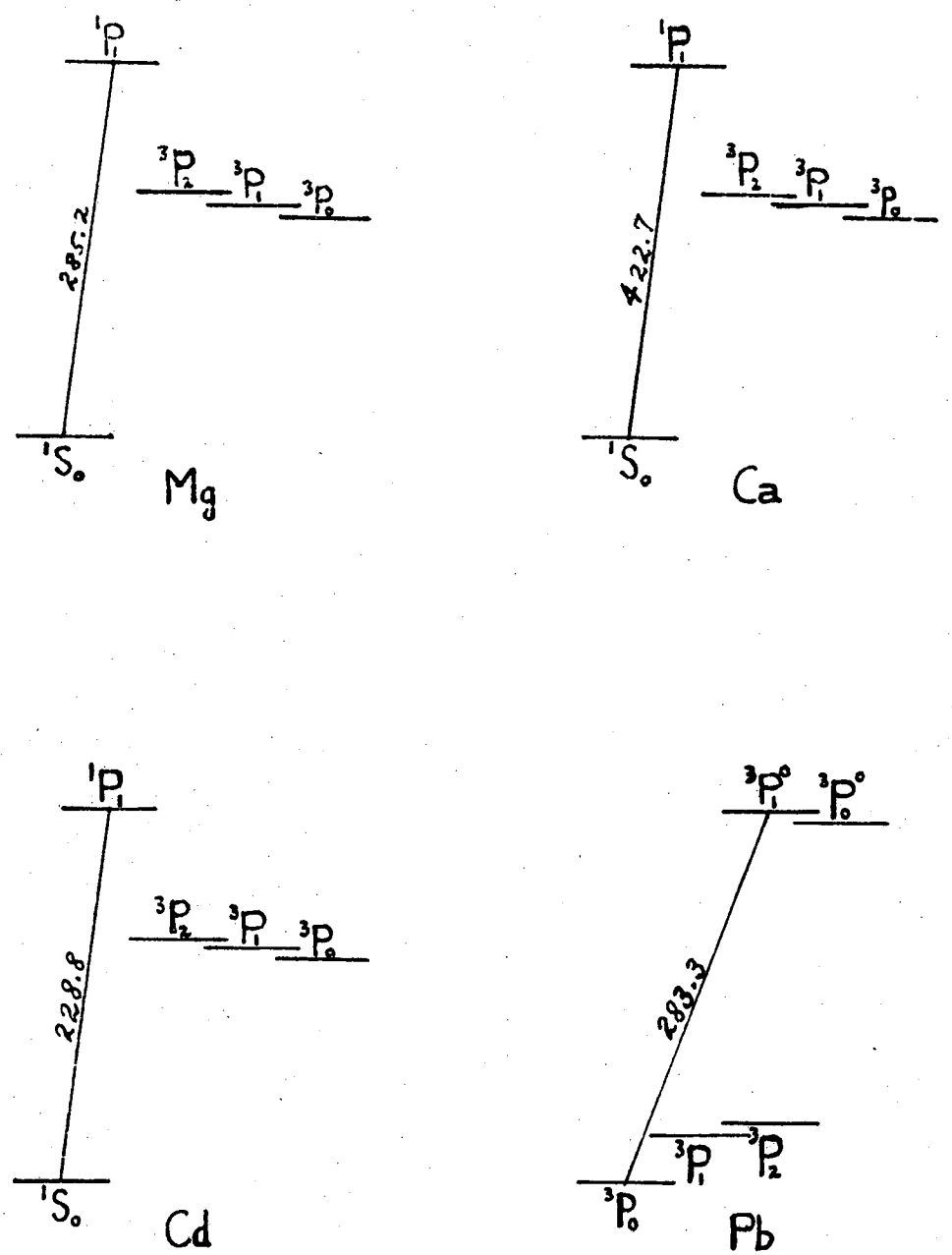

XBL 699-5678

Figure 7

mental results were obtained from a liquid hydrogen dewar system. The detailed investigation of effects upon spectra were obtained with the cryo-tip system. Argon, krypton, xenon and SF_6 have been used as matrices.

2. Calcium

The calcium atom has the same ground state ^1S as a magnesium atom and its electron configuration is $4s^2$. The lowest energy of an allowed atomic transition lies at 23652.3 cm^{-1} to ^1P state. Since it is a $^1P \leftarrow {}^1S$ transition it should have the same absorption feature as magnesium atom.

The calcium in granules was provided by Gallard Schlesinger, Chemical Mfg. Corp., Carle Place, N. Y. The purity was 99.9%. The sample is heated at 550°C for many hours and at 650°C for half an hour before deposition. The cell is around 600°C when deposition takes place. The spectral analysis, performed by Dr. John Conway, shows that the sample is very clean with the exception of Mg and Sr. There is about 0.3% by weight of Mg and 0.1% Sr. Experiments took place in both a liquid hydrogen dewar and Cryo-tip system both types of furnaces were used. Only krypton and xenon were used as matrices. The spectral region investigated was between 2200A to 6000A.

3. Cadmium

The cadmium is a IIB element in the periodic table. It has an electron configuration of (Kr) $4d^{10}5s^2$. Its lowest allowed electron transition is $^1P \leftarrow {}^1S$, with a transition energy of 43692.5 cm^{-1}. The isolation of Cd in rare gases has been reported by many other investigators. It was done again under an accidental condition.. The Cd was present because hard soldering material which has a high Cd content has been used in soldering the thermocouple to the Knudsen cell in the early period of this research. The success of identification of Cd in matrices shows that the matrix

isolation method might be used as a means for identifying small amounts of impurities in a sample.

4. Lead

Lead has a ground electronic state of ^3P with an electronic configuration of (Xe) $4f^{14}5d^{10}6s^2 6p^2$. The strongest transition from the ground $^3P_0$ state is $6p7s\ ^3P_1 \leftarrow 6p^2\ ^3P_0$ which occurs at 2833A (35287 cm^{-1}) in the gas phase. The total angular momentum of a ^3P state is 2. So the ground state has substates $^3P_0$, $^3P_1$ and $^3P_2$. From the gas phase spectrum we know that $\Delta E(E_{^3P_1} - E_{^3P_0}) = 7819.35\ cm^{-1}$ and $\Delta E(E_{^3P_2} - E_{^3P_0}) = 10650.47\ cm^{-1}$. Because of these large difference between the $^3P_0$ and the other two states we could expect that most Pb atoms trapped in rare gas matrices at 20K to be in the $^3P_0$ state. The $62p\ ^3P \leftarrow 6p^2\ ^3P_0$ transition involves the excitation of an outer electron from a 6p to a 7s orbital and involves a large change in overlap with the matrix atomic wave functions. The transition is expected to be shifted to higher energies and should show a relatively large shift.

The metallic lead was provided by the American Smelting and Refining Co. with purity of 99.999+% with chemical spectral analysis showing maximum impurity for Mg < 1 ppm, Fe < 1 ppm, Cu < 1 ppm. The lead atomic beam was generated from carbon resistance furnace. Kr and Xe were used as matrices. The liquid hydrogen dewar system was used. Only very dilute mixtures of Pb in rare gas were used.

5. Barium

Barium has the same type of the lowest energy transition as magnesium and calcium. Barger and Broida[32] studied barium doped argon solid. The spectrum showed fifteen absorption lines which were dependent on matrix and observation conditions. The strong overall features of the spectrum

were assigned to transitions involving the $^1P_0$ and $^3p_1$ state, the fine structures were due to removal of orbital degeneracy, site effects and impurities. The $^1P \leftarrow {}^1S$ transition appears to 5535.5A in gas phase.

Barium metal was provided by Research Organic/Inorganic Chemical Corp. with a purity of $99.5^+\%$. A stainless steel Knudsen cell was used. A tungsten foil is inserted between the Knudsen cell and the quartz tube to prevent the attack of the quartz by barium.

6. Silver

See Appendix A.

C. Results

1. Magnesium

The absorption spectra of magnesium in argon, krypton and xenon were photographed in the region between 6000A and 2200A. For a very dilute metal atom in krypton and slow deposition a very distinct triplet is observed at 2856A. The same triplet appears at 2900A when xenon is used. No absorption band is observed in argon. It seems that there are problems for isolating metallic atoms in argon at 20°K. Other investigators also had problems in isolating metallic atoms in argon matrix unless they used a lower target temperature, i.e. liquid helium. The reason for this difficulty in isolating some of the atoms at liquid hydrogen temperature is not yet understood. It may partially be due to high mobility of the argon atoms on the target surface which in turn causes the nucleation of the metallic atoms. The rate of the deposition of rare gas on the target plays a very important role in the appearance of the spectral feature.

The experimental results of magnesium atoms isolated in rare gas matrices are tabulated in Table I. The lowest temperature

Table I. Absorption spectra of matrix-isolated Mg at 20 K

Matrix	A	cm^{-1}	splitting (cm^{-1})	transition
Free atom	2852.12	35061.6		$^1P \leftarrow {}^1S$
Kr	2852	35060		
	2830	35333	273	
	2816	35512	179	
Xe	2952	33874		
	2934	34088	214	
	2915	34300	212	

used in isolation was 18 K. Schnepp[13] isolated magnesium in argon, krypton and xenon at 4.2 K. His results are tabulated in Table II for comparison. The spectra of magnesium obtained in this work are shown in Fig. 8. A photograph showing temperature dependence of the spectra appears in Fig. 9. A graph showing temperature shift is shown in Fig. 10. In this particular experiment the temperature ranged from 20 K to 55 K and then recooled back to 20 K. In many other experiments the triplet absorption disappeared when the target was warmed up to 65 K, and at the same time the pressure of the vacuum system increased. This may indicate the loss of the matrix because no absorption spectrum appeared upon recooling. Table III shows the dependence of wavelength upon temperature. Also the transparency of matrix at short was length region dropped as the matrix warmed to 50 K or higher. Recooling did not show any reversibility of transparency in short wavelength region.

With high metallic concentrations (greater than 1 at%) there are bands in the ultraviolet region that might be due to dimers while the triplet absorption becomes a broad band. It does not resolve into a triplet upon annealing or warm up. This is quite different in comparison with the broad band obtained from fast deposition because the latter resolves into triplet upon annealing. This may mean that the former is the absorption of magnesium dimer because Mg_2 molecule in gas phase has a spectrum around the Mg resonance absorption region.[33] The spectrum of Mg_2 will be discussed in greater detail in the next section. Experiments were carried out with the concentration of magnesium ranging from M/R = 100 to 1500. Here M stands for matrix gas and R stands for trapped species.

For warmup experiments in Xe the shortwave length component of the triplet shifts to the blue with a gradient of 2 cm^{-1}/K. The center one shifts to a longer wavelength with a gradient of 1 cm^{-1}/K and the

Table II. Absorption spectrum of Mg $^1P \leftarrow {}^1S$ transition in solid matrices.

	At 4.2°K*		At 20°K†	
	A	cm^{-1}	A	cm^{-1}
	2955	33840	2952	33874
Xe	2937	34050	2934	34088
	2920	34240	2915	34300

* O. Schnepp, J. Phys. Chem. Solids, 17, 188 (1961).

† This work.

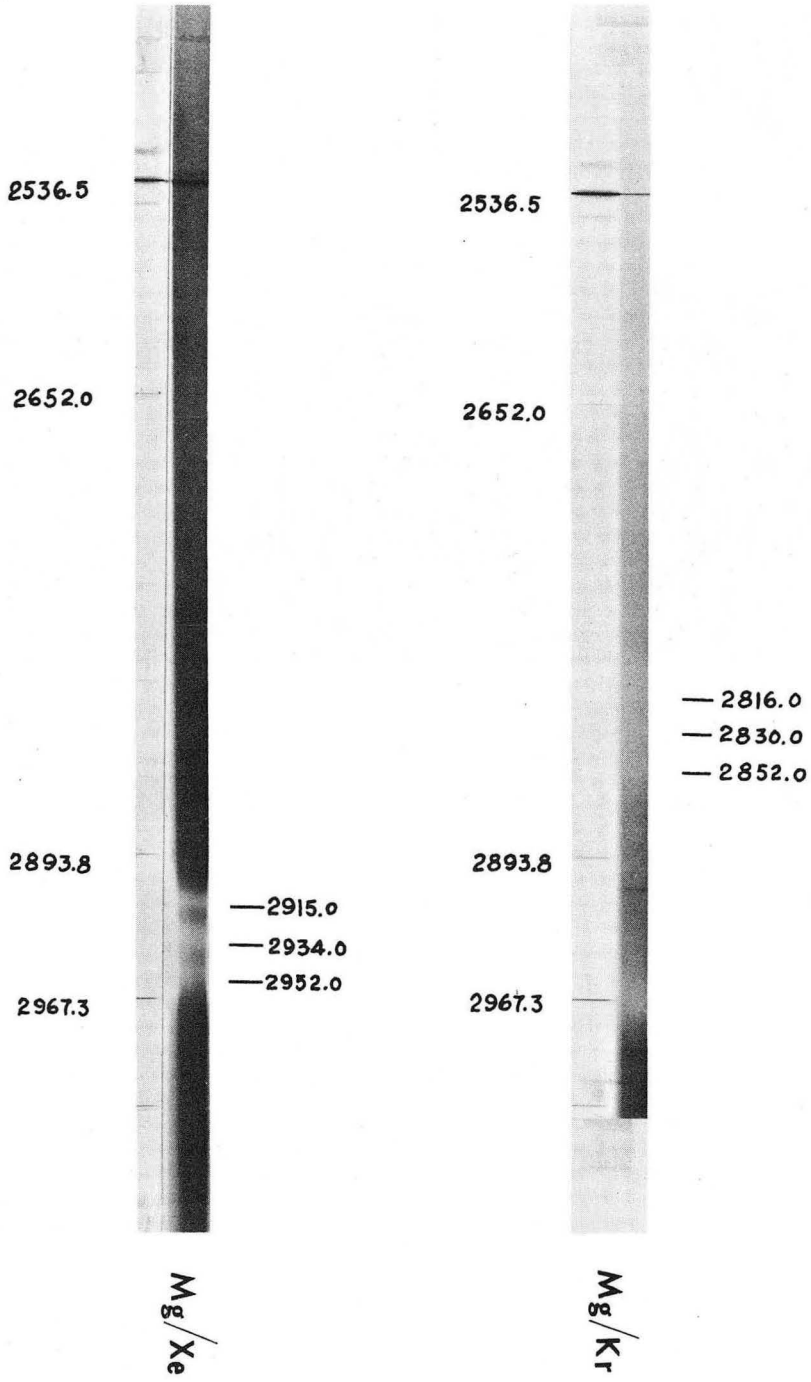

XBB 699-6107

Figure 8

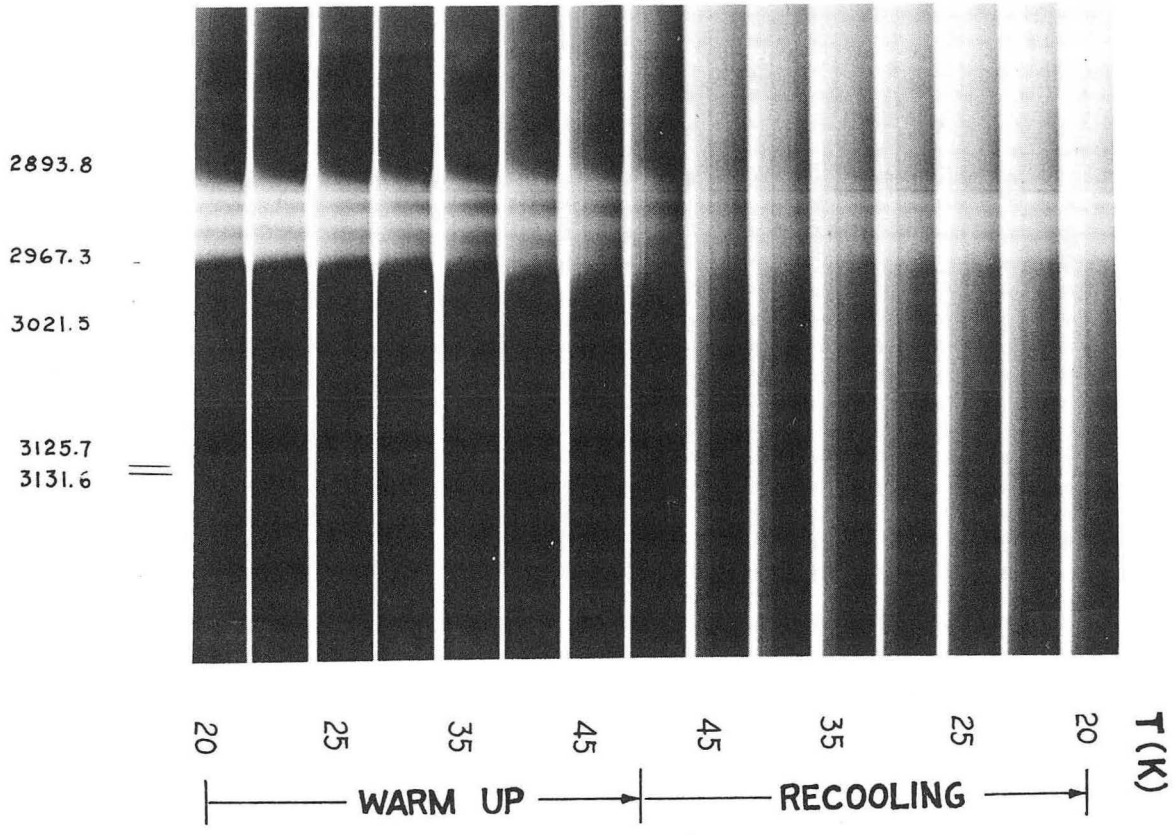

XBB 699-6108

Figure 9

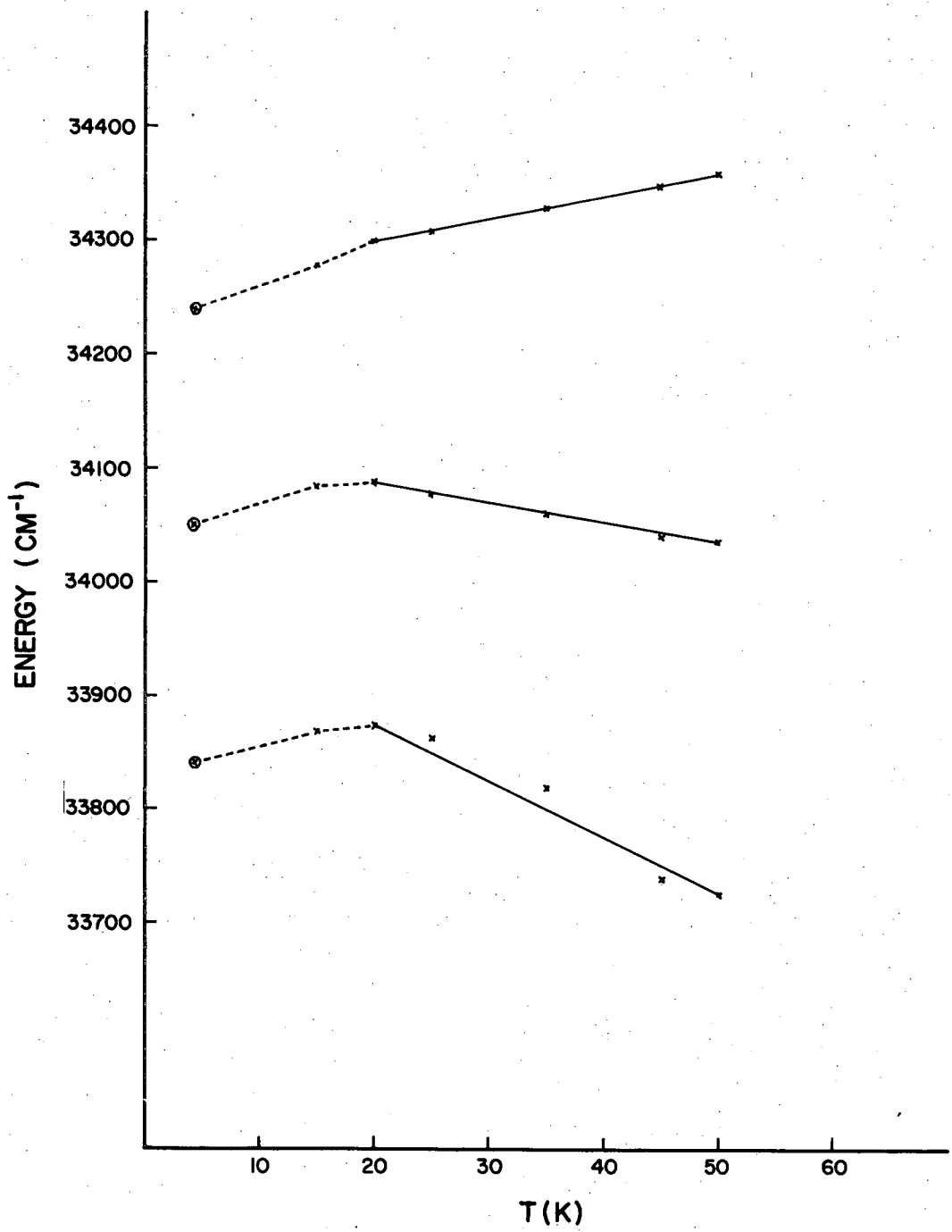

XBL 699-5676

Figure 10

Table III. Absorption features of Mg in xenon as a function of temperature

Temperature (°K)	Frequency (cm^{-1})		
20	34300	34088	33874
25	34309	34080	33864
35	34330	34060	33819
45	34350	34040	33737
50	34362	34037	33725

longer wavelength components shifts to the red with a gradient of 1.6 cm^{-1}/K.

For Mg in Kr it is very difficult to isolate Mg in Kr at 20 K or higher but it could easily be isolated at 18°K and a triplet is observed in the region of 2830 A. This triplet shows approximately the same temperature dependence shift as in Xe. In Xe the triplet stays until the target temperature exceeds 65 K but in Kr the triplet disappears as soon as the target temperature goes above 45 K.

The triplet observed in Xe at 20 K is shifted to the red compared with the gas phase $^1P \leftarrow {}^1S$ transition, while in Kr it is shifted to the blue.

The splittings between the triplet in Xe at 20 K are approximately 213 to 300 cm^{-1}, while in Kr at the same temperature the spacing between the shorter wavelength component and the center one is approximately 280 cm^{-1} and the spacing between the center one and the longer wavelength one is only 180 cm^{-1}.

No spectrum is observed for magnesium trapped in SF_6 matrix with $M/R \approx 500$.

2. <u>Calcium</u>

The calcium atoms were isolated in Kr and Xe matrices. Up to now no experimental results have been reported in any literature. This should be the first time that calcium atoms are trapped in rare gas matrices. In the gas phase the transition from the ^1S ground state to the lowest allowed state ^1P is at 23652.3 cm^{-1}. In Kr at 18 K a triplet absorption appears at 23884 cm^{-1} (or 4187 A). This is shifted to the blue for about 230 cm^{-1} from the gas phase transition. In Xe at 18 K the triplet appeared 23051 cm^{-1} (or 4338 A). This shifted 600 cm^{-1} to the red compared to the gas phase value, which is large compared to the shift in Kr.

By passing the Kr through a microwave discharge cavity, a second triplet appears to the red of the one observed without discharge. This new triplet has a central component at 20650 cm^{-1} (or 4842A). The spacings of the triplet splitting are 176 and 174 cm^{-1}. This might be due to multiple site because it is not easy to relate this transition to any other gas phase transition.

The warmup of calcium in Xe matrix shows that the short wavelength component has a shift of 2 cm^{-1}/K to the blue, the central one has a shift of 1.4 cm^{-1}/K to the red and the long wavelength one shifts to the red about 2 cm^{-1}/K. This phenomenon is very similar to the one displayed by a magnesium atom in a xenon matrix.

The M/R used for isolating calcium range from 200 to 1000.

The experimental results of calcium atoms isolated in rare gas matrices are tabulated in Table IV. A typical temperature dependence of the calcium spectrum in Xe is shown in Fig. 11 and the wavelength vs temperature is tabulated in Table V.

3. Cadmium

The isolation of cadmium atom in rare gas matrices has been reported.[22,23,27,34] Duley's results are based on a much higher metallic concentration and he observed diffuse bands. The triplet he observed is approximately 200 A wide at 4.2 K. Roncin's results were probably for high dilution and the total band was approximately 40 A wide at 4.2 K. Merrithew's result showed a partially resolved triplet at 20 K and has a width comparable to Duley's.

Since cadmium is present as a small percentage of impurity the concentration of admium in rare gas solid is very dilute. A distinct

Table IV. Absorption spectra of the calcium $^1P \leftarrow {}^1S$ transition in solid matrices at 20°K

Matrix	A	cm^{-1}	splitting (cm^{-1})	transition $^1P \leftarrow {}^1S$
Free atom	4226.73	23652.3		
	4212	23743		
Kr	4187	23884	141	
	4156	24060	176	
	4377	22840		
Xe	4337	23052	212	
	4311	23192	140	

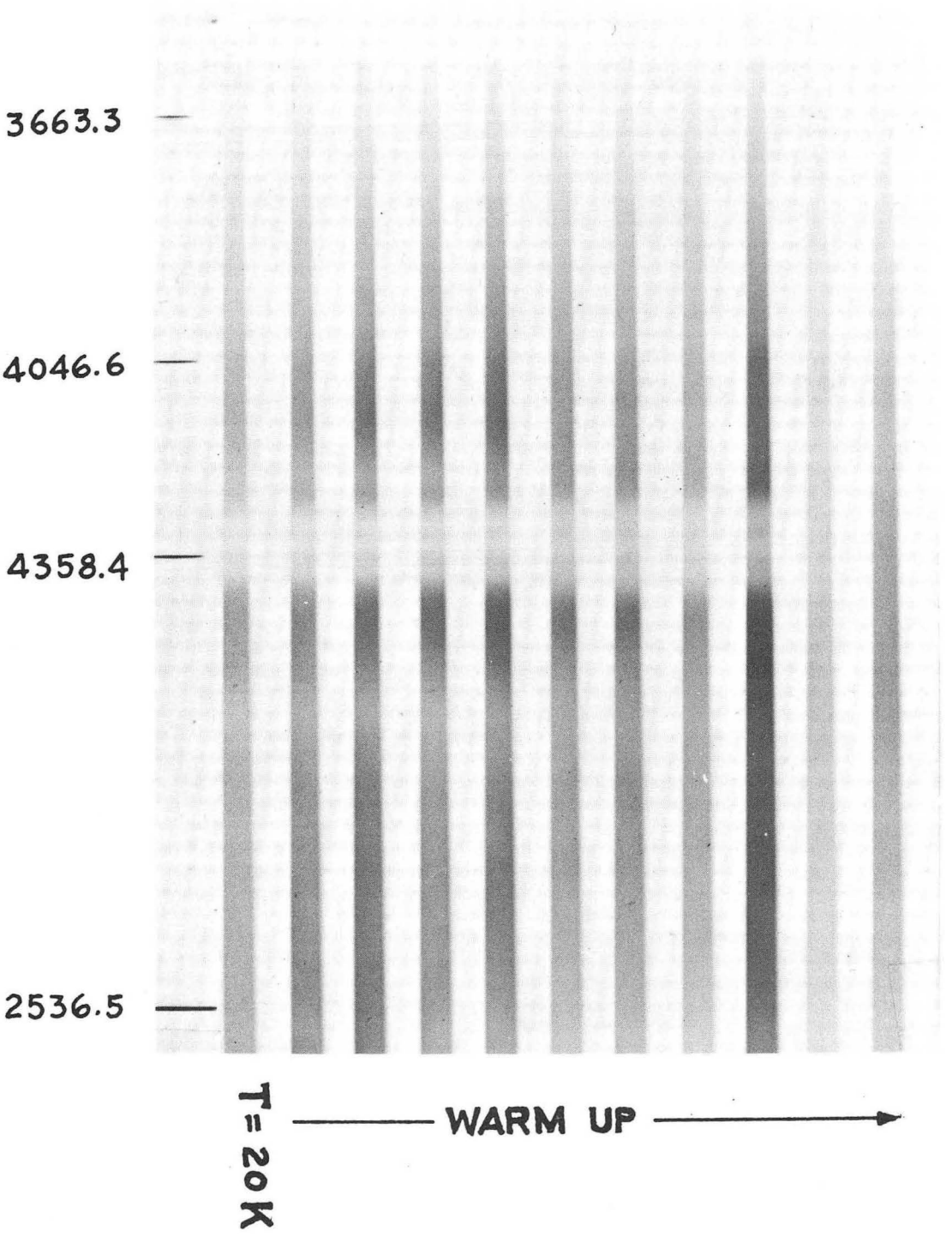

XBB 699-6114

Figure 11

Table V. Absorption features of calcium in xenon as a function of temperature.

Temperature (°K)	Frequency (cm^{-1})		
18	23205	23051	22852
20	23213	23072	22833
30	23233	23060	22814
40	23246	23044	22795

triplet appears in the region of 2200 A. Experimental results are shown in Table VI. The results of other investigators are given for comparison. The observed spectrum is shown in Fig. 12.

The half width of the Cd triplet absorption in Xe at 20°K is approximately 60 A. The warmup experiment shows that the short wavelength component shift to the blue while the other two long wavelength components to the red. Roncin's results at 4.2 K and 20 K indicate all three components of the Cd triplet shift to the blue. This may suggest that the site where the Cd atom is isolated at 4.2 K is not a stable one or the neighboring atoms of the Cd atom are not in the best ordered form.

The spacings among triplets are 200 and 400 cm^{-1} between the red component and the center and between the center and the blue component, respectively.

4. Lead

Lead in rare gas matrices has been studied by Duley.[29] The allowed transition with the lowest energy is a ^3P - ^3P transition. In this work the experiments were carried out with high dilution in krypton and xenon at 20 K. No triplet was observed but there was a band at 2600 A and another band at shorter wavelengths. The experimental results are shown in Table VII together with Duley's results. The spectra are shown in Fig. 13.

In gas phase the strongest allowed transition from the ground $^3P_0$ state of Pb is

$$(6p7s)\,^3P_1 \leftarrow {}^3P_0(6p^2)$$

which occurs at 2833 A. In the Xe matrix the strongest band is at 2649 A and in the Kr matrix it is at 2613 A. These are the values closest to the gas phase values. If we could identify them with 2833 A in gas phase then the shift would be quite large. The shifts are 2979 cm^{-1} in Kr and 2467 cm^{-1} in Xe. By comparison with Mg, Ca or Cd the shift

Table VI. Absorption spectra of the cadmium $^1P \leftarrow {}^1S$ transition in xenon matrix

Temperature (°K)	A	cm^{-1}	Splitting (cm^{-1})	Investigator
	2288.02	43692.5		Free atom
20	2369	42200	200	This work
	2358	42400	410	
	2335	42810		
4.2	2367	42250	190	Roncin
	2353	42440	260	
	2342	42700		
20	2367	42250	250	Roncin
	2353	42500	220	
	2340	42720		
10±5	2369	42210	290	Duley
	2353	42500	360	
	2333	42860		
15	2364	42300	180	Shirk and Bass
	2354	42480	270	
	2339	42750		
4.5	2357	42420	220	Merrithew, Marusak and Blount
	2344	42640	230	
	2332	42870		

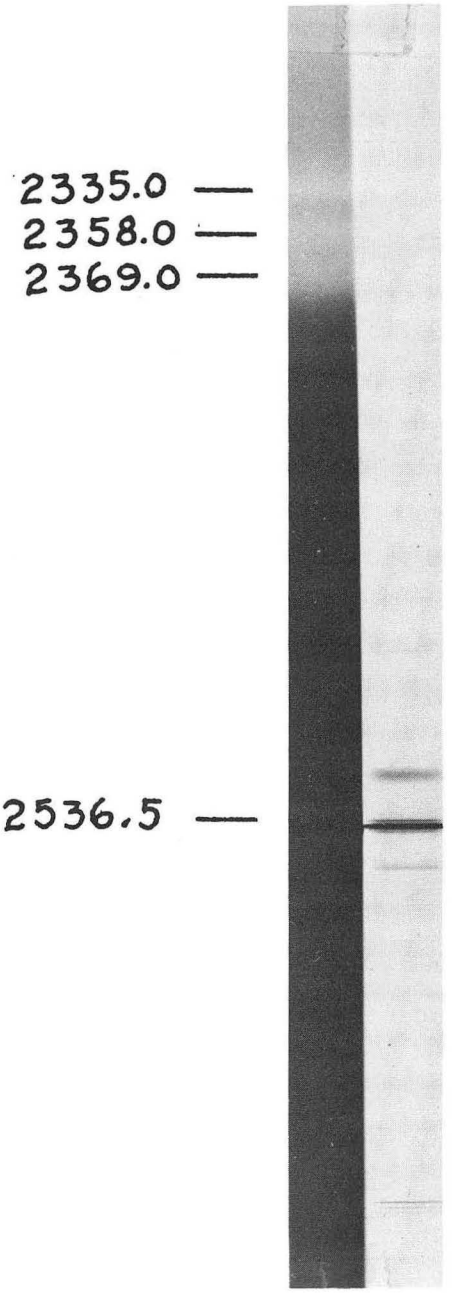

XBB 699-6112

Figure 12

Table VII. Absorption spectra of the lead in solid matrices

Temp.	Matrix	A	cm^{-1}	Transition	Investigator
	Free atom	2833	35287	$^3P_1^\circ \leftarrow {}^3P_0$	
20	Kr	2613	38266	$^3P_1^\circ \leftarrow {}^3P_0$	This work
		2397	41726	?	
	Xe	2647	37754	$^3P_1^\circ \leftarrow {}^3P_0$	
		2544	39304	?	
4.2	Kr	2617	38210	$^3P_1^\circ \leftarrow {}^3P_0$	Duley
		2453	40770	$^3D_2^\circ \leftarrow {}^3P_1$ (?)	
	Xe	2647	37780	$^3P_1^\circ \leftarrow {}^3P_0$	
		2553	39170	$^3D_2 \leftarrow {}^3P_1$ (?)	

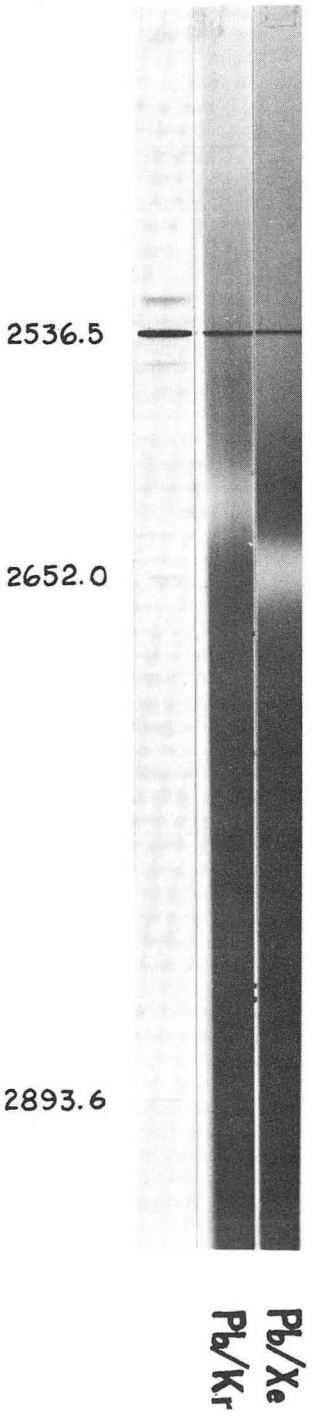

XBB 699-6111

Figure 13

from the gas phase is quite large. If we try to relate this transition in matrices to $^3D_2 \leftarrow {}^3P_1$ we would get very little shift from the gas phase value. This seems very improbable because initially we have to populate the $^3P_1$ state which is about 7819 cm^{-1} higher in energy than $^3P_0$. With a target temperature at 20 K a Boltzmann distribution would give almost no population for a $^3P_1$ state.

It is very difficult to connect any other absorption features to their gas phase counterpart. It is also hard to relate them to dimer formation. Pb_2 is a very stable molecule. It has a gas phase molecular band in the 5100 A region. With higher lead pressures a molecular band is observed by Chang in both Xe and Kr matrices.[35]

More experimental data are needed in order to clarify the assignment of transitions of Pb atom in matrices.

5. Barium

The experimental results of barium isolated in rare gases are not conclusive enough for identification and more experiments are needed to be done in order to confirm the assignment of transitions. A broad band is observed in the region around 5700 A but not resolvable. In gas phase the $^1P \leftarrow {}^1S$ transition, the lowest allowed transition, takes place at 5535.5 A (18065.8 cm^{-1}). The results are shown in Table VIII.

6. Silver

See Appendix A.

D. Discussion

As mentioned in Section IIIA there are difficulties in interpreting the spectra of isolated atoms in matrices. This is not only because of the problem of standardizing the conditions for isolating atoms but also because of the limited knowledge about the interaction between isolated

Table VIII. Absorption spectra of the barium in solid matrices

Matrix	A	cm^{-1}	Splitting (cm^{-1})	Transition
Free atom	5535.5	18067		$^1P \leftarrow {}^1S$
	4770	20964		
Kr	4853	20603	361	?
	4938	20249	357	

atoms and their neighbors or the field they are in.

From the results obtained in Section IIIB we will now try to explain the phenomena by using some existing concepts such as, crystal field theory, size effect, polarizability, or phonon-solute interaction. Many other concepts can be used to interpret the results. The relationship between F-center and metal doped matrices has been discussed by Brewer, et al.[8] and King's[7] thesis. The relationship between high pressure atomic absorption and matrix isolated atoms has been presented by Roncin.[36] Here we will only discuss the matrix shift, splitting, temperature effect and mixed metal effects. The explanation will not only be based on the results obtained by this work but also on the data that have been published by various authors around the world. A literature survey of the atoms trapped in matrices is given by B. Meyer.[132]

1. Matrix shift

a. Size effect. In most of the spectroscopic investigations of the matrix isolated atoms to date the center of gravity of the dominant group of absorption lines shifts from the center of gravity of the corresponding free-atom transition. The magnitude of shift ranges from a few cm^{-1} to a few hundred wave numbers, but for some transitions it may go up to a few thousand wave numbers. The magnitude of the shift seems to depend on the electronic transition. Matrix shifts are probably determined by two opposing types of interaction. On excitation, the electronic charge cloud surrounding the trapped atom tends to expand and therefore may cause stronger bonding interaction with the matrix atoms, thus tending to lower the energy. On the other hand, it has recently been shown[133] that the surrounding "solvent" tends to restrict the electron cloud of the "solute" and thus raise its energy by a restricting box type effect. For example, in lead the matrix shift in Kr is about 2979 cm^{-1}

$6p7s\ ^3P_1 \leftarrow 6p^2\ ^3P_0$. This is quite a large blue shift but it is possible because an electron is forced to jump from one principal shell to another. In a solid it will take more energy to overcome the repulsive electron clouds from the neighboring atoms. While for Mg in Kr we have

$$3s3p\ ^1P \leftarrow 3s^2\ ^1S.$$

This transition takes place in the same principal shell but to different orbitals with a relatively small energy difference. We would expect a small shift only. Testing the average energy of the triplets, the shift of Mg $^1P \leftarrow {}^1S$ transition in Kr is only 240 cm^{-1} to the blue. For calcium in Kr the blue shift is about 243 cm^{-1} for the $4s4p\ ^1P \leftarrow 4s^2\ ^1S$ transition.

b. Polarizability. The effect of polarizability upon the spectral shift will be discussed qualitatively only. More information about the structure of doped matrix is needed for quantitative calculation.

It has been observed in the study of matrix-isolated atoms that blue shifts decrease in the order of argon, krypton, xenon. This is also the order of increasing polarizability and lattice parameter.

In order to relate the polarizability with the observed matrix shift it is necessary to take a closer look at the crystal structure of the rare gases.

A rare gas atom is spherically symmetric in free space, but not so in a crystal[37-39] because of the compression by surrounding atoms. An atom in a closepacked lattice has twelve nearest neighbors and has six "windows" facing the second neighbors. At these windows the electron density should be different and hence the atom has an electrical multipole. It is easily seen that in a hexagonal closepacked lattice,[40] this multipole is an octapole.[41] The octapole interaction between the nearest neighbors is repulsive.[42]

When this occurs, the molecule has an electric moment and will show a polarization not only by distortion, but also by orientation. We therefore may expect that the amount of orientation created by the field increases as the disturbance due to temperature motion decreases.

Since the lattice parameter of the rare gas is temperature dependent we should observe a shift in matrix as we change the temperature of the matrix. The experimental results show a red shift of the center of gravity of the absorption band. This is what would be expected because as the temperature is increased the lattice parameter as shown by Losee and Limmons[43] increased as temperature increases.

c. Multiple sites . In a crystal different lattice sites have different interactions toward the trapped atoms. Atoms may be trapped in a more neutral or repulsive site.[11] A neutral site is characterized by similar matrix shifts in both electronic states involved in the transitions, leading to an almost unshifted absorption. Such a site could consist of a loose cluster of rare-gas atoms formed by rapid cooling of the condensing gas at low temperature. The repulsive site could be due to a denser, partially annealed crystal formed through reaggrangement of the loose clusters.

The atom may be trapped in a low symmetry site, i.e. the trapped atoms are perturbed by an immediate environment for which only two-fold rotational symmetry axes exist. Or the atom may be trapped in high symmetry site. The low symmetry site is probably an impurity site in which the lattice is strongly distorted in the neighborhood of the trapped atom. The higher symmetry site may be a site with most of the nearest neighbor being present. It seems reasonable to assume that the

energy of excitation for a higher symmetry site is considerably higher than that of a site of lower symmetry. It is thus possible to account for the observed differences in shift and stability of the different sites on this basis. Annealing processes have been reported to account for the disappearance of some of the unstable sites. In this case the crystallites would grow in size as the low temperature deposit warms up. Most of the unstable sites would be converted into stable sites or would be evaporated. If the former process is of major importance, the intensity of the triplet absorption feature should increase in intensity as the unstable band disappears. (This has not been done with great detail so it is hard to make any definite conclusions from the observed disappearance of bands.) Because of the broadness of the bands observed, it is very difficult to observe the change in intensity of absorption while some of the bands, which may have been caused by the unstable site, disappears.

There are indications of existence of multiple sites, e.g. ESR work of noble metal by Zhitnikov,[14] optical absorption and ESR work of Rb by Kupferman and Pipkin,[12] and optical absorption of alkaline metal by Meyer.[11]

2. Splitting

a. Crystal field splitting. Among the many important problems which remain unsolved is the structure of the deposited solid which determines the crystal field acting on the atoms. The solid affects the energy levels of trapped atoms in a way which is formally equivalent to the Stark effect produced by crystal fields encountered in the study of the optical and magnetic properties of compounds of the transition elements.[45-48] The major difference in the metallic atom rare gas system is the fact that the forces acting on the metallic atoms probably arise from the polarizability of the rare gases, and are therefore much weaker and have much

shorter range than do the forces occurring in crystals containing ions and electric dipoles. We expect, therefore, any splittings of levels of metallic atoms by the solid rare gas to be much smaller than the splittings found in ionic systems, and the levels and hence the spectral lines of metallic atoms to be much sharper in the rare gas than in the ionic system. These splittings are, however, large compared to the Stark splittings produced by laboratory.

The magnitude of splitting of a state and the number of resulting levels depends on the details of the crystal field and of the multiplet seperation of the free atom. Due to the short range of forces, the field acting on atoms depends mainly on the arrangement of molecules nearest to the atoms. This arrangement is not yet known. In fact it is not certain whether the deposited material has the crystal structure of rare gas corresponding to the depositing temperature and contains the atoms as lattice defects, or whether the material is deposited in an amorphous layer whose structure is similar to that of a super-cooled liquid.

In many cases, the orbital degeneracy of the excited state of an atomic impurity is lifted in the crystal. A small decrease in symmetry from the full three-dimensional rotation group is sufficient to split a $^2P_{3/2}$ state into two components yielding a triplet for the transition $^2P_{1/2,3/2} \leftarrow {}^2S_{1/2}$ of noble atoms, i.e. gold, silver, copper, but much lower symmetry is required to split a $^1P_1^0$ state into three components as observed for the transition $^1P_1^0 \leftarrow {}^1S_0$ of Ca in rare gas matrices. Atomic energy levels with a higher degeneracy, as for example the $^6P^0_{7/2,5/2,3/2}$ levels of Mn in Ar,[15] exhibit in most cases a complete lifting of this degeneracy. One must assume that the trapping sites are all of a uniformly low symmetry.

A relatively detailed description of the splitting of an atomic energy level by a crystal field was given in Duley's thesis.[29] A detailed description, therefore, is not necessary in this context.

When an atom is placed in a crystal, the symmetry of its environment which previously in the free state was that of a three-dimensional rotation group with inversion, is reduced. This reduction in symmetry means that all directions are no longer equivalent as they were for the free atom. Crystal field theory allows a prediction to be made of how much degeneracy is removed by a field of give symmetry and provides expressions for the magnitude of the splitting energies.

For a ^1P state under a weak field of D_2 symmetry it will split as shown in Fig. 14.

For a ^3P state under a weak field of D_2 symmetry it will split as ^1P state. Experimental results shows that in order to relate the observed multiplet to crystal field splitting the weak field with symmetry no higher than D_{2h} has to be assumed. But it does not tell us whether it is any lower.

In this model, the neighboring rare gas atoms of the metal atom are treated as structureless, orbital-less points which set up an electrostatic field due to their polarizability. Since the force holding the rare gas atoms together in forming crystal is primary a van der Waals force, it is hard to imagine that the interaction field in this kind of crystal would provide such a large splitting, i.e. 150 cm^{-1} to 500 cm^{-1}. The crystal structure of pure rare gases is face centered cubic (fcc), and therefore no removal of orbital degeneracy of the atomic P state is to be expected for a perfect substitutional site.[49] Therefore distorted impurity sites have to be considered in an effort to interpret the experimental

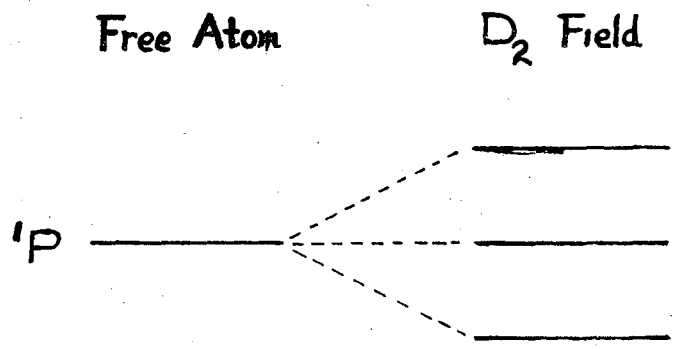

XBL 699-5677

Figure 14

observations. M. Brith and O. Schnepp[14] investigated the covalent and the dispersion interactions between the impurity atom and the host lattice and the contributions of these interactions to the splitting energy of the atomic excited P states of magnesium in a distorted lattice site in solid argon. They conclude that the experimentally observed multiplet structure can be explained on the basis of physically reasonable models of asymmetric impurity sites. In particular, an impurity site with more than one adjacent vacancy is the most physically reasonable configuration.

There is also a problem of interpreting the increasing splitting as a function of temperature because as the temperature of the rare gas solid increases the lattice parameter increases and the polarizability decreases. This means that the field strength should decrease and also the magnitude of splitting, but as we observed in magnesium, calcium and cadmium warmup experiments and other observations by many investigators, there are always two components which shift to the red and one to the blue even though the center of gravity of the triplet absorption shows a red shift in all cases. The reversibility of the magnitude of splitting with temperature clearly shows that there is an unknown factor that governs the splitting and which is a temperature dependent variable. This also tends to reject Brith and Schnepps vacancy assumption because formation of vacancy should be able to take place during warmup and the number of vacancy should change which would change the symmetry of the impurity site.

Although the crystal field theory provides a qualitative understanding of the splitting in energy levels, it does not fully explain the blue and red shifts. More work has to be done in order to understand the interaction between metal atoms embedded in rare gas matrices for interpreting splitting.

b. Atomic pairs. The existence of multiplet structure has been interpreted as evidence of the removal of orbital degeneracy by the environment of a host lattice (Brith and Schnepp) or in terms of the Jahn-Teller effect (McCarthy and Robinson), but as mentioned in the previous section it is not very conclusive.

Recently, Andrews[26] has suggested, and his suggestion was reinforced by Merrithew,[27] that possibly some of the components of the multiplet structure could be explained by interactions between pairs of foreign atoms trapped at non-nearest-neighbor sites in the host lattice. Assuming that the interacting pair of trapped atoms can be treated as a weakly bound diatomic molecule, the interaction energy between atoms trapped at various sites can be obtained from known diatomic potential curves. Since the region of the observed multiplet is within the region of non-nearest-neighbor interacting pair's transition for many of the studied atoms, i.e. Hg, Li, Mg, etc., this proposed interpretation is highly possible.

But more recently, King studied the codeposition of silver and gold, vaporized simultaneously in electron bombardment heated Knudsen cells, with krypton at 20°K. He showed that within experimental error the "pure" metal bands experience no shift in the presence of other metal and that no new features appear. This is evidence that none of the three strong bands are due to solute-solute interaction. If they are, we should have observed an isotopic-substitution type effect, but much larger, due to AgAu. This is again confirmed in this work. See Fig. 15, Mg-Cd (with $M/R \approx 1000$) mixed metal melted system and compared with the pure spectra. There are no shifts or extra features. Also the study of copper-gold alloy in krypton by King shows that no shifts of the bands from their position in

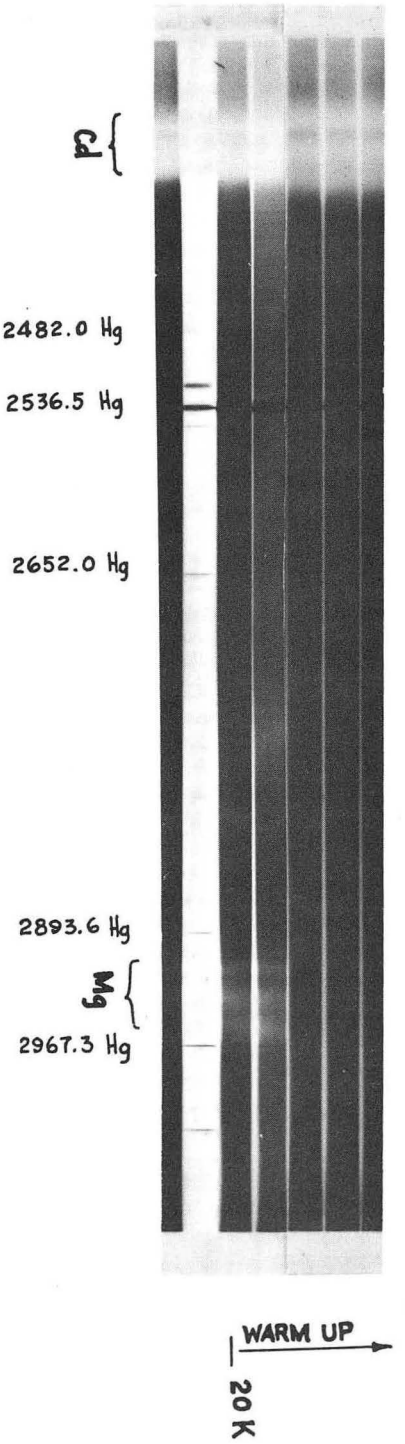

XBB 699-6106

Figure 15

the pure metals and no appearance of new bands. This again justifies the conclusion that the three prominent bands in the spectrum of each metal are due to well isolated atoms. Different ratios of metal mixture had been used with no evidence of mixed metal interaction at the concentration raises studied.

Recent work on Pb with high Pb concentration in Xe by Chin-An Chang[35] shows that a spectral line corresponding to $^3P \leftarrow {}^3P$ transition appears at the same time as a molecular band 5000 A. This molecular band intensity increases as the temperature of the Pb increases. This band corresponds to the Pb_2 gas phase transition and has a very similar vibrational spacing.

3. Temperature Dependence

As we mentioned before the appearance of the absorption spectra of trapped atoms in rare gas matrices depends on the temperature of the rare gas matrices. If we have too cold a temperature the metal atoms may be trapped in all kinds of different sites and give rise to extra absorption feature. If the target is too hot then we may not be able to prevent the metal atoms from forming polymers or aggregates and this in fact may give rise to some complicated absorption features. In the former case it is possible to anneal the crystal and eliminate some of the unstable sites. This, however, requires good experimental setup for temperature control. In the latter case it is of very little use towards understanding of the spectrum.

For well isolated metal atoms in rare gas matrices we normally see a distinct triplet for a $^1P \leftarrow {}^1S$ transition. As the temperature of the matrix increases, the triplet displays two types of shift: a. the center of gravity of the triplet shifted to the red; b. two components of the longer wavelength shifted to the red while the shorter wavelength

component shifted to the blue.

Type (a) can be explained in terms of the increase of intermolecular distance. The interaction potential drops off quite fast as the temperature increases. Evidence of the temperature dependence of lattice parameter has been given by Lasee and Limmons.

A type (b) shift is not at all understandable, especially the blue shift of the shorter wavelength component. This is partially due to the lack of a clear understanding of the multiplet structure. The reversability of the splitting as a function of temperature shown in Fig. 9 tends to discount the systematic occurrence of vacancies in the metal atoms immediate neighborhood. According to M. Brith and O. Schnepp more than one vacancy is required in order to account for the observation of three nearly equally spaced splitting components.

4. Mixed Metal Effects

Andrews[26] has suggested that some of the features in atomic absorption could be due to long-range non-nearest neighbor solute-solute interaction. If we assume that one of the features in triplet is due to atomic transition and the others are due to solute-solute interaction then, by depositing mixed metals we should be able to see the effect on the other features. In order to test this hypothesis different metals have been codeposited in xenon at 20° K with different atomic percentages. Results show no visible effect at all. The spectra of the pure metals are the same as the spectra of the mixed metals. Mg-Cd ($M/R \approx 1000$) and Mg-Ca ($M/R \approx 500$) are the systems under study. Their spectra of pure metal and their mixed metal spectra do not show any visible difference as shown for Mg-Cd in Fig. 15. The results of King for Ag-Au and Cu-Au systems also show no effect at all. These results tend to disprove Andrew's hypothesis.

The warm up spectra in Fig. 15 show that the magnesium triplet disappears while the cadmium triplet remains. This seems to indicate that Mg may be trapped in certain regions where it is easy to warmup and loose matrix while Cd may be trapped in a bigger region and remains isolated while warmup takes place.

IV. ABSORPTION SPECTRA OF SOME SIMPLE MOLECULES TRAPPED IN SOLID RARE GASES

A. Mg_2

1. Introduction

Most of the chemically stable molecules possess characteristics of either or both of the two well-known types of bonding, homopolar and heteropolar. A third type of bonding is called polarization or van der Walls bonding. The small attractive forces between rare gas atoms, responsible for their deviations from ideal gas behavior and for their liquification at sufficiently low temperatures, are called van der Walls forces. Molecules whose binding energy is mainly due to van der Walls forces are called van der Waals molecules. All diatomic molecules of rare gases and elements from group IIa and IIb are considered as van der Walls molecules. The following are the electronic configurations of the lowest states of some typical diatomic molecules formed from elements of group IIa:

$$Mg_2: KKLL\ (3S\sigma_g)^2\ (3S\sigma_u)^2$$
$$Ca_2: KKLLMM\ (4S\sigma_g)^2\ (4S\sigma_u)^2$$

Other molecules like Zn_2, Cd_2, Hg_2 have been observed spectroscopically and their stabilities are known.

From Section III we saw the importance of the concentration of metal atoms in the matrix for interpreting the spectroscopic data. The temperature dependent diffusion and the formation of dimer are all pertinent factors in the appearance of the spectrum. Appendix B shows that the dimer is of negligible concentration compared to the monomer in the Knudsen cell, but this does not have to be so when the beam collides on the target. With the rate gas atoms moving around it is always possible for the metal

atom to form dimer and/or aggregates. Because of this, the understanding of the dimer or polymer spectra is necessary prior to the investigation of spectra of high temperature molecules in rare gas matrices synthesized by a diffusion mechanism.

Many of the van der Waal molecules and metallic dimers have been spectroscopically observed both in gas phase and in rare gas matrices. See Table IX and Table X references.

The most thoroughly studied van der Waal molecules are Hg_2 and Cd_2 and their dissociation energy limits have been estimated.

For Hg_2 absorption, fluorescent and emission spectra in the gas phase are observed with $D_o \approx 0.06 \pm 0.003$ eV. London[50] used the dispersion measurement data of Wolfsohn[51] to calculate the dissociation energy of Hg_2 theoretically on the basis of polarization binding and obtained the value of 0.086 eV for an equilibrium separation of 3.5A between the two Hg atoms.

Recently, Freedhoff[52] suggested a systematic means for identifying the molecular features associated with a given atomic transition in the spectra of impurity trapped in solids. Guided by the similarity of the Hg and Cd spectra and by their appearance, the 48,330 cm^{-1} and 47,640 cm^{-1} bands of Hg in Ar and Kr respectively are identified with the transition $(^1S_0 + {}^1P_1)\ {}^1\Sigma_u \leftarrow (^1S_0 + {}^1S_0)\ {}^1\Sigma_g$ of Hg_2. Using the experimental data of Brewer, et al.,[16] Freedhoff obtained binding energies of 0.008 eV from the observations of Hg in Kr and 0.009 eV from Hg in Ar. This is about a factor of ten smaller than the gas phase value.

For Cd_2 the absorption and fluorescent spectra are observed upon discharge in the gas phase. The dissociation energy of Cd_2 has been reported to be 0.087 eV by Kuhn and Arrhenius.[53] Cram[54] analyzes the bands of Cd_2 lying on either side of the atomic line and can only account

Table IX. Studies on gas phase homonuclear diatomic molecules of group II elements

Molecules	Methods	Year	Author	Reference
Ba_2	-	-	-	-
Be_2				
Ca_2	Emission	1931	Hamada	33
		1968	Kovalyonok	56
Cd_2	Absorption	1927	Jablonski	62
		1927	Mohler, Moore	63
		1928	Winans	64
		1928	Jablonski	65
		1929	Winans	55
		1929	Winans	66
		1932	Robertson	67
		1933	Kuhn, Arrhenius	53
		1935	Robertson	68
		1935	Winans, Cram	69
	Emission	1931	Hamada	33
		1934	Cram	54
		1951	Garton	70
	Fluorescence	1921	Van der Lingen	71
		1925	Kapuscinski	73
		1927	Jablonski	62
		1930	Mrozowski	72
		1934	Cram	54
	Theoretical	1939	King, Van Vleck	74
Hg_2	Absorption	1922	Franck, Grotrian	75
		1925	Koernicke	76
		1931	Winans	77
		1932	Khun, Freundenberg	78
		1937	Kuhn	79
		1944	Winans, Heitz	80
		1952	Winans, Heitz	81
		1953	Winans, Heitz	82
	Emission	1931	Hamada	33
	Fluorescence	1929	Mrozowski	83
	Theoretical	1930	London	50
		1939	King, Van Vleck	74
		1952	Winans, Heitz	81
Sr_2	-	-	-	-

Table IX. (Continued)

Molecules	Methods	Year	Author	Reference
Mg_2	Absorption	1955	Sthapitanonda	58
		1969	Balfour	57
	Emission	1931	Hamada	33
		1955	Sthapitanonda	58
Zn_2	Absorption	1927	Mohler, Moore	63
		1928	Winans	64
		1929	Winans	55
		1929	Winans	66
	Emission	1931	Hamada	33
	* *	*	* * * *	
	Review	1950	Herzberg	61
		1953	Gaydon	84

Table X. Studies on matrix isolated homonuclear dimer of metal

Molecule	Matrix	Wavelength region	Year	Author	Ref.
Cd_2	Ar,Kr,Xe	2000Å 2200Å	1966	Duley Freedhoff	33 52
Hg_2	Ar,Kr,Xe	2250Å 2070Å	1965 1967	Brabson Freedhoff Duley	9 52 23
Li_2	Ar,Kr,Xe	 5000Å	1967 1967	Andrew Belyaeva	26 28
Mg_2	Kr,Xe	3400-2800Å	1969	Wang	
Pb_2	Kr,Xe	5100Å		Chang	35
Tl_2	Ar,Kr,Xe		1965	Brabson	9
Zn_2	Ar,Kr,Xe	2300Å 2500Å 2700Å	1966	Duley	29

for the spectra by assuming a $(^1S_0 + {}^1P_1)\ {}^1\Pi_u \leftarrow (^1S_0 + {}^1S_0)\ {}^1\Sigma_u$ transition. Potential curves of Cd_2 molecule have been derived empirically from his spectroscopic analysis.

According to Freedhoff, Duley's[29] observed absorptions of 36,620 cm^{-1} and 35,900 cm^{-1} in Ar and Kr respectively may be identified with the $(^1S_0 + {}^1P_1)\ {}^1\Sigma_u - (^1S_0 + {}^1S_0)\ {}^1\Sigma_g$ transition of Cd_2. This identification is strengthened by the observed vibrational structure of the band in Ar[29] with spacings of 80 ± 20 cm^{-1} at higher temperature 40°K.

Zn_2 spectra have been reported by Winans[55] and Hamada[33] in gas phase. Recently Duley has assigned some of the absorption feature of Zn in rare gas matrices to Zn_2 molecule.

No Be_2, Ba_2, Sr_2 spectra have been reported. Ca_2 gas phase spectra in the 4227A resonance line region of $^1P_1 \leftarrow {}^1S_0$ transition have been reported by Hamada.[33] Kovalyonlk, et al.[56] reports a rotational analysis of the orange bands of Ca_2 in the 5900 A region. But both of these works are not very definite. In Kovalyonok's work he reports that Ca_2 has r_e = 1.35A while for CaO, r_e = 1.82A. If we compare r_e of Ca_2 with r_e (=3.88A)[57] of Mg_2, we would think that it is very unlikely for Ca_2 to have a r_e = 1.35A. More work for Ca_2 is needed to clear up the ambiguity.

Mg_2 gas phase spectra have been studied by many investigators. Hamada has studied the emission spectra of Mg_2 with a hollow cathode system. The hollow cathode used was a closed iron tube 6 cm in length and 2 cm in diameter. An iron cover which had a small aperture of 2 or 3 mm was screwed on the open end of the tube. The magnesium metal was inserted into the hollow space of the cathode. The most favorable conditions for the excitation of molecular spectra required a comparatively low voltage and weak current. The metallic vapor glowed intensely at the small

aperture of the cathode and the pressure of the vapor was high enough to produce molecules.

Sthapitanonda[58] has studied the Mg_2 absorption spectra by vaporizing magnesium nitride in a McDanel porcelain tube with flat quartz optical window being held under pressure by two Teflon gaskets inside the stainless steel flanges. The furnace was capable of temperatures up to 1700°C; but the highest temperature used was only 1400°C.

Recently Balfour[57] at Ottawa has done a high resolution study of Mg_2 vapor. He has used the mass 24 and 26 isotopes of magnesium in a stainless steel tube (somewhat like a King furnace) at about 1000 K. The Mg_2 spectrum is a many-line spectrum with no obvious band heads. His spectroscopic data are tabulated in Table XI. This seems to be the most reliable analysis to date.

As we discussed in Section III the appearance of absorption feature depends upon the concentration of the metal atom in the matrix. It would be necessary to segregate and identify the effects of aggregation and site perturbation. There is real promise that the spectra will reveal the energetics of growth of metallic aggregates and this could contribute importantly by closing somewhat the gap between diatomic molecules and the metallic state.

2. Experiments and Results

The experiments are the same as for the atomic absorption of magnesium atom in rare gas matrices and are described in Section II. The only change is that higher magnesium concentrations were used. The M/R ratio was well below 100. The Mg_2 spectra have been observed in both Kr and Xe matrices. They appear in Fig. 16. The results are tabulated in Table XII. Most of the bands in the long wavelength side of the $Mg(^1P \leftarrow {}^1S)$

Table XI. Spectroscopic data for Mg_2 molecule*

	$X^1\Sigma_g^+$	$A^1\Sigma_u^+$
T_0	0	—
ω_e	51.1 cm^{-1}	190.6 cm^{-1}
$-\omega_e\chi_e$	-1.65 cm^{-1}	1.15 cm^{-1}
r_e	3.889Å	3.081Å
D_e	424 cm^{-1}	—

* Balfour, W. J., Can. J. Phys., 1969, to be published

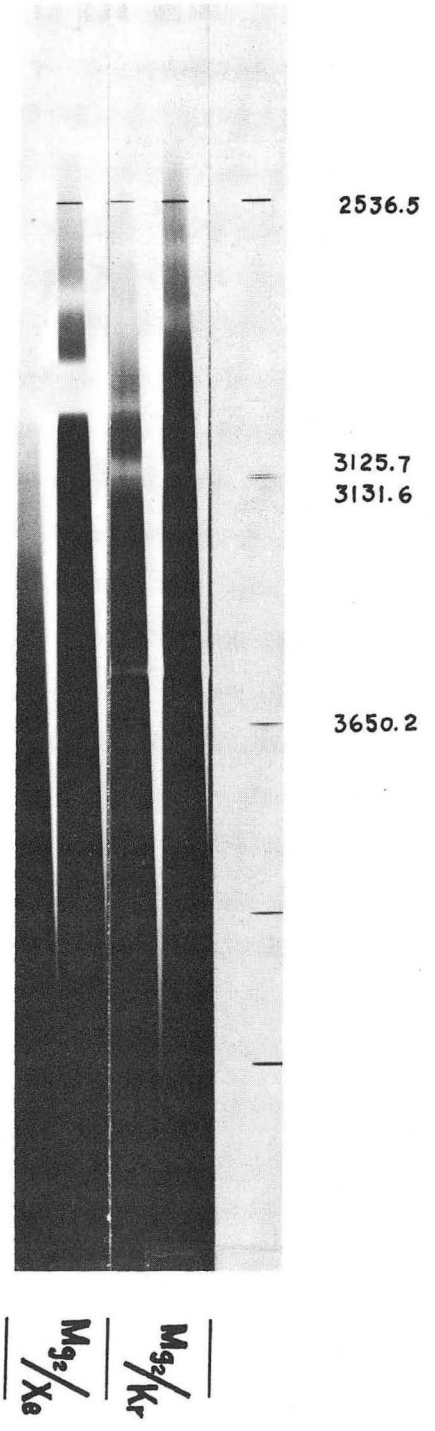

XBB 699-6115

Figure 16

Table XII. Absorption features of Mg_2 in solid matrices

Xe		Kr	
A	cm^{-1}	A	cm^{-1}
		3534	28295
3247	30798	3112	32130
3130	31948	2974	33625
2932	34106	2779	35985
2730	36630	2646	37800
2619	38182		

resonance line can be accounted for as Mg_2 molecular bands while those on the short wavelength side are definitely due to the multiple site effect, because they disappear upon warmup while all the others remained. This is also confirmed by the experiments with high dilution but fast condensation, since the short wavelength bands disappear upon annealing while the triplet absorption remains and no molecular band on the long wavelength side of the magnesium resonance transition are observed. This is shown in Fig. 17.

3. Discussion

The results of gas phase spectra suggest that the ground electronic state of the van der Waal molecules may be unstable or have a very shallow potential minimum. For these molecules one finds very low value for dissociation energies[56,60] and high value for r_e, internuclear distance.

Potential curves representing the ground and excited electronic states may often be drawn from the information obtained from both absorption and emission spectra of the same system. Herzberg[61] has shown such potential curves for van der Waals molecules and has given an excellent discussion on their interpretation. Potential energy diagrams of Hg_2 and Cd_2 in matrices have already been suggested[52] but are subject to change, of course, if new observations can be obtained.

Balfour reported the Mg_2 $X^1\Sigma_g^+$ state has $D_e = 424\ cm^{-1}$ with r_e = 3.889A while for $A^1\Sigma_u^+$ r_e = 3.081A. From these spectroscopic data and using the following equation

$$D_e = \frac{\omega_e^2}{4\omega_e X_e}$$

we obtain $D_e \approx 7847.8\ cm^{-1}$ for $A^1\Sigma_u^+$ state. Using the value 35300 cm^{-1} for Mg $^1P \leftarrow {}^1S$ in Kr as the dissociation limit for $(^1S_0 + {}^1P_1)$ $A^1\Sigma_u^+$

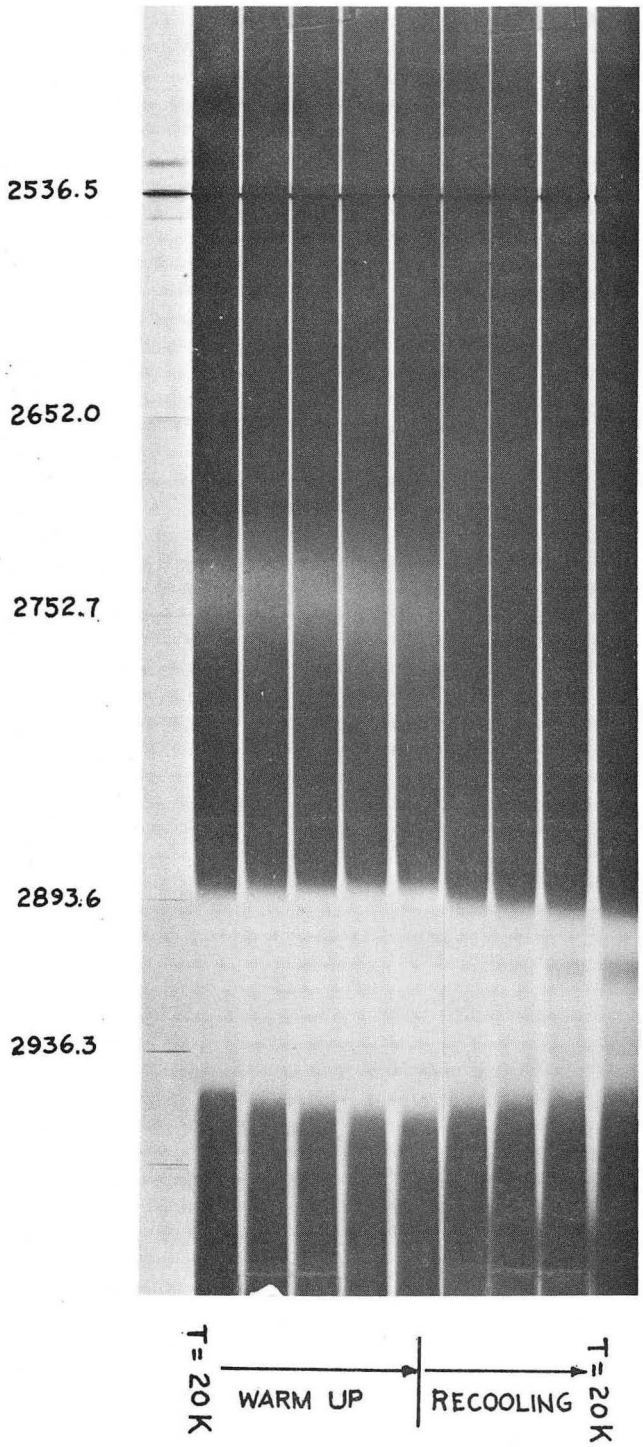

XBB 699-6110

Figure 17

state, r_e = 3.081A and the shape of potential curve described by Freedhoff we get the potential curve of an $A^1\Sigma_u^+$ state in a Kr matrix (see Fig. 18).

This portion of work can only be regarded as a small effort towards the understanding of dimerization of metal atoms in matrices. One conclusion we can make is that the Mg_2 molecule which is observed must be formed in the process of producing matrices rather than in the Knudsen cell. The detailed mechanism for the formation of dimer in matrices is still very uncertain. It has to form before being completely trapped in the target because no observable Mg_2 molecular spectra appear in the warmup experiment of matrices showing only the atomic features. Also the warmup and quenching experiments of Mg atoms in rare gas matrices seem to indicate that Mg atoms do not move around once they are in the rare gas solid and the only particles that are moving around are rare gas atoms which possess high mobility. The mobility of Mg atoms is very small while some other ligher atoms may have high mobility in rare gas solid even at temperature below liquid hydrogen temperature, e.g. Li has such a high mobility that both Andrews[26] and Belyaeva[28] were able to observe the increase in intensity of the bands that they consider to be Li_2.

There are many stably bonded dimers of metallic atoms being isolated in rare gas matrices, i.e. Pb_2, Bi_2, Tl_2. Chang's result for Pb_2 is the most interesting one because a distinct band system is observed and it corresponds very closely to the Pb_2 gas phase transition while the atomic transition which is assigned to $^3P \leftarrow {}^3P_0$ transition, appears as a singlet rather than a triplet.

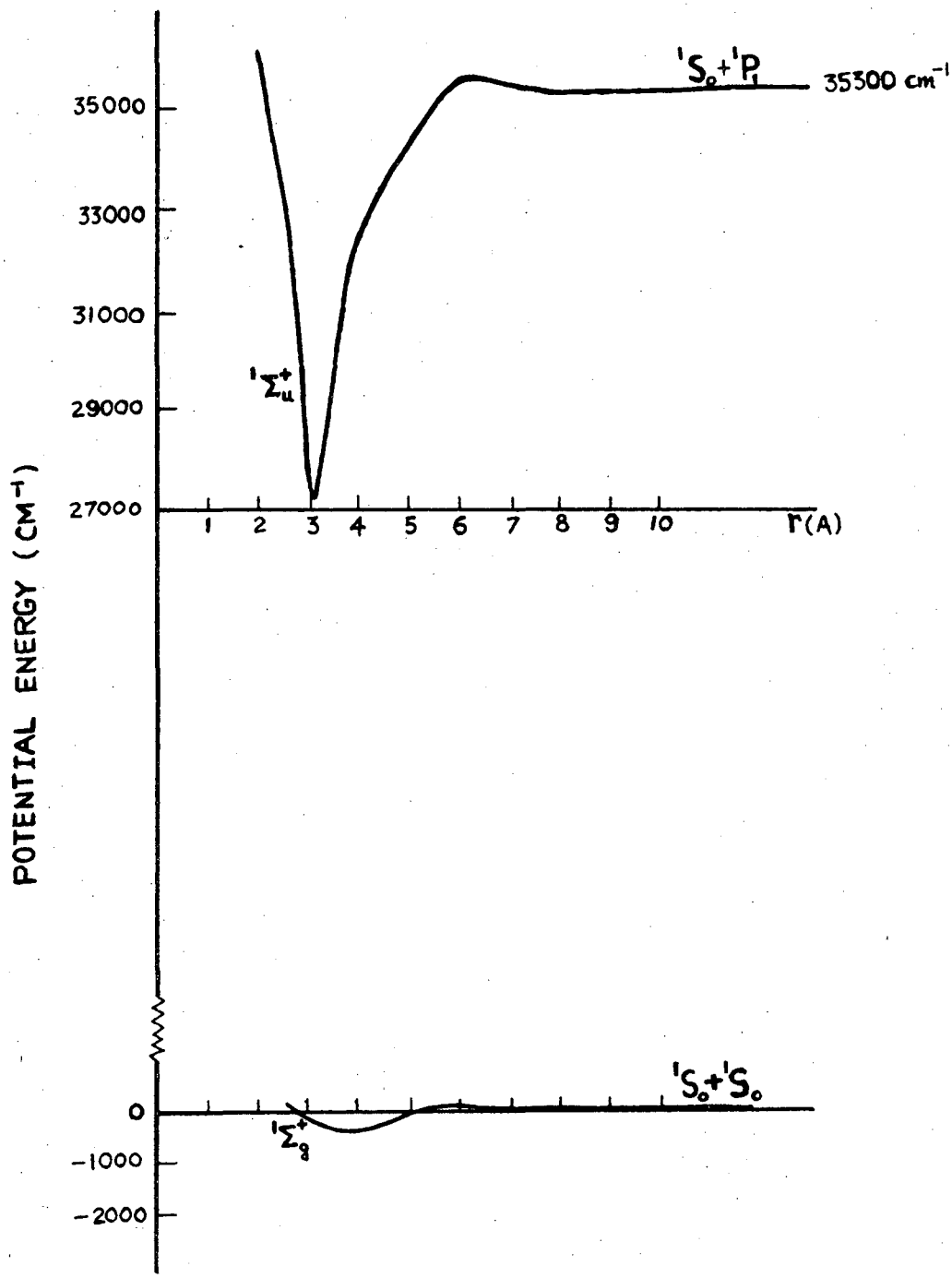

XBL 699-5681

Figure 18

B. O_2

1. Introduction

Oxygen atom, oxygen molecule and ozone are some of the reactants to be used in synthesizing metallic oxides in rare gas matrices. The ultraviolet, visible and infrared spectra are very important information for understanding and interpreting the spectra of the final products and the possible reaction mechanism.

In this section we will deal primarily with the absorption spectra of pure oxygen and oxygen in different matrices.

The ultraviolet absorption of oxygen in the region 2400 to 3000A in condensed phases has been studied by McLennan, Smith, and Wilhelm.[85] They observed a number of bands corresponding to the "high pressure" bands in gaseous oxygen reported by Finkelnberg and Steiner.[86] Prikhotko[87] studied the absorption spectrum of O_2 in the crystal lattice of O_2-N_2 and O_2-Ar at liquid hydrogen temperature. In the region 2400 to 2800A she found that all spectra consisted of a series of absorption bands arising during transition from the normal level $^3\Sigma_g^-$ to some excited level. Every band of this series is a triplet. ω_0 diminishes quite rapidly, changing from 760 cm^{-1} to 360 cm^{-1} over a range of 10 members of a series. These bands coincide with the absorption spectra of solid oxygen, and have a structure identical with the "high pressure" bands. From her data she calculated a potential energy curve for the upper state of the transition which was very similar to the $A^3\Sigma_u^+$ state of the Herzberg bands. The thickness of her crystal was about 10 to 20 mm. Hörl[88] prepared thin polycrystalline layers of solid α-oxygen by deposition from the gas phase onto surfaces liquid helium cooled to near 4.2 K, with film thickness estimated to be a few hundredths of a millimeter. Between 2400 and 2700A a number of

broad diffuse bands were observed with half-widths of the order of 200 to 300 cm^{-1}. Hörl suggested the bands in the solid were the Herzberg bands of oxygen ($A^3\Sigma_u^+ \leftarrow X^3\Sigma_g^-$) shifting to shorter wavelengths by about 90 to 120 cm^{-1}. Dressler[20] and Schnepp[89] studied thin layers of oxygen deposited in mixtures with argon and nitrogen on a surface at 4.2°K. Between 1750 and 2000A, eleven bands, 50 to 150 cm^{-1} broad, were observed and identified as the Schumann-Runge bands of oxygen ($B^3\Sigma_u^- \leftarrow X^3\Sigma_g^-$). By measuring the isotope shift produced with O_2^{18} they established that the bands in the solid were shifted toward longer wavelengths by roughly 300 to 400 cm^{-1}. Bass and Broida[90] studied the condensed phases of oxygen over the wavelength range 1750 to 2900A and observed both the Schumann-Runge bands of O_2 and the diffuse oxygen bands. Observations had been made in liquid and crystalline argon and nitrogen at temperatures between 60 and 90°K. The observed spectra show little change between the solid and liquid matrix and are quite similar to the spectra observed at 4.2°K. Schnepp[91] studied the absorption spectra of oxygen in solid solutions in nitrogen, argon, krypton, xenon and neon in the spectral region of the Schumann-Runge bands at liquid helium temperature. Series of ten or more bands have been measured in each case but the widths of the bands for neon and xenon as hot lattices are considerably larger than in the other solids, where the absorptions are relatively narrow and can be accurately measured. The vibrational structure is identical with that of the gas for low vibrational quantum numbers of the excited electronic state ($B^3\Sigma_u^-$) but for higher levels the differences are very marked.

Landau[92] studied the absorption spectrum of solid oxygen in the wavelength region from 12,000 to 3300A and found the electronic band systems of O_2 with ground state $^3\Sigma_g^-$ and upper states $^1\Delta_g$, $^1\Sigma_g^+$, $^1\Delta_g + {}^1\Delta_g$,

$^1\Delta_g + {}^1\Sigma_g^+$ and $^1\Sigma_g^+ + {}^1\Sigma_g^+$. All these systems were investigated in detail in the α-form of the solid at ~21°K. Prikhot'ko[93] studied the absorption spectrum of the α-modification of oxygen at 4.2°K. Oxygen crystals were prepared by sputtering the gas onto a cold quartz window cooled to the liquid helium temperature. Prikhot'ko[94] studied the absorption spectrum of solid oxygen in greater detail at 1.3 K. Prikhot'ko[95] studied the spectra of the high temperature β- and γ-modifications. This study was intended to gain comprehensive understanding of the absorption features of the various modifications of solid oxygen, which differ in crystal structure and in magnetic properties.

2. Results and Discussion

The experimental set up was the same as described in Section II. The pure oxygen gas was mixed with various amounts of rare gases ranging from 5 to 20% oxygen.

No molecular absorption bands were observed in the region of 4000A-2500A or in the region of 4000 to 650 cm^{-1}. The lack of spectra may be due to insufficient O_2 concentration or too thin a layer. When Mg atoms were deposited with the O_2-rare gas mixtures with the same quantity as in the experiment with O_2-rare gas alone, we observed molecular spectra in the region of 4000-2500A in all three rare gas matrices. At first this molecular system was thought to be molecular oxygen absorption. But from a comparison of this molecular system in rare gas matrix and the molecular system of solid oxygen by various investigators and in the gas at standard pressure it is easy to see the different characteristics of this molecular system from the others, as will be shown in Table XVIII, the vibrational frequency of the molecular system obtained from this work has an average around 1000 cm^{-1} for initial terms while the α phase solid

oxygen has a value approximately equal to 750 cm^{-1} for the first few vibrational levels as shown in Table XIV. Also the absorption features of this work is almost structureless while the solid oxygen work shows triplet structure. The only similarity is the intensity distribution - the intensity increases with the vibration number. For O_2 this type of distribution should be expected from the relative positions of the potential energy curves of the ground and excited states.[96,97] A stronger proof that the molecular system observed in this work is not due to O_2 or its polymer is that its vibrational frequencies are quite different from both the vibrational frequencies of solid oxygen obtained by Prikhot'ko and the gas phase value as reported by Wallace.[99]

A comparison of the vibrational frequencies in the crystal and gas series reveals their similarity and provides additional grounds for concluding that absorption in the crystal should be associated with the same electronic transition as in the gas, i.e. with the transition $^3\Sigma_u^+ \leftarrow {}^3\Sigma_g^-$. Table XIIIshows the similarity of some of the spectroscopic constants of $^3\Sigma_u^+$ state in the free molecule and in the crystal of oxygen. The work of O_2-N_2 and O_2-Ar by Prikhot'ko[87] also gives a very similar spectroscopic data compared to the observed oxygen absorption band system in crystal and in gas. This also proves that the molecular system observed in this work is not due to oxygen but some other molecular species. The band does not appear without depositing magnesium together with the oxygen-rare gas mixture. This tends to suggest that the molecular absorption observed has to be some magnesium-oxygen molecules. Another experiment also gives a strong indirect proof that this molecular absorption is the result of the magnesium-oxygen compound. The proof is the observed spectra of calcium with oxygen-rare gas mixtures which does give molecular spectra

Table XIII. Constants of the $A^3\Sigma_u^+$ state of O_2 in the crystal and in the free molecule

Constants (cm^{-1})	Crystal[93]	Gras[98]
ν_{00}	34120 34280 34420	34193
$\Delta G_{v+1/2}$	800	810
$\Delta^2 G_{v+1/2}$	34	33
$\omega_e X_e$	17	16.5
ω_e	834	843
ω_0	817	826

Table XIV. Frequencies of the series of $^3\Sigma_u^+ \leftarrow {}^3\Sigma_g^-$ in the spectra of solid oxygen and gas phase

	Solid [a]			Gas [b]
(v',v")	α-phase T=22 K cm-1	β-phase T=26 K cm-1	γ-phase T=48 K cm-1	cm-1
0,0		34160		35008
1,0	34918	34955	34905	35780
2,0	35679	35710	35685	36526
3,0	36408	36445	36400	37235
4,0	37110	37145	37100	37910
5,0	37777	37810	37765	38546
6,0	38405	38435	38395	39138
7,0	38997	39030	38990	39681

[a] A. F. Prikhot'ko, T. P. Ptukha, and L. I. Shanskii, Ukrainski Fizicheskii Zhurnal, 12 (7), 1166 (1967).

[b] L. Wallace, Astrophysics, J. Suppl. No. 68, 7, 165 (1962).

in the 5000A region, but never in the region below 4000A. In magnesium and calcium experiments the only difference is the metal and it causes a change in the position of the appearance of spectra. From this evidence we are very sure that the molecular spectra appeared in each case is the result of some oxygen-alkaline earth molecules and not oxygen alone. The reason we say that it contains oxygen is that it does show proper isotope shift when we substitute oxygen 16 with oxygen 18. A detailed discussion of these molecular band systems and their absorbers will be given in Section IVD.

C. O_3

1. Introduction

Interest in the products condensed at 20°K from dissociated oxygen (i.e., oxygen which has been passed through an electric discharge) has been stimulated by a number of recent investigations in this field. Observations of molecular bands which occur when the products condensed at 20°K from oxygen passed through a discharge and the metal atoms from the furnace are warmed indicate that oxygen atoms may be trapped in the deposit at low temperatures. Evidence in favor of this explanation has also been inferred from calorimetric measurements[100] and infrared absorption.[101] The evidence of the existence of oxygen atoms in the matrices at 20°K also makes possible the formation of either ozone in the matrices or ozone produced possibly by the discharge and cocondensed in the matrices with the oxygen molecules and oxygen atoms. This makes it necessary for us to understand more about the spectral behavior of ozone in the matrices prior to the synthesis of metallic oxides in the matrices.

The data presented here are the results of an investigation of the ultraviolet, visible and infrared absorption spectra of the products condensed from oxygen-rare gas mixtures passed through an electrical discharge.

2. Experimental

The low temperature systems used are the same as that described in Section II except that in the present work both the external windows are of cesium iodide and the target is of cesium bromide. In the dissociated oxygen experiments, the discharge is initiated in a quartz tube, which has a small orifice of 1 mm diameter, away from the collector surface and the axis of the tube has an angle of 11.2 degrees from the normal of the center of the collector to make sure that the oxygen-rare gas beam will cross the metal atom beam which has an angle of 8.6 degrees on the center of the collector. The details of this arrangement are shown in Fig. 19. Air Products research grade gases are employed without further purification. For isotope studies O_2^{18} of purity 99.85%, with 0.13% O_2^{17}, from Isomet Corporation, Palisades Park, New Jersey, were used. The source of power for the discharge is a 100-w, 2450-Mc microwave generator.

The spectra are obtained with spectrometers mentioned in Section II.

3. Results and Discussion

The infrared absorption bands of a film of discharged products are listed in Table XV. The agreement with the spectrum reported for the gas phase[102] is good, indicating that there is relatively little distortion of the molecule in the solid. As the film is warmed up no significant changes occur in the spectrum except for a tendency of the bands to broaden as the melting point of the matrix is approached.

From the discharged oxygen-xenon mixture condensation we observe

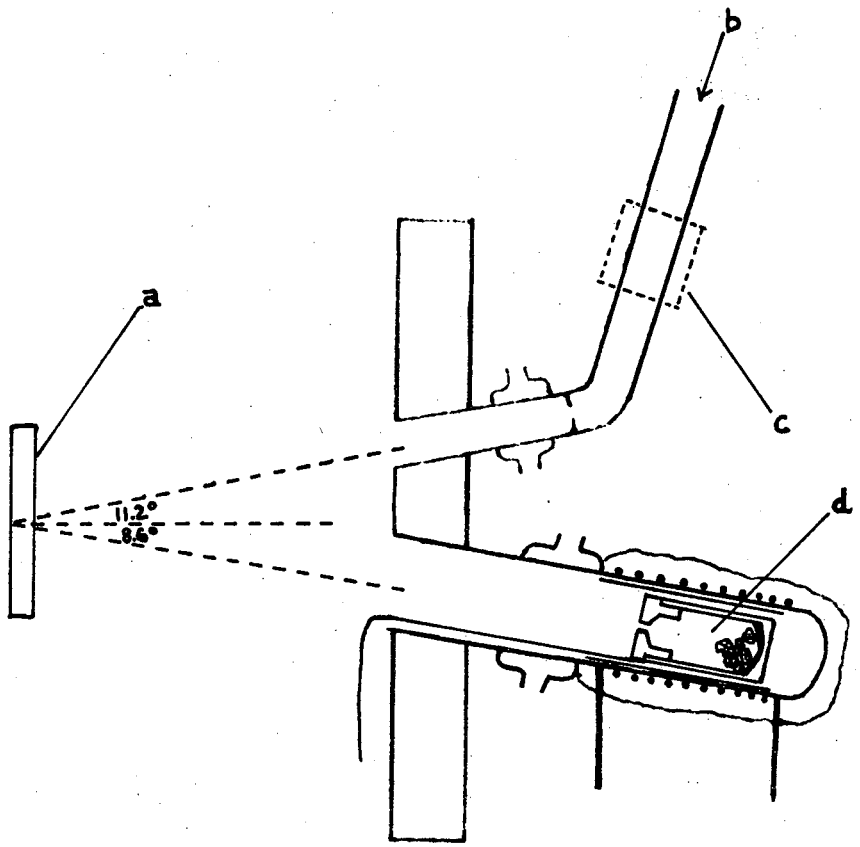

XBL 699-5679

Figure 19

Table XV. Infrared absorption bands of ozone in solid matrices

Kr (cm^{-1})	Assignment	Xe (cm^{-1})	Remarks
3687		3700	(OH?)
	ν_3	2350	CO_2
		1650	
1595	ν_2	1630	(H_2O)
1528		1535	
1036	ν_3	1032	O_3
998		980	
698			

a very strong absorption with a doublet at 1032 and 1025 cm^{-1}. Also a feature at 2150 cm^{-1} has been assigned by Harvey[101] to be $2\nu_1$ of ozone but this assignment is very uncertain since the 2150 cm^{-1} band is very weak and may be due at least in part to the presence of a trace of CO. Also this band was not observed in discharged oxygen-krypton mixture. The oxygen-18 does not show this band either. So it is fairly certain that 2150 cm^{-1} is not due to $2\nu_1$.

The 1043 cm^{-1} band does show red shift in both Kr and Xe while Harvey reported that in pure oxygen a blue shift showed.

The experimental result of discharged oxygen-18 in xenon gas is shown in Table XVI and the results of Harvey and Bass,[101] and Wilson and Badger[102] are also shown in the same table for comparison. The spectra are shown in Fig. 20. From the isotope shift we can easily see that there is close agreement between the spectra reported for solid and that for the gas phase.

The strong ultraviolet absorption is probably associated with the ultraviolet system in ozone, observed as long ago as 1889 by Liveing and Dewar.[103] Because of the thinness of the film no band as reported by Bass[104] is observed in the visible region. From the schematic cross section[105] of the ozone potential surface, we see that we would expect a strong diffuse continuum in the ultraviolet region for ozone absorption because the upper state is a repulsive state. There are strong absorptions below 2800A which go all the way to the short wavelength sensitivity edge of a 103-a-o plate in both discharged oxygen isotope experiments. These should be ozone absorption.

The results of this study of ozone in rare gas matrices provide important information for the work in the next section. One important aspect is that no new molecular band has been observed during the warming

Table XVI. Infrared absorption bands (cm^{-1}) of ozone in various phases and xenon matrix

O_3^{18}/Xe [a] T=20°K	O_3^{16}/Xe [b] T=20°K	O_3 [b] T=4.8°K	O_3 [c] Gas phase	Assignment [b]	Remark
3700	3700				(OH)
3680					
2980		3060	3050	$3\nu_3$	
		2800	2800	$\nu_1+\nu_2+\nu_3$	
	2350				(CO_2)
		2150		$2\nu_1(?)$	(CO)
2100		2100	2105	$\nu_1+\nu_3$	
1900		2060		$2\nu_3$	
1625	1600		1740	$\nu_2+\nu_3(?)$	(N_2O_4)
	1535				
1090		1120	1110	ν_1	
1038					
1008					
{978, 970}	{1032, 1025}	1050	1043	ν_3	
660		704	705	ν_2	

[a] This work

[b] K. B. Harvey and A. M. Bass, J. Mol. Spect. 2, 405 (1958).

[c] M. K. Wilson and R. M. Badger, J. Chem. Phys. 16, 741 (1948).

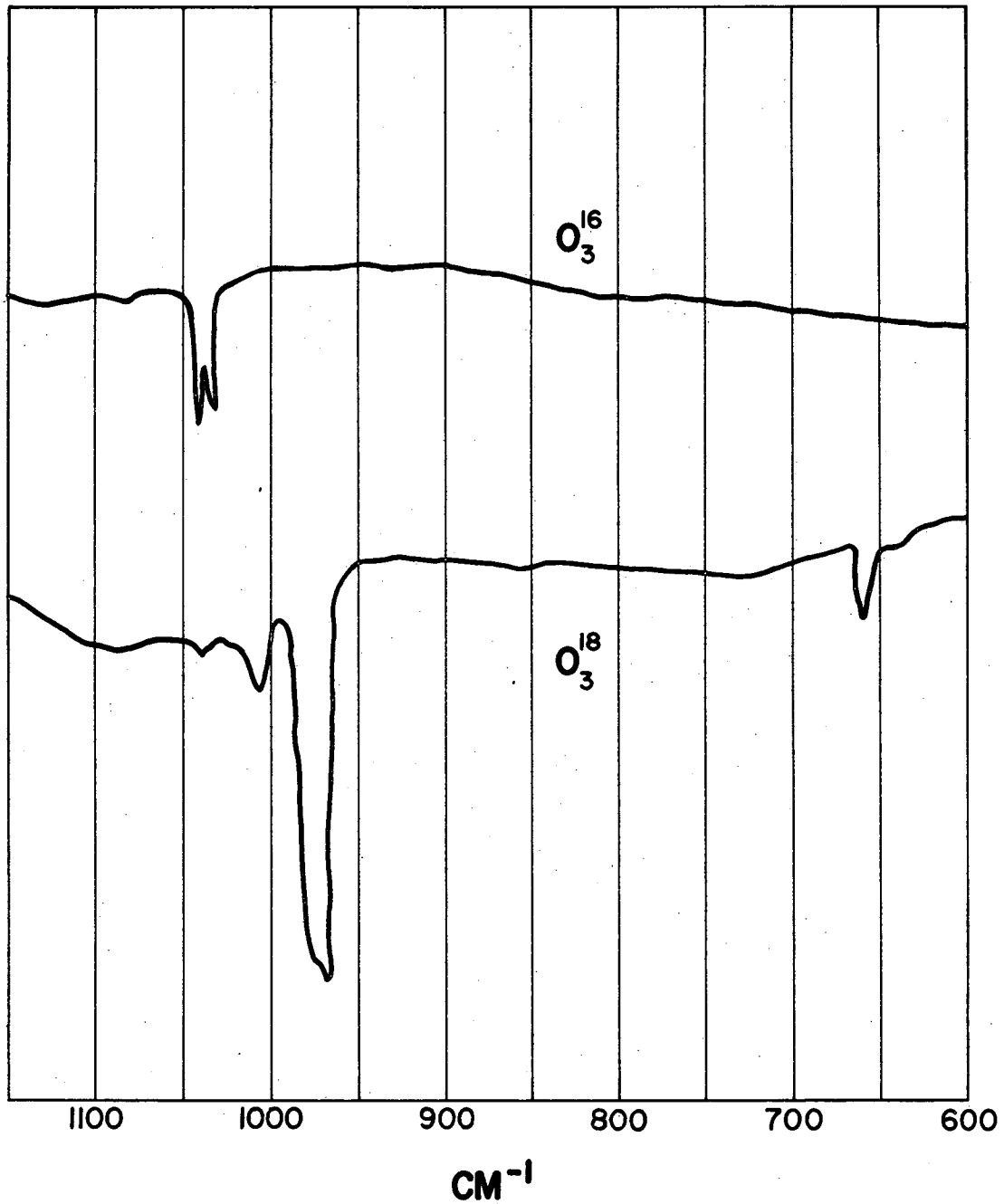

XBL 699-5682

Figure 20

process of the condensed discharged products. This evidence simplifies the interpretation of the molecular bands observed in experiments in the next section, carried out under the same experimental conditions with addition of metallic atoms only.

It is very difficult to estimate the concentration of oxygen atoms being trapped in the matrices because no noticeable increase in ozone concentration occurred during the warming process. But it is hardly necessary to point out, however, that these experiments do not preclude the presence of high concentrations of oxygen atoms since it is possible that the trapped atoms may combine directly to form oxygen molecules, without changing the ozone concentration.

D. MgO, CaO, BaO

As was pointed out before precise information on low-lying energy levels of high temperature molecules is needed to calculate the proper values of their thermodynamic properties. A survey of the spectroscopic literature for the alkaline-earth oxides shows that a great deal of uncertainty, confusion, and speculation still exist despite intensive research in this area in recent years.

In view of the importance of spectroscopic and thermodynamic data in the problem of high temperature chemistry of the alkaline earth oxides, it is essential to include the following survey as an integral part of this thesis.

1. Energy Levels of MgO, CaO

A very informative analysis for BeO, SrO, and BaO has been published by Sullivan.[106] There is no need to discuss them here, except to present some supplementary references for their spectroscopic data. We will also discuss the energy levels of gaseous MgO and CaO molecules.

a. Magnesium oxide. Several band systems have been observed for magnesium-oxygen in discharge or flame but only a few of them had been analyzed. These are the red system[107-110] assigned to $B^1\Sigma^+$-$A^1\Pi$, the green system[107-114] attributed to $B^1\Sigma^+$-$X^1\Sigma^+$ and the two violet systems assigned to $C^1\Sigma^-$-$A^1\Pi$ and $D^1\Delta$-$A^1\Pi$.[115-116] Brewer and Green[117] recently assigned a number of previously unassigned band systems in the violet region to the MgO molecule. Based on the near equality of spectroscopic constants of $C^1\Sigma^-$ and $D^1\Delta$ states, Green discussed the possibility that these two states are not singlets but might be components of a triplet. Also a closer look at the results of Sullivan's green system[106] and Green's green system[118] reveals that Sullivan's green system has at least a few more band heads than Green's work. Sullivan's spectrum is taken from a diffusion flame source with a total pressure of 200 Torr and oxidizer mixture of 10% O_2-90% Ar while Green's spectrogram is taken from a closed reduced pressure arc with about 1-10 Torr of oxygen. Higher energy heads have also been observed by V. A. Sokolov and N. A. Nazimov.[119] Brewer suggests that the inability to observe the higher energy heads in reduced pressure systems may imply that the upper state of the green system may predissociate and the molecules could fly apart before they could emit radiation. But in a flame, recombination processes may offset the dissociation process and enough highly excited molecules would emit radiation to make observation possible. A high resolution study of the higher vibrational levels of the $B^1\Sigma^+$ might be able to pin-point the dissociation limit of this state and indirectly help in locating the unknown state.

Many other bands have not been analyzed or assigned. This is due in part to the complexity of their appearance. There are many practical difficulties in trying to establish the order of energy of the low-lying

electronic states. An energy level diagram for MgO is given in Fig. 21.

The solid line levels are the observed states and the dotted levels are the predicted states. The scheme of prediction has been described by Brewer.[1] Some adjustments have been made and the estimates given by Brewer and Green[117] had been incorporated. This energy-level diagram is in no way an accurate description but it could serve as a guide for locating some of the possible transitions and their assignments.

b. CaO. Only three band systems have been assigned to the diatomic oxide CaO. These systems are the extreme red system ($A^1\Sigma$-$X'^1\Sigma$),[120] blue system ($B^1\Pi$-$X'^1\Sigma$),[121] and ultraviolet system ($C^1\Sigma$-$X'^1\Sigma$).[121] All correspond to transition between singlet states. The bands in the near infra-red region have been shown by Hauge[122] to be part of the extreme red system mentioned before.

There are also band systems in the green and orange regions of the spectrum. Hauge's oxygen isotope substitution experiments show that the emitter of the green bands very likely contain only one oxygen per molecule but there is the possibility that CaOH is the emitter. In the case of the orange band system, Hauge has not observed any oxygen isotope shift. Recently Kovalyonok[56] did a rotational analysis of the orange system and concluded that Ca_2 was the emitter.

The known states of CaO and the predicted states, using the same prediction scheme as in MgO, are shown in Fig. 22.

2. Matrix Work of Magnesium-Oxygen, Calcium-Oxygen and Barium-Oxygen Compounds

A few high temperature techniques, i.e. flames, arc discharge, etc., have been used to obtain the gas phase spectrum of alkaline oxides, but many of the observed spectra are too complicated to make analysis possible.

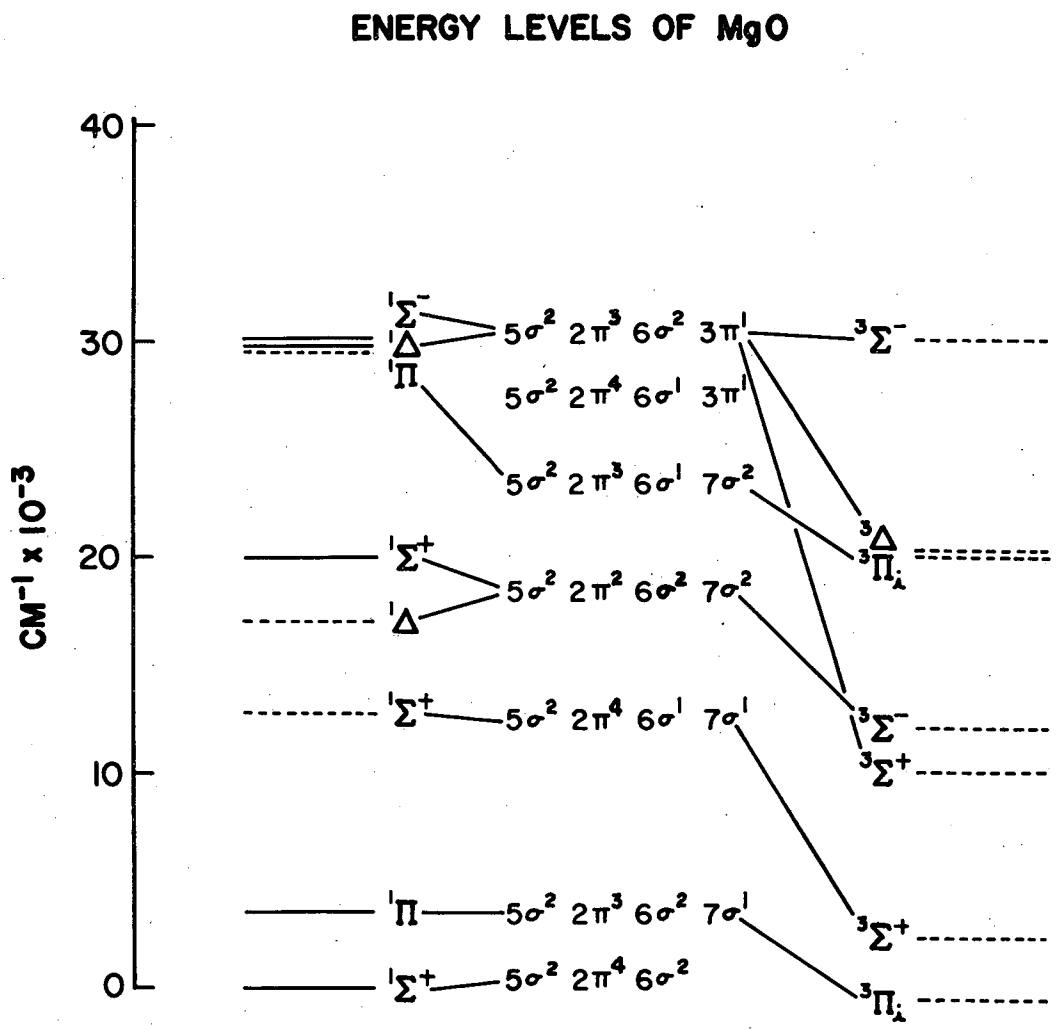

XBL 699-5684

Figure 21

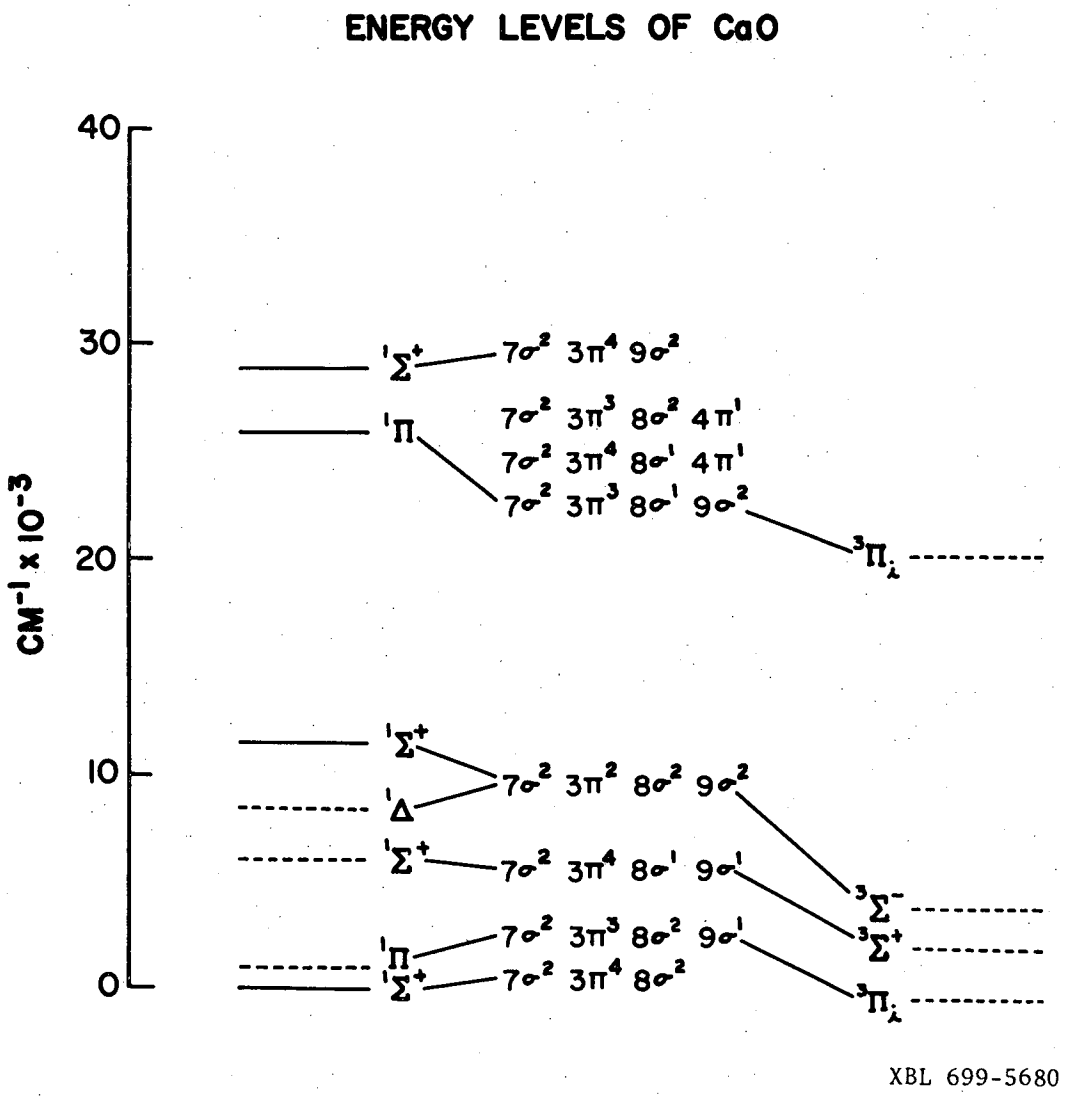

XBL 699-5680

Figure 22

The complexity of these spectra may be due to the high temperature environment (highly excited levels), hydroxides, or polymers.

The matrix isolation method gives an alternative to study the spectra of these high temperature molecules. The advantages offered by this method are: 1) molecules can be accumulated over a long period of time from weak sources, and 2) the spectra are greatly simplified because only the ground state is significantly populated at temperature typically used. Because of weak interactions with the rare gas atoms, it might be expected that the energy levels of the trapped molecules would not be much different from their gas-phase values, and that the absorption spectrum observed in the matrix would be easily correlated to the gas phase spectrum. This helps us to sort out the uninterpretable region of the spectrum if it does include the low energy transitions.

a. Experimental. The alkaline earth-oxygen compounds are obtained by first condensing alkaline earth metal and oxygen in rare gas matrices at the same time. Then the matrices are warmed to such a temperature that oxygen atoms or molecules could diffuse, while the matrix gas remains in a solid form, and finally the matrix is recooled. The furnace used is shown in Fig. 19. The details of this system have been described in Section II. The typical experimental parameters are tabulated in Table XVII.

Here the rate of metal deposit is obtained by weighing the target before and after a trial run of depositing pure metal alone. The rates of gas deposit were measured by a flow meter and it was assumed the condensation coefficient to be 1. The method of estimation of M/R gives a higher value than the actual ratio on the target because of the uncertainty of the condensation coefficient and scattering of the rare gas plasma from the discharge. This would imply that in the target we may

Table XVII. Experimental parameters for synthesizing of MgO

Target temperature for deposition	18 or 20 °K
Target temperature for observation	18 — 65 °K
Rate of metal deposit	6.1×10^{-10} mole/sec
Rate of rare gas deposit	1.6×10^{-6} mole/sec
Rate of oxygen deposit	4×10^{-7} mole/sec
Rare gas:oxygen:metal	2700:700:1

actually have higher concentrations than have been used.

b. Results.

i. MgO

(a) Electronic spectra of magnesium + oxygen.

Magnesium atoms isolated in rare gas matrices are reacted with oxygen atoms, oxygen molecules, and ozone which are codeposited. There are at least three molecular band systems in ultraviolet and visible regions. These bands' appearance depends very much on the condition of the matrix and the method of deposition. By passing the oxygen-rare gas mixture through a discharge cavity we observe a strong broad absorption in the 2537A region. This broad band is thought to be ozone absorption as discussed in Section III. The deposition of magnesium metal at the same time as the discharged products of oxygen-rare gas mixture give a strong magnesium triplet absorption with very little shift from the triplet absorption obtained by deposition magnesium with pure rare gas alone. But in warming up the target from 20°K to approximately 35°K, a molecular band appears in the region from 2400A to 4000A while the magnesium triplet disappears. From the previous experience of warmup experiment of pure magnesium metal isolated in matrices, we know that the magnesium triplet should stay in the matrix up to a temperature as high as 55°K with a slight increase in triplet splitting but should not disappear. The disappearance of the magnesium triplet at 35°K and the appearance of the molecular bands should serve as a strong evidence that magnesium atoms were oxidized by either oxygen atoms or ozone molecules which could diffuse in the matrix. The molecular bands observed are shown in Fig. 23 and 24 and the measured wavelengths are in Table XVIII.

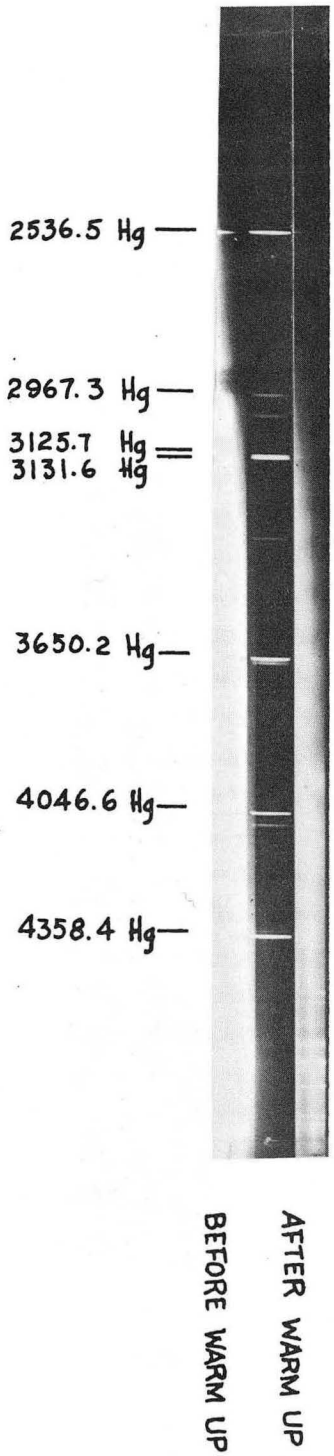

XBB 699-6109

Figure 23

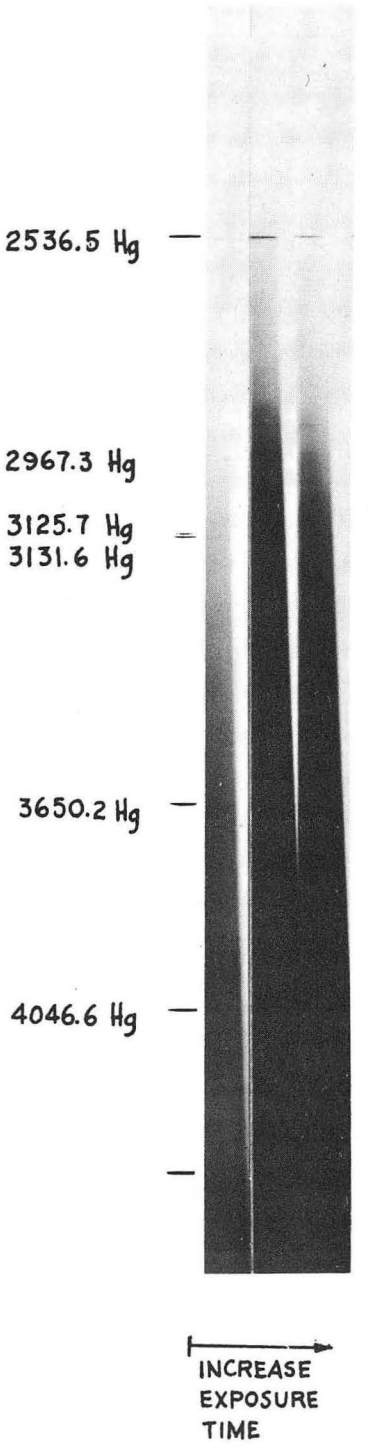

XBB 699-6113

Figure 24

Table XVIII. Ultraviolet absorption spectra of Mg + O_2 (discharged) in rare gas matrices

Ar		Kr		Xe	
A	cm^{-1}	A	cm^{-1}	A	cm^{-1}
2558	39087	2566	38961	2574	38850
2632	37988	2628	38056	2639	37892
2701	37025	2692	37154	2707	36948
2767	36144	2964	36176	2786	35891
2854	35042	2841	35198	2865	34910
2941	34000	2936	34062	Mg absorption band	
3037	32925			3046	32829
3142	31827			3152	31725
3237	30896			3239	30873
3355	29804			3346	29890
3481	28730			3472	28800
3637	27497			3609	27710
3777	26475			3758	26606
3936	25408			3925	25477

As discussed in Sections IVB and C, this molecular band system is not due to oxygen molecules or ozone alone. Without magnesium in the matrix we do not observe any molecular system in this region. Also the result of calcium + oxygen reaction products does not give any molecular band in this region. If this band system is due to oxygen molecules it should appear in the calcium + oxygen experiments or upon isolation of pure oxygen molecules in matrices. More experiments are necessary in order to make a conclusive determination and assignment of this band system. Also a similar band in the region of 5000-3750A as in a Ca + O system is observed with Mg + excess oxygen in rare gas (rare gas:oxygen= 1:1). This system does not appear with small oxygen concentration.

(b) Infrared spectra of magnesium + oxygen molecules

The reaction of magnesium atoms or polymers with oxygen can form many possible different molecules, i.e., MgO, MgO_2, Mg_2O, MgO_3, etc. Many of these molecules are not stable in high temperature environment or they may disintegrate or disproportionate into other molecules. But most of them are stable at low temperature, i.e., Mg_2O,[123] $Mg(O_2)_2$.[124]

Many absorption bands are observed in the region from 4000 to 550 cm^{-1}. By trapping Mg and O_2 in xenon matrix a band appears in 3700 cm^{-1}. This is considered to be the hydroxyl OH stretching band of $Mg(OH)_2$. The reported value of OH stretching[125,126] is 3698 cm^{-1}. This band does not appear very often. Its appearance would imply that the system is not quite dry. There are two strong sharp bands, one at 1528 cm^{-1} and the other at 995 cm^{-1}. These two bands increase as the metal concentration. By discharging the oxygen-rare gas mixture these two bands become invisible and a strong band at 1026 cm^{-1} appears and it increases faster than any other absorption as deposition time increases. This band may be due to MgO_3. Bands like 1583 cm^{-1}, 1015 cm^{-1} and 780 cm^{-1} are observed with an undischarged gas mixture, but the area under these

peaks increases very slowly in comparison with the two strong sharp absorptions.

All the observed bands in xenon matrix are also observed in the krypton matrix except for a little shift due to the different matrix gas. The observed bands are tabulated in Table XIX. The results of the magnesium atom reacted with the discharged oxygen rare-gas mixture are shown in Table XX. The results from the xenon matrix are almost the same as in krypton except for a small matrix shift. No features in either case, i.e. undischarged or discharged gas mixtures, can be related to the fundamental vibrational frequency of MgO $X^1\Sigma^+$ state. But with the oxygen isotope substitution experiment we should be able to distinguish the features that are due to MgO or magnesium oxygen compound with more than one oxygen atom per molecule.

ii. CaO

(a) Visible spectra of calcium + oxygen

Calcium atoms and oxygen molecules have been codeposited with rare gases at 18°K on CsBr target. Molecular bands appear in the region of 5000-3750A. The xenon-matrix absorption spectra of $Ca+O_2^{16}$ and $Ca+O_2^{18}$ are shown in Fig. 25. This figure comes from the densitometer tracing and was normalized by using an arbitrary base line. The bands are, in general, rather broad. The wavelengths of the bands are tabulated in Tables XXI and XXII.

The (0,0) bands of most of the systems observed in krypton and xenon matrices are established by the replacement of ^{16}O by ^{18}O in $Ca+O_2$. This isotopic substitution causes only a small shift in the (0,0) bands, but increases shift to the red of the (1,0),(2,0), etc., levels in a particular system. The isotope shift also seems to indicate that all the observed

Table XIX. Infrared absorption of Mg + O_2 in solid matrices (in cm^{-1})

O_2	Kr	Xe	Remark
	3730		$\nu_3(H_2O)$
	3710	3700	$(OH)_2$ Mg(?)
	1586	1583	$\nu_2(H_2O)$
	1528	1528	MgO_x
1150	1016	1015	MgO_y
842	996	995	MgO_z
798		780	
700			
668			

Table XX. Infrared absorption of Mg + O_2 (discharged) in solid matrices

O_2	Kr	Xe	Assignment
	3740		$\nu_3(H_2O)$
	3710		$(OH)_2Mg$ (?)
	2350		$\nu_3(CO_2)$
	1590		$\nu_2(H_2O)$
		1550	
	1528	1538	MgO_x
1150			
1030	1035	1026	ν_3 (O_3) ?
	1015		MgO_y
	995		MgO_z
842	820		
798			
700		698	
668			

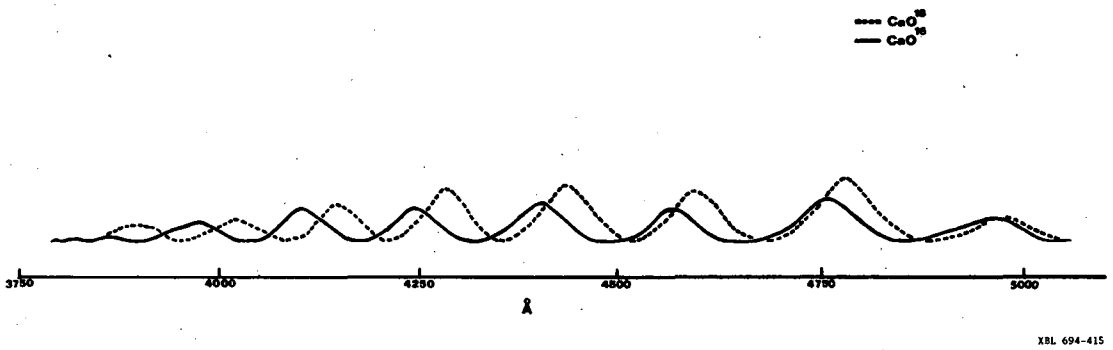

Figure 25

Table XXI. Absorption bands of CaO in a Xe matrix at 18°K

v'	CaO^{16} λ, Å	CaO^{16} ν, cm^{-1}	CaO^{16} $\Delta G'_{v+1/2}$, cm^{-1}	CaO^{18} λ, Å	CaO^{18} ν, cm^{-1}	CaO^{18} $\Delta G'_{v+1/2}$, cm^{-1}	$\nu-\nu_i$, cm^{-1}	$\rho = \frac{\nu^i_{osc}}{\nu_{osc}}$
0	4968.4	20127		4976.9	20093		24	
			889			816		0.918
1	4758.4	21016		4782.6	20909		107	
			887			849		0.968
2	4567.7	21893		4596.0	21758		135	
			820			780		0.951
3	4402.8	22713		4436.9	22538		175	
			826			811		0.981
4	4248.3	23539		4282.9	23349		190	
			839			793		0.945
5	4102.1	24378		4142.1	24142		236	
			758			732		0.965
6	3978.3	25136		4020.3	24874		262	
			745			796		1.07
7	3863.8	25881		3895.6	25670		211	

Table XXII. Molecular bands of Ca + O_2 in krypton matrix at 18°K

CaO^{16}			CaO^{18}		
λ,A	ν,cm^{-1}	$\Delta G'_{v+1/2}$,cm^{-1}	λ,A	ν,cm^{-1}	$\Delta G'_{v+1/2}$,cm^{-1}
4910	20367		4918	20333	
		811			738
4722	21178		4746	21071	
		829			763
4544	22007		4580	21834	
		778			826
4389	22785		4413	22660	
		916			787
4219	23701		4265	23447	
		719			813
4083	24492		4122	24260	
		397			548
4034	24789		4031	24808	
		415			777
3966	25214		3893	25685	

bands belong to the same system because of a systematic increase in an isotope shift.

For $Ca+O_2^{16}$ in krypton the bands tend to split as the v' value goes up and this makes it difficult to interpret the spectra. The O_2^{18} substitution does not make the interpretation easier and it is very difficult to find the corresponding band in both oxygen isotopes. There is a possibility that at least two band systems are overlapping each other in this region and they may belong to different absorbers with different numbers of oxygen atoms in each molecule. The absence of this type of splitting in a xenon matrix may have been caused by the bands being too broad or the xenon not being a good matrix for the study of electronic transitions.

There is no band in the region 2300A-6000A other than the one mentioned.

There is no analyzed CaO gas phase band in this region nor is there any observed CaO electronic state with the same spectroscopic characteristic as the one observed in the matrix, but there are many unanalyzed bands in this region in the gas phase. If the observed band does belong to CaO then it would serve as strong evidence to support the theory that the observed $X^{1}\,{}^{1}\Sigma$ is not the ground state. It is very likely that CaO has a triplet ground state since none of the singlet-singlet transitions has been observed in the matrices.

From the Ca atomic work in Section III, oxygen work in Section IV, and many calcium-oxygen mixture experiments we can say for sure that the band observed in calcium-oxygen system is due to molecules which contain calcium and oxygen.

The theoretical ratio of $\nu(CaO^{18})/\nu(CaO^{16})$ is 0.9594, but because

of anharmonicity one expects the observed ratio to be slightly higher than this.

(b) Infrared spectra of calcium + oxygen molecules

The infrared spectra of the products from the reaction of calcium atoms with oxygen molecules are not as easily interpreted as one might expect, since they are not always reproducible. Furthermore, relatively little is known about the vibrational spectra of calcium oxides. There are many possible products, e.g. CaO, CaO_2, Ca_2O, Ca_2O_2, OCaO, etc. Whichever product one obtains depends very much on what kind of environment the Ca atoms and oxygen molecules are found. The oxygen isotope substitution is helpful in determining the number of oxygen atoms in a particular molecule.

The infrared absorption bands of Ca + O_2^{16} and Ca+O_2^{18} in both krypton and xenon matrices are shown in Fig. 26 and their positions are tabulated in Table XXIII.

The theoretical ratio of $\nu(CaO^{18})/\nu(CaO^{16})$ is 0.9594. From Table XXIII we obtain a value of 0.946 for 1040 cm^{-1} and 794 cm^{-1} bands in krypton matrices and 0.956 for 695 cm^{-1} band in krypton matrices. A closer look at Fig. 20 and Fig. 26 seems to indicate that the reaction products of Ca+oxygen system are O_3 and CaO.

iii. BaO

Barium oxide has the same number of outer electrons - eight electrons- as MgO and CaO. Theoretically it should have the same molecular electronic states as MgO and CaO. Our knowledge of the lowest energy state of BaO is more confirmative. The work by Wharton et al.[127] indicates that the lowest observed electronic level $X^{1}\Sigma$ is the ground state and that there

Table XXIII. Infrared absorption of Ca + O_2 in rare gas matrices (in cm^{-1})

	Assignment	O_3	CaO	O_3
Kr	O^{16}	1040	794	695
	O^{18}	984	758	665
	$\rho = \frac{\nu^{i}_{osc}}{\nu_{osc}}$	0.946	0.955	0.956
Xe	O^{16}	1038	794	691
	O^{18}	980	750	660
	$\rho = \frac{\nu^{i}_{osc.}}{\nu_{osc.}}$	0.944	0.944	0.955

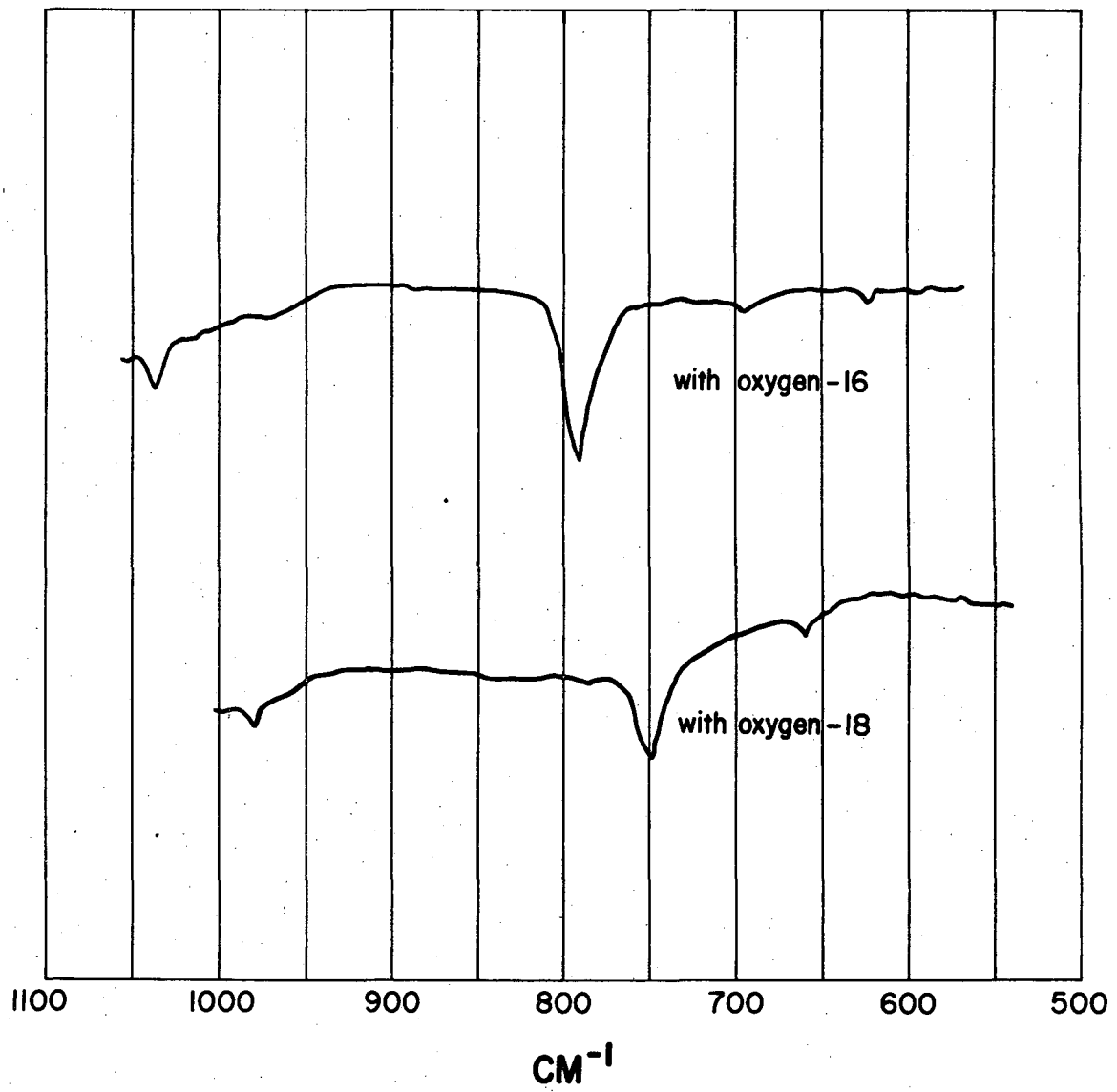

XBL 699-5683

Figure 26

are no states within 4000 cm^{-1}. But this does not mean that it is a singlet state. It is still possible that this state is one of the components of a triplet state. Possibly, because the splitting of this heavy molecule is so large that it does not effect the thermodynamic calculation too much. Also the dissociation energy of the BaO molecule obtained from the Birge-Sponer extrapolations agrees very well with the thermodynamic study whereas there is a large discrepancy for MgO and CaO between their spectroscopic study and thermodynamic study. An added advantage of studying BaO is that we can obtain fairly large amounts of BaO molecules by vaporizing the BaO solid at relatively low temperature. For MgO and CaO, however, the mass spectrometry studies show that they vaporize mostly into atomic species and they also need a relatively high temperature to have enough molecular concentration for absorption studies. This would create problems for isolation of impurity due to radiation heating. If we can obtain the same spectrum of BaO by these two processes: (a) synthesizing BaO the same way as MgO and CaO, and (b) vaporizing BaO directly from the BaO solid, then we can make a more confirmative conclusion for the result we obtain from synthesizing MgO and CaO. This method can be utilized for snythesizing many other high temperature molecules.

The experiments of synthesizing BaO has been done and molecular bands have been observed in the visible region. Infrared spectra of barium+oxygen has been recorded. The source of barium available was not very pure. This caused difficulty in the analysis of the spectra but nevertheless the primary results seemed to indicate there is a band system which resembles observed singlet-singlet transition in the gas phase with a slight matrix shift. There are many bands in the infrared spectra. Oxygen isotope substitution is needed in order to make the assignment of each band.

More experiments are needed in barium oxide studies in order to have a better understanding. The positions of observed absorption bands are shown in Table XXIV. The infrared spectra are shown in Fig. 27. A summary of assignments of each infrared band is in Table XXV.

c. Discussion

The measurement of the optical spectra of MgO, CaO and BaO began with the purpose of making quick confirmatory investigations of the gas phase results. However, several interesting facts immediately became apparent: 1) The perturbations of the molecules in matrices are great, as evidenced by band widths. 2) The vibrational spacings appear irregular but within the accuracy of measuring the peak positions, it is not clear that the irregularity is real. 3) The molecular bands observed from reaction products of Mg + oxygen and Ca + oxygen cannot be related to any of the analyzed gas phase transitions. 4) The oxygen isotope shift increases systematically with v'.

The reactions of alkaline earth atoms with oxygen produce many different molecules, i.e. MO, MO_2, $M(O_2)_2$, M_2O, $M(O_3)_2$, etc. Infrared spectra of these molecules are not known because most of them are ionic in character or their ions are not infrared active. For example, we would not expect to see any infrared spectra of peroxide ion, $O_2^=$, or superoxide ion, O_2^-, because their geometrical structures suggest that they are infrared inactive. Also peroxide ion provides no absorption in the visible region whereas the O_2^- at room temperature has an absorption spectrum in the visible. Thus all superoxides are colored, and their color range is yellow to orange.

Table XXIV. Molecular bands of Ba + O_2 in Kr matrix at 20 K

λ,A	ν,cm^{-1}	$\Delta G'_{v+1/2}$,cm^{-1}
4518	22135	
		606
4397	22741	
		935
4220	23694	
		850
4074	24544	

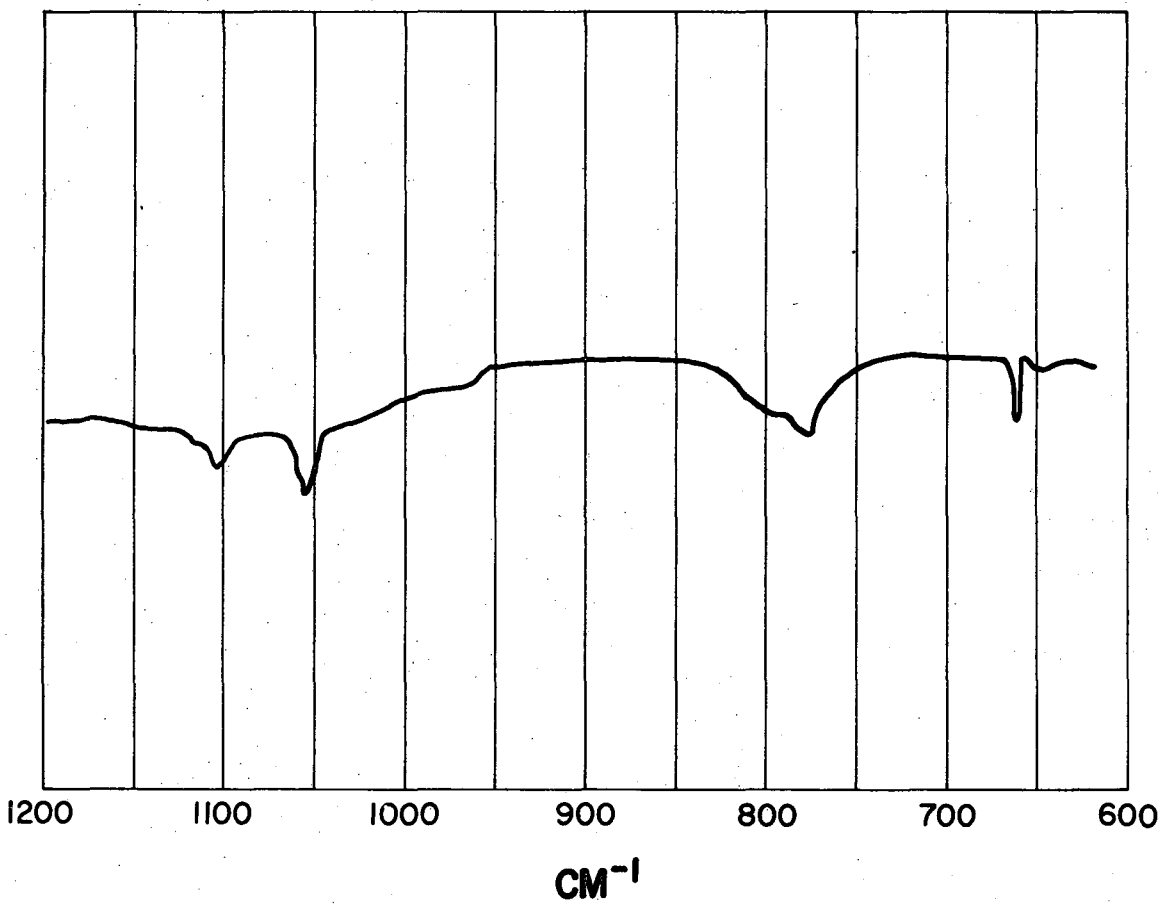

XBL 699-5675

Figure 27

Table XXV. Infrared absorption of Ba + O_2 in rare gas matrices (in cm^{-1})

T=20°K O_2	T=18°K Kr	T=20°K Xe	Assignment
3800		3850	
3730	3730	3750	(OH) (?)
3320			$\nu_1(H_2O)$
	2370	2375	
2350	2340	2350	$\nu_3(CO_2)$
1640			
1620			$\nu_2(H_2O)$
	1109	1105	BaO_x
	1056	1055	BaO_y
	780	780	BaO_z
		662	$\nu_2(CO_2)$

Spectra of O_2^- have been reported.[128] Single crystals of NaCl, KCl, and KBr are grown from the melt in an oxygen atmosphere, and their optical absorptions spectra are measured at 300, 77, and 4.2K. The weak absorption band caused by oxygen is the same in all three crystals, and does not vary with temperature. The band has a maximum absorption at 5.0 eV (40335 cm^{-1}) and a half-width of 1.0 eV. At 300 K, 12 to 15 peaks are resolved, and at 4.2 K each of these peaks split into 4 to 6 components. From the optical results and from paramagnetic resonance experiments,[129] it is concluded that O_2^- ions are responsible for the absorption. Rolfe[130] also has studied O_2^- fluorescence emission spectra at 4.2 K in NaF, NaCl, NaBr, KCl, RbCl, KBr, RbBr, and KI, and he estimates the ω_e value for ground state to be 1170 cm^{-1}, and an unharmonicity $\omega_e X_e$ of 8.5 cm^{-1}.

The absorption band in the visible region observed in this work normally appears only when there is a high oxygen concentration. ($\sim Xe:O_2:M = 1000:1000:1$). The band observed in the Ca+oxygen system seems to give a systematic isotope shift. And very likely it is due to an absorber that is made up of more than one oxygen atom. The products are yellow in color. In many respects they resemble the O_2^- absorption in alkaline halide crystals yet the vibrational spacing of this band system is $\sim$ 300 cm^{-1} off from that of O_2^- in alkali halide crystals. It should be noted too that this band does not appear when alkaline earth atoms and oxygen are deposited without the rare gas. This would also tend to reject the possibility of O_2^- as the absorber. A metallic atom has to be deposited in order to have the spectra. This would lead us to conclude that the molecular band system in the visible region is due to some alkaline earth oxide molecules with more than one oxygen atom per molecule. Observation of this molecular band with a slow deposition rate

and a very dilute metal concentration would suggest that the molecular absorber has only one alkaline earth atom per molecule but this would need further evidence for confirmation. Alkaline earth isotope substitution would be helpful.

The molecular band in the region from 2500 to 4000A in Mg + oxygen systems appears only when the oxygen-rare gas mixtures are discharged. This means that we should have a mixture of oxygen atoms and ozone other than oxygen molecules. The deposition of discharged products without metal failed to show any molecular structure in this region except a continuum in the 2500A region which should be due to ozone[105] as discussed before. This seems to suggest that the molecular band is due to some alkaline earth metal oxide absorber. The concentration experiments would suggest that there is one alkaline earth atom per molecule. The number of oxygen atoms per molecule is hard to estimate without an oxygen isotope substitution result. The appearance of a 1016 cm^{-1} band in the Mg + oxygen/xenon (through discharge) would suggest the production of magnesium ozonide. This band has a shift of approximately 16 cm^{-1} from the ozone 1032 cm^{-1} band. No ozone infrared band has been observed when metal is deposited together with discharged oxygen mixture. The appearance of a molecular band with the disappearance of a magnesium triplet absorption would tend to suggest that the molecular band may be due to the reaction of magnesium atom and oxygen atom and not the ozonide because the diffusion of magnesium and ozone are not considered to be important compared to oxygen atoms. More experiments are necessary to make a more confirmatory identification of the molecular species.

The green system of the MgO gas phase transition which lies around 5000A has been thought to involve the transition from the ground

electronic state. If this is really so, then we should observe it in the matrix too. Even taking "matrix shift" into consideration we find it difficult to relate the observed violet band to any of the analyzed band systems or states that are involved. Actually the large matrix effects are not unusual among matrix isolated atomic spectra, but this is not so for molecules, i.e. TiO, ZrO, HfO,[131] etc.

The infrared spectra of a Ca + oxygen system have three features that we consider to be due to calcium oxide compounds. From the relative intensity change and the ν_i/ν ratio we would suggest that 1038 cm^{-1} and 691 cm^{-1} bands are due to an O_3 molecule with more than one oxygen atom per molecule, and the 794 cm^{-1} band is probably due to CaO.

The electronic transition in the visible region shows a regular oxygen isotope shift.

Based on the results of the infrared bands we would consider that CaO is the major species that is being trapped, and we would suggest that the strong band system is due to transition of CaO. There is no other band system in the other spectral regions. This would mean that the CaO bands that overlapped with other bands in the observed spectra should be the transition of CaO involving the ground state. A quick examination of the CaO gas phase spectrum in the corresponding region does show some band system but they are still unanalyzed. A full understanding of these gas phase band systems would be helpful in determining the ground or low-lying electronic states of CaO.

V. CONCLUDING REMARKS

The present work indicates the importance of the study of concentration, temperature dependence of matrix-isolated atomic spectra of Mg, Ca, Ba, Cd and Pb. It also indicates the importance of the study of the crystal structure of the doped crystal prior to interpretation of multiplet splitting.

Results of alkaline earth-xoygen reaction products are very interesting but these can only serve as a small effort towards understanding of the spectroscopic characteristic of these high temperature molecules and the feasibility of matrix isolation techniques in synthesizing high temperature molecules. It is evident that there is a need for more detailed study of the alkaline earth oxides using infrared and mixed isotopes in order to have a better understanding of the species trapped in the matrices.

ACKNOWLEDGEMENTS

I am deeply grateful to Professor Leo Brewer for his insight and guidance throughout this work.

I also thank all who have been part of Professor Brewer's research group, and all of the technicians, machinists, glass blowers, and others who have helped in my research.

This project was performed under the auspices of the United States Atomic Energy Commission.

TABLE I. Silver absorption lines.

Matrix	Absorption maxima at 20°K (cm^{-1})	Comparison with gas-phase spectra: Shift assuming small splitting, $^2P_{1/2}$	Shift assuming small splitting, $^2P_{3/2}$	Shift assuming large splitting, $^2P_{1/2}$	Shift assuming large splitting, $^2P_{3/2}$
Xenon	29 710	158		158	
	30 423	871			−50
	30 595		122	1043	
	30 925		452		452
Krypton	30 881	1329		1329	
	31 857	2305			1384
	32 334		1861	2782	
	33 286		2813		2813
Argon	30 930	1378		1378	
	31 732	2180			1259
	32 929		2456	3377	
	33 522		3049		3049

target, had a radially cut effusion hole, 1.02-mm diam, and was shielded by tantalum foil with a 6.4 mm× 9.55-mm aperture. In a typical experiment the silver vapor pressure was computed to be 3×10^{-4} torr from the furnace temperature of 840° to 880°C as measured with an optical pyrometer. The experimental arrangement is shown in Fig. 1.

The matrix gas flow was controlled by an independent inlet system and the quantity of condensed gas was estimated from the geometry of the system and the calibrated leakage rate.[2] During deposition the cryostat pressure, measured at a point 7.6 cm above the target, was always less than 8×10^{-6} torr. The estimated value of M/R (moles of matrix/moles of radical) was typically of the order of 1000.

The silver (99.95%, Englehard Industries, Incorporated) and Linde high-purity rare gases were used without further purification. In a typical experiment about 0.4 mM of matrix were deposited at a rate of about 0.2 mM/h. With liquid hydrogen in the cryostat the pressure before deposition was less than 5×10^{-6} torr and during deposition rose to 8×10^{-6} torr.

For warmup experiments the liquid hydrogen was allowed to evaporate and successive spectra were photographed continuously as the matrix warmed up. Up to 50°K the target temperature increased at approximately 10°K/min. In some experiments the matrix warmup was quenched by the reintroduction of liquid hydrogen.[2]

Spectra were photographed in the region 2400–4000 Å using a Jarell–Ash $f/6.3$ Czerny–Turner spectrograph with a 2160-lines/mm grating blazed for 3000 Å giving a first-order dispersion of 5 Å/mm.

RESULTS

General

In the gas phase the resonance lines of silver occur at 3280.7 Å (30 473 cm^{-1}) for the $^2P_{3/2}\leftarrow{}^2S_{1/2}$ transition, and 3380.9 Å (29 552 cm^{-1}), for the $^2P_{1/2}\leftarrow{}^2S_{1/2}$ transition. In each of the three matrices studied, at 20°K, four absorption lines appeared at shorter wavelengths than the gas wavelengths. The smallest shifts were observed in xenon and the largest in argon with xenon and krypton showing the most clearly resolved spectra. Changes of a factor of 5 in the M/R ratio did not affect the spectra. Table I lists the wavenumbers of the absorption maxima observed for the three matrices. Typical microphotometer tracings of spectra obtained from what we believe are well-isolated silver atoms are shown in Fig. 2. During warmup experiments some bands exhibited further shifts with respect to the gas-phase transitions which were, within the experimental accuracy, linear functions of temperature.

Xenon

The absorption spectra of well-isolated silver atoms at 20°K showed three distinct but partially overlapping regions of comparable intensity. The central region, with a total half-width of about 400 cm^{-1}, consisted of a doublet, the longer-wavelength portion accounting for approximately two-thirds of the total half-width. The half-width of each of the outer maxima was about 180 cm^{-1}.

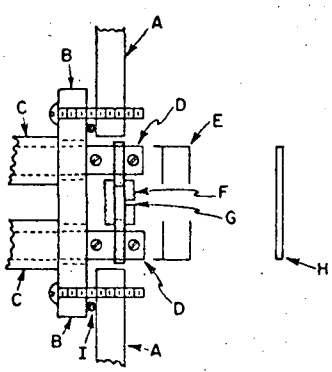

FIG. 1. Arrangement for carbon resistance furnace, scale approximately 1:1. A, vacuum chamber wall; B, flange; C, Kovar–ceramic seal for water-cooled electrodes; D, copper electrodes; E, radiation shield; F, carbon resistance furnace; G, effusion hole; H, sapphire target maintained at 20°K; I, vacuum O ring.

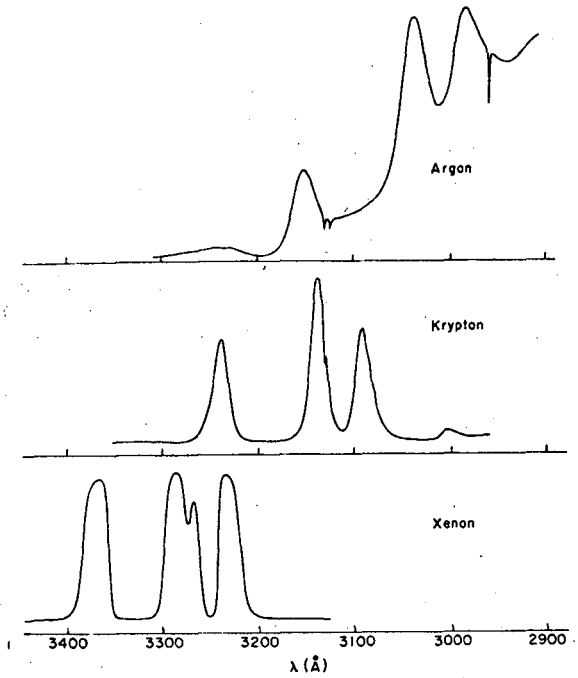

FIG. 2. Absorption spectrum of well-isolated silver atoms in rare-gas matrices at 20°K. The sharp emission lines are mercury.

The effect of warming the matrix is shown in Figs. 3 and 4. The following points were observed: (1) The position of the short-wavelength component of the central doublet remained constant and its intensity relative to the other bands decreased considerably. (2)

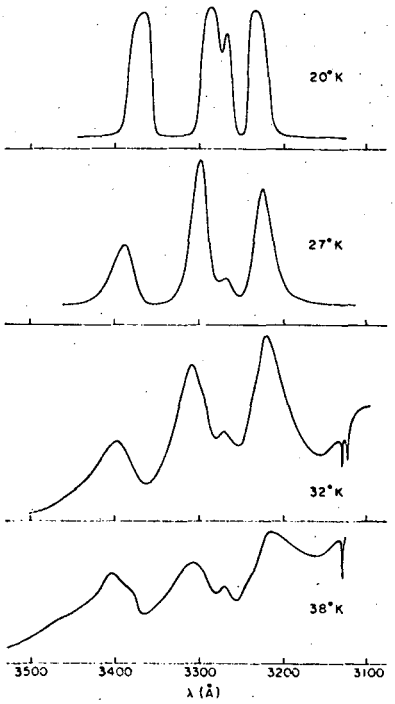

FIG. 3. Effect of temperature on the absorption spectrum of silver in xenon. The sharp emission lines are mercury.

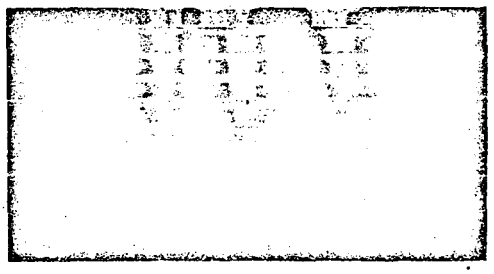

FIG. 4. This photograph shows clearly the effect of increasing temperature on the absorption spectrum of silver in xenon. The bottom exposure was taken at 20°K. The band on the left occurs at ~3400 Å, the band on the right at ~3200 Å.

The long-wavelength component of the doublet shifted towards longer wavelengths at ~14 $cm^{-1}/°K$. (3) The long-wavelength band also shifted to longer wavelengths at approximately 24 $cm^{-1}/°K$. (4) The short-wavelength component shifted to shorter wavelengths

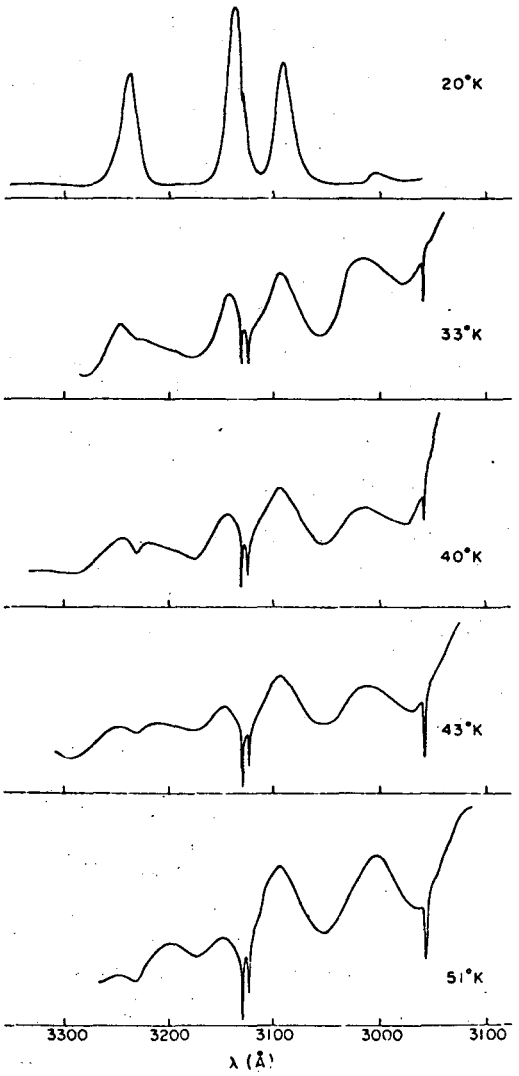

FIG. 5. Effect of temperature on the absorption spectrum of silver in krypton.

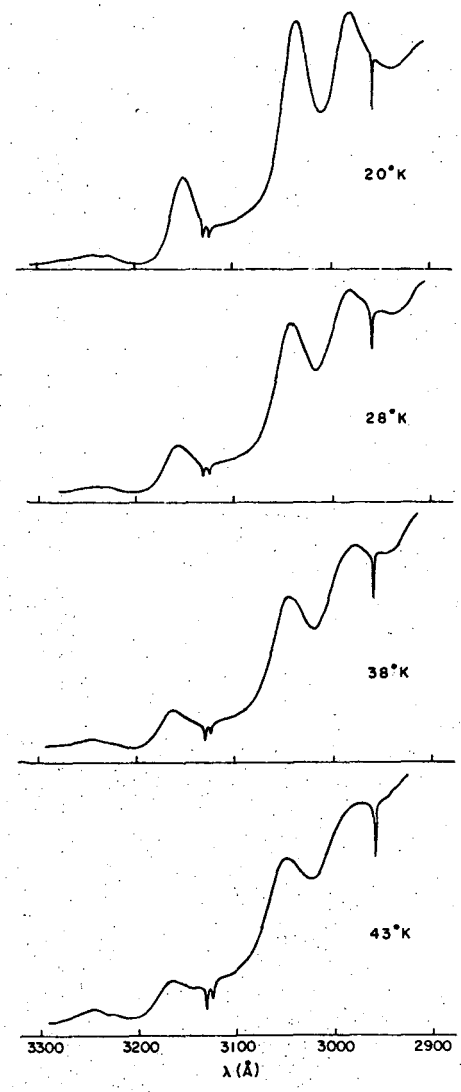

FIG. 6. Effect of temperature on the absorption spectrum of silver in argon. The sharp emission lines are mercury.

at ~11 cm^{-1}/°K. (5) At 35°K the half-width was about twice that at 20°K. (6) When the matrix was warmed to ~45°K and then rapidly quenched to 20°K the original structure and bandwidth were obtained.

Krypton

For krypton the absorption spectrum of well-isolated silver atoms showed three distinct bands of similar intensities with half-widths of about 170 cm^{-1}. These were similar to those observed with xenon but there was no central doublet. However, another weak band was observed at shorter wavelengths.

Spectra obtained as the matrix warmed up are shown in Fig. 5. Up to 40°K none of the three strong bands showed any significant shift. A new band appeared at longer wavelengths and between 40° and 50°K this energy band showed a blue shift of ~23 cm^{-1}. (In some krypton matrices another weak band appeared at 25 541 cm^{-1} and remained constant when the temperature changed.) At 50°K the half-width was nearly twice that at 20°K. On rapidly quenching a matrix warmed to 50°K the original structure and bandwidth were again recovered.

Argon

The absorption spectrum of silver atoms in argon showed three distinct absorptions of comparable intensity with another weaker band at longer wavelengths. The half-widths were approximately 300 cm^{-1}. During warmup experiments the high-energy band showed a small blue shift of ~3 cm^{-1}/°K and the other bands showed red shifts of similar magnitudes. In all cases the half-widths had doubled at about 40°K and above 45°K the bands disappeared. Once a warmup experiment was started it was difficult to quench argon matrices before the absorption bands disappeared and reversible temperature effects were not observed with these matrices. Spectra obtained as the matrix warmed up are shown in Fig. 6.

DISCUSSION

In each of the three matrices four absorption features were observed. Since these bands occurred only when the matrices were left below the estimated diffusion temperature,[9,10] it might be assumed that the spectra are due to isolated silver atoms and their interaction with the host lattice. If it is assumed that the four features are due to doublet splitting of each of the gaseous spectral lines, the assignment of the features depends upon one of two possible assumptions: (a) The splitting is small, or (b) the splitting is comparable to or greater than the $^2P_{3/2}-{}^2P_{1/2}$ energy difference. The energy shifts with respect to the gaseous spectrum are listed in Table I and the splittings are shown in Table II. From studies of the parameters listed in Tables I and II no clear pattern emerges. On the assumption of either small or large splitting the splitting is always greater for the $^2P_{1/2}$ level than for the $^2P_{3/2}$ level. For the large splitting case, there is a consistent increase of splittings from Xe to Kr to Ar. Also on this basis the blue shifts from the gas-phase transitions increase from Xe to Kr to Ar (with the exception of the two of the lines in Ar). These blue shifts follow the trends observed with other atomic species in rare-gas matrices where in general the argon matrix shows the largest blue shift and xenon, the most polarizable matrix, shows the

[9] Small impurities diffuse rapidly and cannot be preserved for periods of many minutes if the temperature is allowed to rise to ~0.5 times the melting point of the pure matrix material; see G. C. Pimentel, "Radical Formation and Trapping in the Solid Phase," Ref. 10.

[10] *Formation and Trapping of Free Radicals*, A. M. Bass and H. P. Broida, Eds. (Academic Press Inc., New York, 1960).

TABLE II. Energy splitting of silver absorption lines.[a]

Gas-phase transition[b]	Small splitting assumption			Large splitting assumption		
	Xe	Kr	Ar	Xe	Kr	Ar
29 552 $^2P_{1/2}$	713	976	802	885	1453	1999
30 473 $^2P_{3/2}$	330	952	593	502	1429	1790

[a] In cm^{-1}.

[b] Gas phase separation $^2P_{3/2}-{}^2P_{1/2}$ is 921 cm^{-1}.

smallest.[1,2,5,11] In the gas phase the $^2P_{3/2}\leftarrow{}^2S_{1/2}$ transition is stronger than the $^2P_{1/2}\leftarrow{}^2S_{1/2}$ transition; however it is not clear how these different intensities are reflected in the matrices.

The reason for the splitting of the expected two absorption bands into the observed four bands is not known. It may be due to the removal of the orbital degeneracy of the P states of the trapped atoms as suggested for magnesium atoms in argon matrices.[12] Distorted impurity sites with more than one adjacent vacancy would have to be considered to explain the experimental observations. So far no information is available about the silver atomic sites. Different lattice sites have been quoted in studies of alkali atoms.[3] For mercury in inert-gas matrices[2] it was believed that multiple sites were not responsible for the splitting of the triplet state ($^3P_1$). The large multiplet splitting in the gas for the ^2P state of gold provides a less ambiguous correlation between the matrix and gas spectra. Preliminary work on Au isolated in Kr shows a single feature at 2612 Å (2675 Å in gas) and a doublet at 2333 and 2360 Å (2427 Å in gas) which suggests that the matrix provides a weak electric field which can split a $^2P_{3/2}$ state but which can only shift a $^2S_{1/2}$ or $^2P_{1/2}$ state. This behavior can be reconciled with the silver observations if the relatively weak components for Ag in Kr and Ar at 3004 and 3233 Å, respectively, are attributed to Ag_2 on the basis of their observation only with relatively large concentrations of Ag. This explanation would not be applicable to xenon matrices where one would have to assume that the field is large enough to split further degenerate terms. The limited amount of experimental data presently available indicate that experimental conditions of deposition can greatly influence matrix spectra.[3,11]

Shift theories for mercury atoms in argon, krypton, and xenon matrices were based on a Lennard-Jones potential between the trapped mercury atom and the rare-gas atoms, but this model breaks down for neon matrices.[1] To explain the observed shifts with alkali atoms in inert-gas matrices, atomic sites were compared with F centers in alkali halide crystals.[11] However, there are insufficient data available at the moment to see if either of these techniques can also be applied to silver atoms in matrices.

During warmup of the matrices both blue and red shifts were observed for the absorption maxima together with increases in bandwidth. Similar red shifts have been observed for copper, gold, and mercury in matrices and the reversibility range (20° to about 50°K) is also comparable.[2,13] The observation of simultaneous red and blue shifts with temperature as observed for argon and xenon constitute a new factor to be considered in matrix work; these temperature shifts are probably due to lattice expansion (~1% over the temperature range studied[14]) and changes in the rigidity of the matrix.[3] Some absorption maxima did not show any temperature shift and this suggests strong interaction between silver atoms and either the matrix or other silver atoms.

The reversibility of line position during annealing suggests that at 20°K silver exists in only one site, namely the most stable. Thus silver differs from Na, K, and Rb, where irreversible loss of a set of lines during annealing[3] and other effects proved the presence of multiple sites. An F-center model[11] which predicts an increase in bandwidth with increasing temperature together with a red shift for impurity absorption lines[15] might possibly be applied here. The present results do not resolve the question of the origin of the observed silver features. It is hoped that additional work with copper and gold and with mixtures of all three metal atoms in a variety of matrices will distinguish solute-solute interaction from multiple site effects. If a clear understanding of the atomic spectra in matrices can be obtained, it will be possible to deal with molecular spectra more confidently.

ACKNOWLEDGMENT

This work was performed under the auspices of the U.S. Atomic Energy Commission.

[11] W. Weyhmann and F. M. Pipkin, Phys. Rev. **137**, A490 (1965); S. L. Kupferman and F. M. Pipkin, *ibid.* **166**, 207 (1968).
[12] M. Brith and O. Schnepp, J. Chem. Phys. **39**, 2714 (1963).
[13] B. Meyer (private communication).
[14] G. L. Pollack, Rev. Mod. Phys. **36**, 748 (1964).
[15] C. C. Klick and J. H. Schulman, Solid State Phys. **5**, 97 (1957).

APPENDIX B

ESTIMATION OF Mg_2 CONCENTRATION IN KNUDSEN CELL

$$M_2(g) \rightleftharpoons M(g) + M(s)$$

Assuming a linear Birge-Sponer extrapolation

$$D_e = D_o + \frac{1}{2}\omega_e - \frac{1}{4}X_e\,\omega_e$$

$$424 = D_o + \frac{1}{2}(51.1) - \frac{1}{4}(1.65)$$

$$D_o = 424 - 25.5 + 0.41$$

$$= \frac{399\ \text{cm}^{-1}}{3.498\times10^2} = 1.141\ \text{kcal/}$$

$$\Delta H_0\ (\text{vap. Mg}) = \underline{\underline{35.28\ \text{kcal}}} \qquad \text{JANAF}$$

$$D_0\ (Mg_2) = 1.141\ \text{kcal}$$

$$\alpha = \frac{\Delta H_0^\circ\ (\text{vap. Mg})}{D_0^\circ\ (Mg_2)} = \frac{35.3}{1.141} = 30.91$$

$$RT\ \ell n\ \frac{P(M_2)}{P(M)} = \Delta H_0^\circ\ (\text{vap. Mg})\ \left(\frac{1-\alpha}{\alpha}\right) + T\Delta(\text{fef})$$

$$(\text{fef})_{M_2} = R\ [(7/2)\ell n\ T + (5/2)\ell n\ M + 2\ \ell n\ d] - 14{,}308 + \text{fef}_{vib} + \text{fef}_{el}$$

$$d_{Mg_2} \approx 3.889\text{Å}$$

$$R = 1.987\ \text{cal/deg mole}$$

$$\omega_e = 51\ \text{cm}^{-1}$$

$$u = \frac{hc\omega}{kT} = 1.4387\ \frac{\omega}{T}$$

For $T = 700°K$

$$u = 1.4387\ \frac{51}{700} = 1.4387 \times 0.07286 = 0.1048$$

$$\text{fef} = 2.3\ R$$

$$fef_{Mg_2} = -1.987 \{\frac{7}{2} \ln 700 + \frac{5}{2} \ln 24.3 + 2 \ln 3.88Å\}$$

$$+ 14.31 - 2.3 R$$

neglecting for the moment $(fef)_{el}$

$$fef_{Mg_2} = -1.987 \{\frac{7}{2} (6.5511) + \frac{5}{2}(3.191) + 2(1.356)\} + 14.31 - 2.3R$$

$$= -1.987 \{22.93 + 7.975 + 2.712\} + 14.31 - 2.3R$$

$$= -83.84 + 14.31 - 2.3 R$$

$$= -74.1$$

$$-fef_{Mg(g)} = 36.9$$

Stull and Sinke

$$-fef_{Mg(s)} = 13.3$$

$$\langle \Delta fef \rangle = - \langle fef_{M_2} \rangle + \langle fef_{M(s) + M(g)} \rangle + 2.2$$

$$= + 74.1 - 36.9 - 13.3 + 2.2$$

$$= 26.1 \text{ cal}/^\circ K$$

$$RT \ln \frac{P(M_2)}{P(M)} = 35{,}300 \left(\frac{-29.94}{30.94}\right) + 700 (26.1)$$

$$= 35{,}300 (-0.968) + 700 (26.1)$$

$$= -34{,}170 + 18{,}270$$

$$= -15{,}900$$

$$\ln \frac{P(M_2)}{P(M)} = - \frac{159}{7 \times 1.987} = - \frac{159}{15.9} = -10$$

$$\log_{10} \frac{Pm_2}{Pm} \approx - \frac{10}{2.303} = -4.34$$

$$\underline{\underline{P_{M_2} \sim 10^{-4.34} P_M}}$$

at 700°K $\begin{cases} P_{Mg} = 8\times10^{-3} \text{ mm Hg} \\ P_{Mg_2} = 8\times10^{-7.34} \text{ mm Hg} \end{cases}$

REFERENCES

1. Brewer, L., Principles of High Temperature Chemistry, in Proceedings of the Robert A. Welch Foundation Conference on Chemical Research. I. Topics in Modern Inorganic Chemistry, November 1962, Houston, Texas, Chapter 3, pp. 47-92.

2. Brewer, L., Nat. Acad. Sci.-Nat. Res. Council, Publ. No. 1470, 3 (1967).

3. Schofield, K., Chem. Rev. 67, 707 (1967).

4. Whittle, E., Dows, D. A. and Pimentel, G. C., J. Chem. Phys. 22, 1943 (1954).

5. Norman, I. and Porter, G., Nature (London) 174, 508 (1954).

6. Brewer, L. and Rosenblatt, G. M., preprint (1969) Dissociation Energies and Free Energy Functions of Gaseous Monoxides.

7. King, B. A., Ph.D. Thesis, University of California, Berkeley, UCRL-18618, 1968.

8. Brewer, L., King, B. A., Wang, J. L., Meyer, B. and Moore, G. F., J. Chem. Phys. 49, 5209 (1968).

9. Brabson, G. D., Ph.D. Thesis, University of California, Berkeley, UCRL-11976, 1965.

10. Weyhmann, W. and Pipkin, F. M., Phys. Rev. A137(2), 490 (1965).

11. Meyer, B., J. Chem. Phys. 43(9), 2986 (1965).

12. Kupferman, S. L. and Pipkin, F. M., Phys. Rev. 166 (2), 207 (1968).

13. Schnepp, O., J. Phys. Chem. Solids, 17, 188 (1961).

14. Brith, M and Schnepp, O., J. Chem. Phys. 39 (10), 2714 (1963).

15. Lee, E. L. and Gutmacher, R. G., J. Phys. Chem. Solids, 23, 1823 (1962).

16. Brewer, L., Meyer, B. and Brabson, G. D., J. Chem. Phys. 43, 3973 (1965).

17. Duley, W. W., Phys. Letters, 19, 361 (1965).

18. Duley, W. W., Proc. Phys. Soc. (London) 88 (4), 1049 (1966).

19. Duley, W. W., Proc. Phys. Soc. 90, 263 (1967).

20. Dressler, K., J. Quant. Spect. Rad. Transfer, 2, 683 (1962).

21. Shirk, J. S. and Bass, A. M., J. Chem. Phys. 49, 5156 (1968).

22. Duley, W. W., Nature, 210, 624 (1966).

23. Duley, W. W., Proc. Phys. Soc. 91, 976 (1967).

24. Duley, W. W., and Garton, W. R. S., Proc. Phys. Soc. 92, 830 (1967).

25. McCarty, M., Jr. and Robinson, G. W., Mol. Phys. 2, 415 (1959).

26. Andrews, L. and Pimentel, G. C., J. Chem. Phys. 47 (8), 2905 (1967).

27. Merrithew, R. B., Marusak, G. V. and Blount, C. Z., J. Mol. Spec. 29, 54 (1969).

28. Belyaeva, A. A., Predtechenskii, Y. B. and Shcherba, L. D., Opt. Spec. (USSR) (Eng. Trans) 24, 233 (1968).

29. Duley, W. W., Ph.D. Thesis, Imperial College, London, 1966.

30. Weltner, W., Jr., McLeod, D., Jr. and Kasai, P. H., J. Chem. Phys. 46, 3172 (1967).

31. Moore, C. E., Atomic Energy Levels, NBS Circular No. 467, Washington (1958).

32. Barger, R. L. and Broida, H. P., NBS Report 8200 (1965).

33. Hamada, H., Phil. Mag. 12, 50 (1931).

34. Guy, M., Roncin, J-Y. and Damany, N., Compt. Rend. 263, 546 (1966).

35. Chang, Chin-An, private communication.

36. Roncin, J.-Y, Damany, H. and Romand, J., J. Mol. Spect. 22, 154 (1967).

37. Kihara, T. J. Phys. Soc. (Japan) 6, 184 (1951).

38. Kihara, T. and Koba, S., J. Phys. Soc. (Japan) 7, (4), 348 (1952).

39. Kihara, T., J. Phys. Soc. (Japan) 15, 1920 (1960).

40. Meyer, L., et al., J. Chem. Phys. 41, 1078 (1964).

41. Debye, P., Polar Molecules, (Dover Publications, Inc., New York, 1929), Chapter II.

42. Kihara, T., Adv. Chem. Phys. 5, 186 (1963).

43. Losee, D. L. and Simmons, R. O., Phys. Rev. 172 (3), 934 (1968).

44. Zhitnikov, R. A., Kolesnikov, N. Y. and Kosyakov, V. I., J. Exptl. Theoret. Phys. (USSR) 43, 1186 (1962).

45. Bleaney, B. and Stevens, K. W. H., Repts. Progr. Phys. 16, 108 (1953).

46. Owen, J., Proc. Roy. Soc. (London) A277, 183 (1955).

47. Koide,S. and Aguchi, T., Adv. Chem. Phys. 5, 189 (1963).

48. Bartolo, B. D., Optical Interactions in Solids,(John Wiley and Sons, Inc. N.Y., 1968).

49. Bethe, H. A., Ann. Physik 3[5], 133 (1929).

50. London, F., Z. Physik. Chem., B11, 222 (1930).

51. Wolfsohn, G., Z. Physik, 63, 634 (1930).

52. Freedhoff, H. S., Proc. Phys. Soc. 92, 505 (1967).

53. Kuhn, H. and Arrhenius, S., Z. Physik, 82, 716 (1933).

54. Cram, S. W., Phys. Rev. 46, 205 (1934).

55. Winans, J. G., Phil.Mag. 7, 555 (1929).

56. Kovalyonok, G. V., et al., Izv. VUZ Fiz. 3, 27 (1968).

57. Balfour, W. J., Can. J. Phys., to be published.

58. Sthapitanonda, P., Ph.D. Thesis, University of Wisconsin, 1955.

59. Dobrotin, R. B., Solid State Chemistry (USSR)Eng. Transl.) 37 (1966).

60. Verhaegen, G., Stafford, F. E., Goldfinger, P. and Ackerman, M., Trans. Faraday Soc. 58, 1926 (1962).

61. Herzberg, G., Molecular Spectra and Molecular Structure. I. Spectra of Diatomic Molecules, (Van Nostrand, New York, 1950), 2nd. ed.

62. Jablonski, A., Z. Physik 45, 878 (1927).

63. Mohler, F. L. and Moore, H. R., J. Opt. Soc. Am. 15, 74 (1927).

64. Winans, J. G., Phys. Rev. 32, 427 (1928).

65. Jablonski, A., Bull. de l'Acad. Pol. d. Sc. et d.L. 10A, 163 (1928).

66. Winans, J. G., Nature, 123, 279 (1929).

67. Robertson, J. K., Phil. Mag. 14, 795 (1932).

68. Robertson, J. K., Nature, 135, 308 (1935).

69. Winans, J. G. and Cram, W. G., Nature 135, 344 (1935).

70. Garton, W. R. S., Proc. Phys. Soc. (London) 64A, 430 (1951).

71. Van der Lingen, J. S., Z. Physik 6, 403 (1921).

72. Mrozowski, S., Z. Physik 62, 311 (1930).

73. Kapuscinski, W., Nature 116, 170 (1925).

74. King, G. W. and Van Vleck, J. H., Phys. Rev. 55, 1165 (1939).

75. Franck, J. and Grotrian, W., Z. techn. Phys. 3, 194 (1922).

76. Koernicke, E., Z. Physik, 33, 219 (1925).

77. Winans, J. G., Phys. Rev. 37, 897 (1931).

78. Kuhn, H. and Frendenberg, K., Z. Physik 76, 41 (1932).

79. Kuhn, H., Proc. Roy. Soc. (London) 158, 212, 230 (1937).

80. Winans, J. G. and Heitz, M. P., Phys. Rev. 65, 65 (1944).

81. Winans, J. G. and Heitz, M. P., Z. Physik 133, 291 (1952).

82. Winans, J. G. and Heitz, M. P., Z. Physik 135, 406 (1953).

83. Mrozowski, S., Z. Physik 55, 338 (1929).

84. Gaydon, A. G., Dissociation Energies, 2nd. ed. (Chapman and Hall, London, 1953).

85. McLennan, J. G., Smith, H. D. and Wilhelm, J. O., Trans. Roy. Soc. Can. 84, 1 (1930).

86. Finkelnberg, W. and Steiner, W., Z. Physik 79, 69 (1932).

87. Poikhotko, A. F., Acta Physicochim (URSS) 10, 913 (1939).

88. Hörl, E., J. Mol. Spec. 2, 42 (1958).

89. Dressler, K. and Schnepp, O., J. Chem. Phys. 42 (1), 2482 (1965).

90. Bass, A. M. and Broida, H. P., J. Mol. Spec. 12, 221 (1964).

91. Schnepp, O., J. Chim. Phys. 63 (1), 189 (1966).

92. Landau, A., Albin, E. J. and Welsh, H. L., Spectrochim. Acta, 18, 1 (1962).

93. Prikhotko, A. F. and Pakhomova, O. S., Opt. i. Spekt 19, 916 (1965).

94. Prikhotko, A. F., Ptukha, T. P. and Shanskii, L. I., Opt. i. Spekt. 22 (3), 373 (1967).

95. Prikhotko, A. F., Ptukha, T. P. and Shanskii, L. I., Ukrainski Fizicheskii Zhurnal 12 (7), 1166 (1967).

96. Vanderslice, T., J. Chem. Phys. 32, 515 (1960).

97. Meason, E. A. and Marsh, W. G., J. Chem. Phys. 33, 614 (1960).

98. Herzberg, G., Can. J. Phys. 30, 185 (1952).

99. Wallace, L., Astrophys. J. Suppl. No. 68, 7, 165 (1962).

100. Broida, H. P. and Lutes, O. S., J. Chem. Phys. 24, 484 (1956).

101. Harvey, K. B. and Bass, A. M., J. Mol. Spect. 2, 405 (1958).

102. Wilson, M. K. and Badger, R. M., J. Chem. Phys. 16, 741 (1948).

103. Living, G. D. and Dewar, J., Proc. Roy. Soc. 46, 222 (1889).

104. Bass, A. M. and Broida, H. P., J. Mol. Spect. 2, 42 (1958).

105. Bailamonte, V. D., Snelling, D. R. and Bair, E. J., J. Chem. Phys. 44 (2), 673 (1966).

106. Sullivan, H. F., Technical Report No. 865, Dept. of Aerospace and Mechanical Sciences, Princeton University, 1969.

107. Mahanti, P. C., Phys. Rev. 42, 609 (1932).

108. Mahanti, P. C., Ind. J. Phys. 9, 517 (1935).

109. Lagerqvist, A. and Uhler, U., Arkiv. fur Fysik 1, 459 (1949).

110. Lagerqvist, A. and Uhler, U., Nature 164, 665 (1949).

111. Ghosh, P. N., Mahanti, P. C. and Makherjee, B. C., Phys. Rev. 35, 1491 (1930).

112. Barrow, R. F. and Crawford, D. V., Proc. Phys. Soc. A57, 12 (1945).

113. Pesic, D. S., Proc. Phys. Soc. A76, 844 (1960).

114. Pesic, D. S., Proc. Phys. Soc. A83, 885 (1964).

115. Brewer, L., Trajmar, S. and Berg, R., Astrophys. J. 135, 955 (1962).

116. Trajmar, S. and Ewing, G. E., Astrophys. J. 142, 77 (1965).

117. Brewer, L. and Green, D., to be published, The Violet Band Systems and Electronic States of Gaseous Magnesium Oxide.

118. Green, D., private communication.

119. Sokolov, V. A. and Nazimov, N. A., Optic Spect. (USSR) (Eng. Transl.) 8, 303 (1960).

120. Hultin, M. and Lagerqvist, A., Arkiv, Fysik 2, 471 (1951).

121. Lagerqvist, A., Arkiv Fysik 8, 83 (1954).

122. Hauge, R. H., Ph.D. Thesis, University of California, Berkeley, (1965).

123. Brewer, L. and Mastick, D. F., J. Am. Chem. Soc. 73, 2045 (1951).

124. Vol'nov, I. I., et al., IZV Akad. Nauk. SSSR, Ser Khim 10, 2365 (1967).

125. Benesi, H. A., J. Chem. Phys. 30, 852 (1959).

126. Mara, R. T. and Sutherland, G. B. B. M., J. Opt. Soc. Am. 43, 1100 (1953).

127. Wharton, L., Kurfman, M. and Klemperer, W., J. Chem. Phys. 37, 621 (1962).

128. Rolfe, J., Lipsett, F. R. and King, W. J., Phys. Rev. 123 (2), 447 (1961).

129. Kanzig, W. and Cohen, M. H., Phys. Rev. Letters 3, 509 (1959).

130. Rolfe, J., J. Chem. Phys. 40 (6), 1664 (1964).

131. Weltner, W., Jr. and McLeod, O., Jr., J. Phys. Chem. 69 (10), 3488 (1965).

132. Meyer, B., preprint 1969 - UCRL-19033.

133. Brown, R. D. and Coulson, C. A., Calcul des Fonctions d'Orde Molecules, p. 311, Editions du Center National de la Recherche Scientifique, Paris (1958).

LEGAL NOTICE

This report was prepared as an account of Government sponsored work. Neither the United States, nor the Commission, nor any person acting on behalf of the Commission:

A. Makes any warranty or representation, expressed or implied, with respect to the accuracy, completeness, or usefulness of the information contained in this report, or that the use of any information, apparatus, method, or process disclosed in this report may not infringe privately owned rights; or

B. Assumes any liabilities with respect to the use of, or for damages resulting from the use of any information, apparatus, method, or process disclosed in this report.

As used in the above, "person acting on behalf of the Commission" includes any employee or contractor of the Commission, or employee of such contractor, to the extent that such employee or contractor of the Commission, or employee of such contractor prepares, disseminates, or provides access to, any information pursuant to his employment or contract with the Commission, or his employment with such contractor.

TECHNICAL INFORMATION DIVISION
LAWRENCE RADIATION LABORATORY
UNIVERSITY OF CALIFORNIA
BERKELEY, CALIFORNIA 94720